University of Groningen

Self-assembled monolayers in organic electronics

Gholamrezaie, Fatemeh

Self-assembled monolayers
in organic electronics

Fatemeh Gholamrezaie

Self-assembled monolayers in organic electronics

Fatemeh Gholamrezaie
Ph.D. thesis
University of Groningen, The Netherlands

RIJKSUNIVERSITEIT GRONINGEN

Self-assembled monolayers in organic electronics

Proefschrift

ter verkrijging van het doctoraat in de
Wiskunde en Natuurwetenschappen
aan de Rijksuniversiteit Groningen
op gezag van de
Rector Magnificus, dr. E. Sterken,
in het openbaar te verdedigen op
vrijdag 5 oktober 2012
om 16:15 uur

door

Fatemeh Gholamrezaie

geboren op 6 januari 1982
te Tehran, Iran

Promotores: Prof. dr. D.M. de Leeuw
Prof. dr. ir. P.W.M. Blom

Copromotor: Dr. ir. S.C.J. Meskers

Beoordelingscommissie: Prof. dr. P. Rudolf
Prof. dr. R. Resel
Prof. dr. M. Orrit

Contents

Chapter 1
Introduction

This chapter gives a brief introduction of organic electronics and of self-assembled monolayers. First a short historical perspective is presented and the charge transport mechanism in organic materials and field-effect transistors is discussed. Subsequently, the importance of self-assembled monolayers and their utilization in field-effect transistors is highlighted. Self-assembled monolayers applied on the source and drain electrodes of organic transistors can be used to modify the charge carrier injection because of the macroscopic dipole moment. Examples of self-assembled monolayers on the gate dielectric of a field-effect transistor are presented. The concept of self-assembled monolayer field-effect transistors is explained. Finally, the use of spectroscopy to investigate the microstructure of the monolayer is introduced. The chapter concludes by presenting the scope of this thesis.

1.1 Historical: from inorganic to organic electronics

Microelectronics, which was born about 50 years ago, has grown into a mature industry and is responsible for driving most of modern technology in today's world. The technology has changed our lifestyle with the introduction of for instance computers, mobile phones and DVD recorders. The basic building block of microelectronics is the field-effect transistor. Many consider it to be one of the greatest inventions of the 20th century. The transistor was first proposed by Julius Lilienfield in 1926.[1] However, the first operating point-contact transistor, shown in Fig. 1.1a, was only reported years later in 1948 by Bardeen, Brattain and Shockley.[2] It took until 1960, when the first metal-oxide-semiconductor field-effect transistor (MOSFET) shown in Fig. 1.1b, was fabricated.[3] The first MOSFETs were made with single-crystalline silicon as the semiconductor and thermally grown silicondioxide as the gate dielectric.[4] The MOSFETs can be combined into integrated circuits (ICs). In the late 1950s and early 1960s the first ICs appeared, presented in Fig. 1.1c.[5] In 1965 Intel co-founder Gorden Moore noticed that the number of transistors per square inch on integrated circuits had doubled approximately every 18 months since their invention. Moore's law predicts that this trend will continue into the foreseeable future.[6] Therefore, the aim of the silicon industry has been increased performance by continuous downsizing of the feature size. However, single crystalline silicon cannot be used for large area electronics where numerous devices are required on low cost substrates, such as pixel drivers for flexible displays.

Plastics are materials renowned for their excellent mechanical properties, such as strength and flexibility, and for being electrical insulators.[7-8] These properties are exploited in many applications, such as insulation around wires and in electrical appliances. Plastics are used in almost every aspect of daily life because they provide high performance and are cheap to make. So it may come as a surprise to learn that some types of plastics can be made into semiconductors or even conductors. A semiconductor is a material of which the electrical conductance can be manipulated by applying an external field. These non-insulating plastic materials belong to the class of so-called conjugated polymers which contain alternating single and double bonds along the polymer chain. The materials are attractive because they can not only be used as semiconductors; they are also as strong and easy to manufacture as other plastics. The discovery of semi-conduction in a polymer film in the 1970s[10,11] triggered the scientific community to explore polymers as an active material in opto-electronic devices. When heavily doped, these polymers can have high electrical conductivity, even exceeding those of metals. The discovery was awarded with the Nobel Prize in 2000 dedicated to Alan J. Heeger, Alan G. MacDiarmid, and Hideki Shirakawa.[12]

The field of organic electronics started in the late 1970s with the demonstration of the first organic electro-optical devices such as thin-film transistors (OTFTs),[13] organic light-emitting diodes (OLEDs),[14] and organic photovoltaic (OPV) cells.[15] Applications are foreseen in displays of mobile phones and cameras, flexible solar panels, and integrated circuits in Radio Frequency Identification (RFID) tags.[16-18] The first organic electronic products reached the market in 2005/2006.
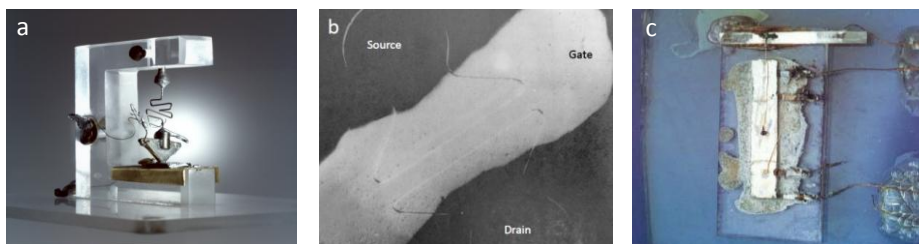
Figure 1.1. (a) Photographs of the (a) first transistor (point-contact transistor)[1] (b) first MOSFET (top view)[4] and (c) first integrated circuit (oscillator).[5]

Passive ID cards used for ticketing or toys that can be mass printed on paper were presented in 2006.[19] The organic electronics market is expected to grow in the coming years. The growth will be in data storage, OLED displays and lighting, photovoltaics, and RFID.[20]

1.2 Organic semiconductors

Organic semiconductors are carbon based compounds that show semiconducting properties. Isolated carbon atoms contain six electrons, two in the 1s and 2s orbital and one in the $2p_x$ and $2p_y$ orbitals. Two carbon atoms can be bound with a single, double or triple bond. Single bonds (σ-bond) are associated with a highly localized electron density in between the carbon atoms.
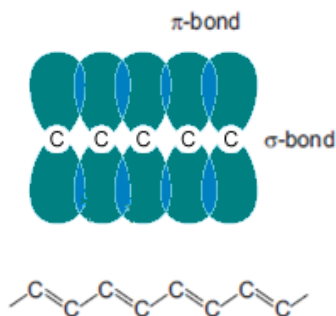
Figure 1.2. Schematic picture of the electronic bonds between carbon atoms (above) and the chemical structure of polyacetylene (below).

Double bonds between separate carbon atoms are formed by hybrizing three valence orbitals (2s, $2p_x$ and $2p_y$) to form three new orbitals: the sp^2-orbitals. Each of the sp^2-orbitals is occupied with one valence electron. The $2p_z$ orbital remains and is occupied by the fourth valence electron. A π-bond is formed by overlap of $2p_z$ orbitals. The electrons in a π-bond are delocalized above and below the plane of the molecule. As an

3

example the electronic bonds of polyacetylene are presented in Fig. 1.2. The energy levels of the π-bonds are concentrated in two bands separated by an energy gap, the band gap. Charge transport occurs either in the Highest Occupied Molecular Orbital (HOMO) or in the Lowest Unoccupied Molecular Orbital (LUMO). A selection of organic semiconductors is presented in Fig. 1.3.
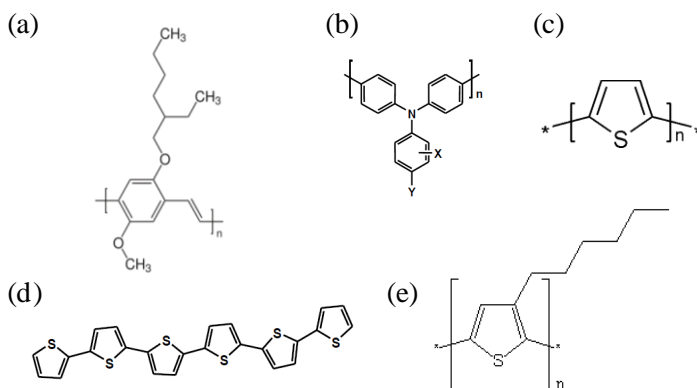
Figure 1.3. Typical organic semiconductors, some of them used in this thesis. (a) poly(2-methoxy-5-(29-ethylhexyloxy)-1,4-phenylene vinylene (MEH-PPV) (b) polytriarylamine (PTAA) (c) polythiophene (d) sexithiophene (T6) (e) poly-3-hexylthiophene (P3HT).

The absence of an ideal three-dimensional (3D) periodic lattice in polymer semiconductors complicates the description of charge transport process in terms of standard semiconductor models. A single crystal has a 3D architecture characterized by an infinite repetition of identical structural units in space. The crystal lattice is characterized by long-range order and strongly coupled atoms.[21] For silicon or germanium the strong coupling results in the formation of two long-range delocalized energy bands separated by an energy bandgap.[21] Charge carriers added to the semiconductor move in these energy bands with a relatively large mean free path.

When an organic molecule is conjugated and defect-free, the π-orbitals are delocalized and extend along the polymer chain.[22] However, due to chemical or structural defects conjugated segments are typically limited to a length of a few nanometers.[23] These conjugated segments vary in size and, consequently, each conjugated part of the molecules has a different local HOMO and LUMO energy.[24] Due to the presence of disordered localized states, the charge transport is modeled by hopping, *viz.* thermally assisted tunneling. The charge carriers hop between localized states at the Fermi level. The shape of the density of localized states (DOS)[25] is usually approximated by a Gaussian[26] or exponential[27] distribution.

1.3 Operation of organic field-effect transistors (OFETs)

The basic building block for organic integrated circuits is the field-effect transistor (OFET). The layout is schematically presented in Fig. 1.4a. The transistor contains three terminals, *viz.* a source, a drain and a gate electrode. In between the source and drain electrode an organic semiconductor is applied. Charge carriers are injected by the source, traverse the channel, and are collected at the drain. The gate is electrically separated from the source and drain electrode by the gate dielectric. The influence of the gate on the channel can be understood by considering the transistor as a parallel plate capacitor, with the gate and the semiconductor representing parallel plates. Applying a negative (positive) bias to the gate electrode may accumulate holes (electrons) in the semiconducting channel. The number of accumulated carriers is proportional to the product of the capacitance of the gate dielectric and the applied gate bias.[28]

Not all induced charge carriers are mobile. Any traps in the semiconductor or at the gate-dielectric-semiconductor interface will be preferentially filled prior to creating mobile carriers. The bias at which the current starts to flow is called the switch-on or threshold voltage (V_{th}). A typical transfer curve, where the source and drain current is monitored while the gate bias is swept, is shown in Fig. 1.4b. The source and drain bias is fixed. When the bias on the drain is much smaller than the bias on the gate, the transistor is operated in the linear regime. When the drain bias is much larger than the bias on the gate, the transistor is driven in saturation. In both regimes, an expression for the current can be derived analogously to the classical inorganic MOSFETs. In the linear regime ($|V_d| << |V_g\text{-}V_{th}|$) the source and drain current is given by:

$$I_{sd}^{lin} = -\mu_{lin} \frac{C_{ox}W}{L}(V_g - V_{th})V_d$$

where W and L are the width and length of the channel, C_{ox} is the areal gate capacitance and μ is the charge carrier mobility. The mobility is derived from the first derivative of the source and drain current to the gate bias as:[29]

$$\mu_{lin} = \frac{L}{V_d C_{ox} W} \frac{\partial I_{sd}}{\partial V_g}$$

In saturation, when $|V_d| >> |V_g\text{-}V_{th}|$, the source and drain current equals:

$$I_{sd}^{sat} = -\mu_{sat} \frac{C_{ox}W}{2L}(V_g - V_{th})^2$$
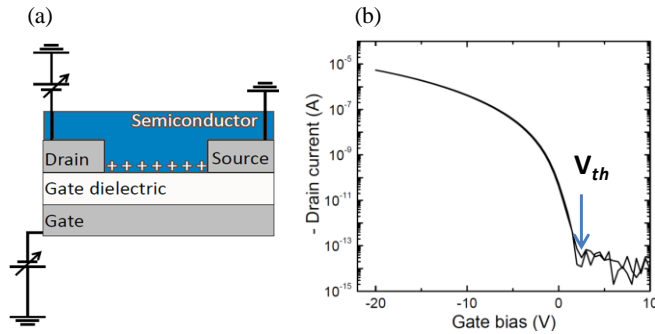
Figure 1.4. (a) Schematic representation of a field-effect transistor (side view) (b) Typical transfer curve of a unipolar transistor comprising a *p*-type semiconductor. At negative gate bias current flows and the current is depleted at positive gate bias.

The mobility can be obtained by taking the second derivative of the source and drain current to the gate bias and by correction for the geometrical parameters of the transistor[29]:

$$\mu_{sat} = -\frac{L}{C_{ox}W}\frac{\partial^2 I_{sd}}{\partial V_g^2}$$
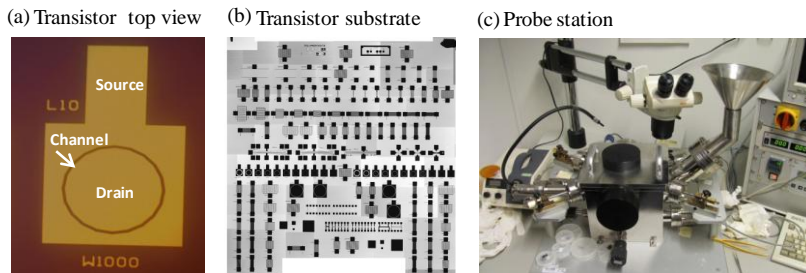
Figure 1.5. (a) Optical microphotograph of a ring transistor with channel length and width of 10 μm and 1,000 μm (top view) (b) Schematic layout of a test substrate with more than 100 ring and finger transistors with varying geometries on a Si monitor wafer made at Philips Research Eindhoven (c) Probe station for electrical measurements under high vacuum (10^{-6} mbar).

The preceding descriptions are useful to extract key device parameters such as threshold voltage and mobility to compare different transistors. The main device architecture that will be discussed in this thesis is the organic field-effect transistors. Fig. 1.5 shows a micrograph of a ring transistor, a schematic layout of a substrate with more than 100 transistors and a picture of the probe station used for electrical measurements of the devices.

1.4 Self-assembled monolayers

Self-assembly is the organization of components into structures without the involvement of humans.[30] In nanotechnology, molecular self-assembly can be used in organic electronics. At the moment for large area processing a top-down technology is being used. Thin films are applied by evaporation, ink jet printing or spin coating and patterned using photolithography. A promising technology for organic electronics is bottom-up self-assembly, where molecules self-organize into complex patterns and structures. By selectively patterning a substrate, in combination with the appropriate molecules, the self-assembly process can be directed. Subsequent patterning steps as needed in a top-down approach can be reduced.[31,32]

An example of self-assembly is a self-assembled monolayer (SAM). In 1980, Sagiv showed the possibility of producing chemically attached monolayers on silicon dioxide, which can be considered as the start of the self-assembled monolayer field.[33] Three years later, Nuzzo and co-workers used the chemical interaction between sulphur and gold to fabricate thiolated SAMs on noble metals.[34] The methods established by Sagiv and Nuzzo can both result in a highly ordered monolayers spontaneously formed from solution.

SAMs gained scientific and industrial interest because of the ease of processing as illustrated in Fig 1.6a. A substrate is dipped in a solution containing the self-assembling molecules. With time a monolayer is assembled on the surface. Reported surface modifications are for instance changes in work function, wettability and adhesion.[35]
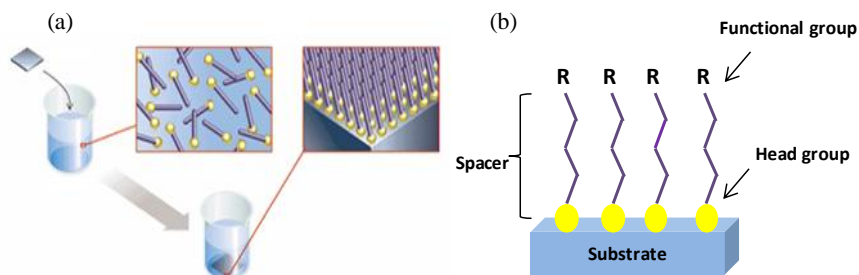
Figure 1.6. (a) Self-assembly solution process. (b) Typical self-assembling molecule containing three ingredients, a head group, a spacer and a functional group.[36]

Self-assembling molecules are usually built of three main ingredients; a head or anchoring group, a spacer and a functional end group.[37] A schematic representation of a typical self-assembling molecule is presented in Fig. 1.6b. The head group reacts with the substrate surface forming a covalent bond. The type of head group therefore depends on the chemical composition of the substrate. The most studied systems are alkyl thiolate ($C_nH_{2n+1}S$) SAMs on Au (111) surfaces.[38] The sulphur atoms of the thiolate molecules form stable bonds to the gold surface and alkyl tails of the thiolate molecules are closely packed by the van der Waals forces which results in a well ordered monolayer. SAMs with similar

structures are formed by alkyl thiolates on a range of other metal surfaces.[39] For Ag and Cu the self-assembly process requires first the reduction of the native oxide because the S linker cannot react with the oxide layer.

The head group can be for example –S–, –SH, –OH, –SiCl$_3$. The surface can be metallic (Au, Cu, Ag, Pd, Pt, Hg) as well as semiconducting (Si, GaAs, etc.) or dielectric like silicon dioxide. The spacer, typically an alkane, is used to separate the functional group from the substrate. In OFETs, self-assembled monolayers can be used to modify the work function of the source and drain electrodes, to control the wetting of deposited semiconductors on the gate dielectric and to adjust the threshold voltage.

1.5 Self-assembled monolayers on electrodes

In OFETs, interface dipoles play an important role in the process of charge injection from the metallic electrode into the active organic layer.[40] An oriented dipole layer changes the effective work function of the electrode due to its internal electric field. The difference between the work function of the electrodes and the highest occupied molecular orbital (HOMO) and the lowest unoccupied molecular orbital (LUMO) of the semiconductor determines the injection barriers of a OFETs. Therefore, the barrier for charge injection can be enhanced or suppressed by changing the work function. SAMs with dipole moments are used to change the local work function.
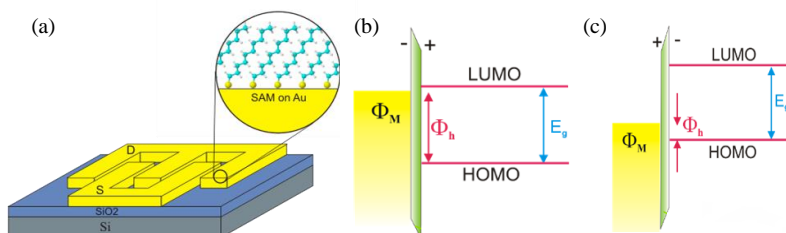
Figure 1.7. (a) Self-assembled monolayer on the gold source and drain electrodes of the finger transistors. Schematic energy level diagrams of metal/SAM/organic interface (b) raising the work function of electrodes for hole injection (c) lowering the work function of the electrodes for hole injection.

Fig. 1.7b illustrates a SAM modified electrodes. In Fig. 1.7b the work function is increased and in Fig. 1.7c, by using a molecule with an opposite dipole moment as compared to Fig. 1.7b, the work function is decreased.[41,42] Moreover, the presence of a SAM can alter the morphology of the semiconductor deposited on top of the electrodes. If the semiconductor is poly-crystalline, the change in morphology caused by SAM modified contacts generally has a larger effect than the change in the work function.

1.6 Self-assembled monolayers on the gate dielectric

A major application of SAMs in organic electronics is to passivate the surface of the gate dielectric. Often a silicon dioxide gate dielectric is used, which is terminated with silanol groups (–Si–OH), that can trap mobile charges.[43] To prevent charge trapping and hence to increase the charge carrier mobility a SAM is applied.[44,45] The driving force for self-assembly on the silicon dioxide surface is the formation of siloxanes, which connect the precursor silane to the surface silanol groups *e.g.* via very strong Si–O–Si bonds.[46] The gate dielectric silicon dioxide is generally passivated with hexamethyldisilizane (HMDS) or octadecyltrichlorosilane (OTS). The gate dielectric Al_2O_3 can also be used. The Al_2O_3 surface is typically passivated with phosphonic acids.

Silane SAMs grown on the gate dielectric can change the morphology of poly-crystalline organic semiconductor which can affect the mobility of the transistor. For example pentacence based FETs modified by an OTS layer on the gate dielectric show an improvement in the transistor mobility.[47] Furthermore, it has been shown that silane SAMs applied on the gate dielectric can adjust the threshold voltage of OFETs based on the chemical composition of the SAM molecules.[48]

1.7 Self-assembled monolayer field-effect transistors (SAMFET)

By studying the thickness dependence of the mobility in thin-film field-effect transistors, it has been shown that the charge-carriers are confined into the first few nanometers of the transistor channel.[49] This "ultrathin" picture of the channel has increased interest in studying charge transport with only a single monolayer as the semiconductor channel. One of the requirements for self-assembled electronics is a self-assembled semiconductor. By designing a self-assembled molecule that anchors to the gate dielectric, with a semiconducting core and a flexible tail, a monolayer transport channel can be formed in between the source and drain electrodes. A major concern is whether the single molecular layer in the SAMFET is able to provide reliable performance with respect to stress and elevated temperature.[31]
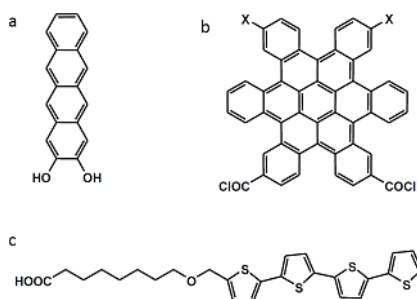
Figure 1.8. Reported semiconducting SAM molecules with an (a) acene (b) hexabenzocoronene and (c) quarterthiophene semiconducting core.

The fabrication of SAMFETs has been attempted by several groups. Systems investigated were functionalized acenes on aluminium oxide,[50] hexabenzocoronene on silicon dioxide,[51] and oligothiophenes with a functionalized short aliphatic linker on both aluminium oxide and silicon dioxide.[52] Chemical structures of the reported molecules are presented in Fig. 1.8. The electrical transport of the SAMFETs was measured as a function of channel length. No current was measured when using few μm channel lengths. Current modulation due to the field-effect was only observed in submicrometer channels. The accumulation layer could not be pinched off, and there was limited current saturation. Moreover, the mobility and the yields were low and the reproducibility poor. The lack of efficient charge transport was due to the presence of defects and to the limited intermolecular π-π coupling between the molecules in the self-assembled monolayers. A prerequisite for functional SAMFETs is a dense and ordered semiconducting monolayer with proper contacts to inject charges into the monolayer.
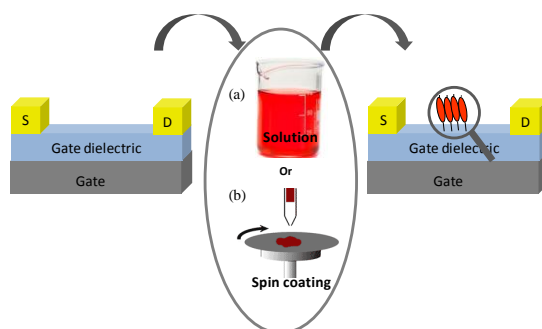
Figure 1.9. Fabrication of a monolayer field-effect transistor (a) Chemisorbed SAM by immersion of a substrate in to a solution containing the active molecule (SAMFET) (b) Physisorbed SAMs fabricated by spin-coating a solution of the semiconducting molecule on the substrate.

One technique to produce a monolayer FET is by spin-coating a solution containing the molecules on the transistor substrate, as shown in Fig. 1.9b. The molecules in the monolayer are physisorbed to the substrate. The interaction energy is low and hence the FET is sensitive to the temperature. Chemisorbed monolayer FETs are more stable.
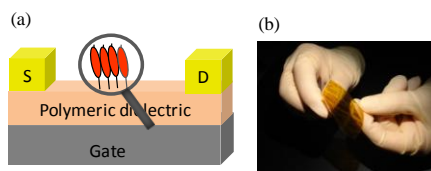
Figure 1.10. Toward flexible monolayer electronics (a) SAMFETs made on a polymeric gate dielectric (SU8) on a Si gate substrate (b) Integrated circuits on a foil (PEN) substrate made at Philips Research Eindhoven.

Recently, Smits *et al.* have demonstrated SAMFETs consisting of an ordered semiconducting self-assembled monolayer. The self-assembling molecule consists of a π-conjugated core with long alkyl chains. The SAMs are made from solution and anchored on the silicon dioxide gate dielectric. A schematic picture is presented in Fig. 1.9a.[53]

SAMFETs open an attractive route to produce low-cost, large-area electronics. A remarkable device complexity could be achieved, including inverters, ring oscillators and code generators, processed on silicon dioxide. This thesis will extend the formation of SAMFETs to polymeric substrates, thereby opening up the field of flexible monolayer electronics. Fig. 1.10a and 1.10b presents the SAMFETs made on a polymeric gate dielectric which will be discussed in the chapter 9. This is the first step towards flexible molecular monolayer electronics.

1.8 Photophysical studies

Organic semiconductors show a strict correlation between electronic and optical properties. In organic materials, including conjugated polymers and small molecules, photophysics plays an important role in understanding both their fundamental properties, their performance and suitability for use in organic devices. Photophysics is the study of the absorption and emission processes, looking at them on different timescales and under different environmental conditions, all in an attempt to understand how the materials behave.

Absorption spectroscopy refers to a spectroscopic technique in which the absorption of radiation by a sample is measured as a function of the energy (or wavelength). The frequencies where the absorption occurs primarily depend on the electronic configuration of the materials. Upon suitable absorption of light in a conjugated organic material an electron moves from the HOMO to the LUMO, forming an excited state. From there the excited state population can undergo a number of different relaxation processes. Some of these processes result in the emission of light and some do not, with the properties of the material defining how often, how quickly and at which frequency such events occur. Fluorescence is the relaxation that emits light. A photo of a fluorescence spectrometer is shown in Fig. 1.11a. In most cases, fluorescence occurs at lower energies or longer wavelength than the absorbed radiation. This is called the Stokes shift, demonstrated in Fig. 1.11b.

In molecular aggregates, the properties of the emission depend not only on the electronic structure of the single molecule, but are also strongly influenced by the molecular packing and coupling in the solid.[54] Arrangement of the molecules can for instance form *H*- or *J*- aggregates. The *J*-aggregate is a molecular arrangement in which the transition moments of individual molecule are aligned parallel to the line joining their centers. The *H*-aggregate is an array of molecules in which the transition moments of individual monomers are aligned parallel to each other but perpendicular to the line joining their centers. The most characteristic feature of *J*-aggregates is that they exhibit a red-shifted peak in the absorption spectrum which is with respect to the molecule absorption.

(a)

(b)
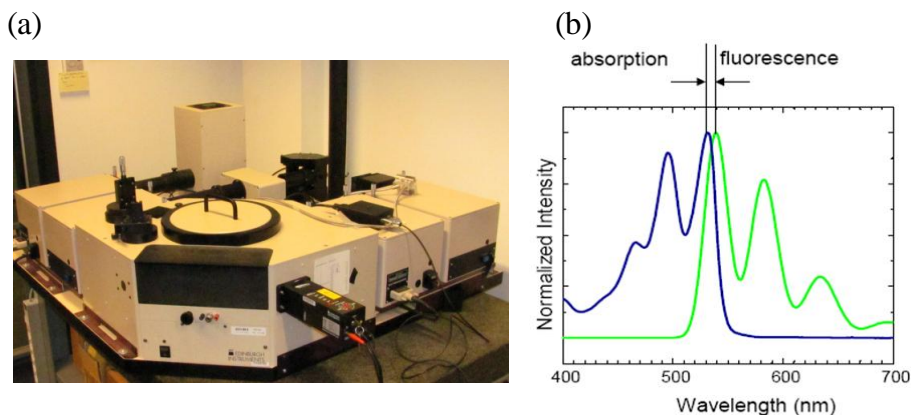
Figure 1.11. (a) Photo of an Edinburgh F900 fluorescence spectrometer (b) The fluorescence spectrum often happens at lower energies as compared to the absorption spectrum which called the Stokes shift.

The absorption spectrum of the *H*-aggregate consists of a blue-shifted band with respect to the monomer absorption. Furthermore the *H*-aggregates have a low fluorescence yield as compared to *J*-aggregates.[55] Therefore, photophysics measurements help to identify molecular packing in the solid.

1.9 Scope and implications of this thesis

A molecular monolayer is only a few nanometers thick, however it can completely change the properties of a surface. Therefore, one of the few practical strategies for bottom-up nanofabrication is using a self-assembled monolayer which can revolutionize nanoelectronics. The basic building of micro-electronic devices is a transistor. Hence, in this thesis the application of SAMs in OFETs is studied. In order to understand the effect of SAMs in OFETs and fabricate monolayer FETs, in particular, the following questions will be answered. The first three questions are related to the performance of OFETs.

1. Is it possible to manipulate the charge injection in OFETs by using SAMs on the source and drain electrodes?
2. Is the charge injection, using SAM modified source and drain electrodes, different in top-gate and bottom-gate transistors?
3. What is the origin of the threshold voltage shift caused by SAMs on the gate dielectric of OFETs?

Subsequently, fabrication of self-assembled monolayer field-effect transistors is investigated. The following questions are studied.

4. How can smooth and densely packed monolayers be formed? Does the microstructure and the molecular packing depend on temperature?
5. Can monolayer transistors be fabricated by spin coating?
6. Can the gate dielectric in SAMFETs be changed from the commonly used SiO_2 to an organic dielectric?

The questions will be addressed in the chapters of this thesis as listed below.

Chapter 2 shows the charge carrier injection of the OFETs can be changed by using self-assembled monolayers on top of the source and drain electrodes. The macroscopic dipole moment of the SAM changes the work-function of the gold source and drain electrode. Two polymers were investigated. Electrical characteristics of the modified transistors were analyzed with the transition line method. Finally, the effect of SAMs on the morphology of evaporated pentacene thin films was investigated.

In **Chapter 3** the modulation of the charge injection in bottom-gate and top-gate transistors is investigated applying SAM to modified electrodes for two semiconducting polymers. The current modulation is more pronounced in the top-gate geometry due to the better defined SAM on the upper surface of the bottom source and drain electrodes.

Chapter 4 discusses the importance of the threshold voltage in OFETs. The value of the threshold voltage is varied by using SAMs on the gate dielectric. The semiconductor after electrical characterization has been delaminated. The surface potential of the SAM has been measured after exfoliation by Scanning Kelvin Probe Microscopy. The surface potential perfectly agrees with the threshold voltage, which demonstrates that the shift is not due to the dipolar contribution but due to charge trapping in the SAM.

Chapter 5 presents liquid crystalline septithiophene (7T) FETs obtained by spin coating. The bulkiness of the end groups enhances the solubility and allows for solution processing. By controlling the concentration monolayer FETs have been fabricated. Electrical characterization and the spectroscopic properties of the monolayer are studied.

In **Chapter 6** the preparation of self-assembled monolayers of a quinque-thiophene derivative is illustrated. The monolayer is self-assembled from solution. The quinquethiophene monolayer forms two-dimensional crystals.

In **Chapter 7** the microstructure of the quinquethiophene monolayer as a function of the temperature is investigated. The layer was studied by grazing incidence X-ray diffraction and by X-ray reflectivity. From transverse shear force microscopy the shape and size of the crystals was obtained. In-situ temperature studies revealed a gradual change of the molecular packing which is irreversible. This chapter presents insights into monolayer formation and into the irreversible evolution upon temperature treatment.

In **Chapter 8** is dedicated to the photophysics of self-assembled monolayers of quinquethiophene on silicon dioxide and quartz substrates. For fully covered monolayers the red-shifted fluorescence and blue shifted absorption as compared to single molecules in solution indicates formation of *H*-aggregates. The spectra of the fully covered monolayer are comparable with reported spectra of oligothiophene crystals. The fluorescence of partially covered monolayer is discussed.

In **Chapter 9** the technology to fabricate SAMFETs on silicon dioxide is extended to fabricate SAMFETs on organic gate dielectrics. A two-dimensional highly ordered SAM directly grown on a polymer surface is demonstrated. Multiple discrete SAMFETs were combined into integrated circuits. The fabrication of the integrated circuits paves the way towards flexible self-assembled monolayer electronics.

References

(1) J. E. Lilienfeld, US Patent 1,900,018 **1926**.
(2) J. Bardeen and W. Brattain, US Patent 2,524,035 **1948**.
(3) D. Kahng, US Patent 3, 102, 230 **1963.**
(4) S. Sze, *Physics of Semiconductor Devices, 2nd ed. (Wiley, New York)* **2002**.
(5) J. S. Kilby, US Patent 3, 138, 743, **1964**. R.N. Noyce, US Patent 2, 981, 877, **1961**.
(6) http://en.wikipedia.org/wiki/Moore's_law
(7) J. H. Burroughes, D. D. C. Bradley, A. R. Brown, R. N. Marks, K. Mackey, R. H. Friend, P. L. Burns, A. B. Holmes, *Nature* **1990**, *347*, 539.
(8) J. J. M.Halls, C. A. Walsh, N. C. Greenham, E. A. Marseglia, R. H. Friend, S. C. Moratti, A. B. Holmes, *Nature*, **1995**, *347*, 539.
(9) G. Yu, J. Gao, J. C. Hummelen, F. Wudl, A. J. Heeger, *Science* **1995**, *270*, 1789.
(10) T. Ito, H. Shirakawa, S. Ikeda, *J. Polym. Sci. Chem*. **1974**, *12,* 11.
(11) C. K. Chiang, C. R. Fincher, Y. W. Park, A. J. Heeger, H. Shirakawa, E. J. Louis, S. C. Gau, A. G. MacDiarmid, *Phys. Rev. Lett.* **1977**, *39*, 1098.
(12) http://nobelprize.org/nobel prizes/chemistry/laureates/**2000**.
(13) A. Tsummer, H. Koezuka, T. Ando, *Appl.Phsy. Lett*. **1986**, *49*, 1210.
(14) C. W. Tang, S. A. VanSlyke, *Appl. Phys. Lett.* **1987**, *51*, 913.
(15) C. W. Tang, *Appl. Phys. Lett.* **1986**, *48*, 183.
(16) Philips Lumiblade, http://www.lumiblade.com
(17) Samsung Omnia, http://omnia.samsungmobile.com
(18) SonyXEL-1,http://www.sony.co.uk/product/tvp-oled-tv/xel-1/tab/technical
(19) http://www.sony.net/SonyInfo/News/Press/201005/10-070E/**2010/**
(20) http://www.marketwatch.com/**2012**
(21) C. Kittel, *Introduction to Solid State Physics*, 7th Ed., John Wiley and son, Inc. **1996**
(22) T. W. G. Solomons, *Organic Chemistry, 5th ed. (Wiley, New York)*, **1992**.
(23) F. Schindler, J. Jacob, A. Grimsdale, U. Scherf, K. Mullen, J. M. Lupton, J. Feldmann, *Angew. Chem.* Int. Ed. 44, **2005**, 1520.
(24) E. Meijer *"Charge transport in disordered organic field-effect transistors"*, PhD thesis Delft University (**2003**).
(25) B. Shklovskii, A. Efros, *Electronic properties of doped semiconductors (Springer-Verlag, Berlin*, **1984**.
(26) W. F. Pasveer, J. Cottaar, C. Tanase, R. Coehoorn, P. A. Bobbert, P. W. M. Blom, D. M. de Leeuw, M. A. J. Michels, *Phys. Rev. Lett.* **2005**, *94*, 206601.
(27) C. Tanase, E. J. Meijer, P. W. M. Blom, D. M. de Leeuw, *Phys. Rev. Lett.* **2003**, *91*, 216601.

(28) P. Stallinga, V. A. L. Roy, Z. X. Xu, H. F. Xiang, C. M. Che, *Adv. Mater*. **2008**, *20*, 2120.

(29) C. Reese, Z. Bao, *Adv. Funct. Mater.* **2009**, *19*, 763.

(30) S. Zhang, *Nat. Biotechnol*. **2003**, *21*, 1171.

(31) M. Halik, A. Hirsch, *Adv. Mater.* **2011**, *23*, 2689.

(32) E. Y. Zarechnaya, L. D. Ubrovinsky, N. Dubrovinskaia, N. Miyajima, Y. Filinchuk, D. Chernyshov, V. Dmitriev, *Sci. Technol. Adv. Mater.* **2008**, *9*, 044209.

(33) J. Sagiv, *J. Am. Chem. Soc.* **1980**, *102*, 92.

(34) R. G. Nuzzo, D. L. Allara, *J. Am. Chem. Soc. **1983**, 105,* 4481.

(35) (a) H. Ma, H. L. Yip, F. Huang, A. K, Y. Jen, *Adv. Funct. Mater.* **2010**, *20*, 1371,(b) S. DiBenedetto, A. Fachetti, M. A. Ratner, T. J. Marks, *Adv. Mater.***2009**, *21*, 1407,(c) D. Braga, G. Horowitz, *Adv. Mater*. **2009**, *21*, 1473, (d) H. Klauk , *Chem. Soc. Rev.* **2010**, *39*, 2643.

(36) http://en.wikipedia.org/wiki/Self-assembled_monolayer

(37) J. C. Love, L. A. Estro, J. K. Kriebel, R.G. Nuzzo, G. M. Whitesides, *Chem. Rev. **2005**, 105*, 1103.

(38) F. Nuesch, F. Rotzinger, L. Si-Ahmed, L. Zuppiroli, *Chem. Phys. Lett*. **1998**, *288*, 861.

(39) S. H. Kim, J. H. Lee, S. C. Lim, Y. S. Yang, T. Zyung, *Jpn. J. Appl. Phys.* **2003**, *43*, 60.

(40) K. Asadi, F. Gholamrezaie, E. C. P. Smits, P. W. M. Blom, B. de Boer, *J. Mater. Chem*. **2007**, *17*, 1947.

(41) B. H. Hamadani, D. A. Corley, J. W. Ciszek, J. M. Tour, D. Natelson, *Nano Lett.* **2006**, *6*, 1303.

(42) (a) N. J. Watkins, L. Yan, Y. Gao, *Appl. Phys. Lett.* **2002**, *80*, 4384, (b) M. Knupfer, G. J. Paasch, *Sci. Technol. A*. **2005**, *23*, 1072.

(43) L. Chua, J. Zaumseil, J. Chang, E. C. Ou, P. K. Ho, H. Sirringhaus, R. H. Friend, *Nature* **2005***, 434*, 194.

(44) G. Ashkenasy, D. Cahen, R. Cohen, A. Shanzer, A. Vilan, *Acc. Chem. Res.* **2002**, *35*, 121.

(45) S. A. DiBenedetto, A. Facchetti, M. A. Ratner, T. J. Marks, Adv. Mater. **2009**, *21*, 1407.

(46) V. Palermo, M. Palma, P. Samori, *Adv. Mater.* **2005**, *18*, 145.

(47) A. Pocchettino, *Accad.Lincei*. **1906**, *15*, 355.

(48) S. Kobayashi, T. Nishikawa, T. Takenobu, S. Mori, T. Shimoda, T. Mitani, H. Shimotani, N. Yoshimoto, S. Ogawa and Y. Iwasa, *Nature Mater.* **2004**, *3*, 317.

(49) G. Horowitz, R. Hajlaoui, P. Delannoy, *J. Phys. III* **1995**, *5*, 355.

(50) G. S. Tulevski, Q. Miao, M. Fukuto, R. Abram, B. Ocko, R. Pindak, M. L. Steigerwald, C. R. Kagan, C. Nuckolls, *J. Am. Chem. Soc.* **2004**, *126*, 15048.

(51) X. Guo, M. Myers, S. Xiao, M. Lefenfeld, R. Steiner, G. S. Tulevski, J. Tang, J. Baumert, F. Leibfarth, J. T. Yardely, M. L. Steigerwald, C. Nuckolls, *Proc. Natl. Acad. Sci.* **2006**, *103*, 11452.

(52) M. Mottaghi, P. Lang, F. Rodriguez, A. Rumyantseva, A. Yassar, G. Horowitz, S. Lenfant, D. Tondelier, D. Vuillaume, *Adv. Func. Mater.* **2007**, *17*, 597.

(53) E. C. P. Smits, S. G. J. Mathijssen, P. A. van Hal, S. Setayesh, T. C. T. Geuns, K. A. H. A. Mutsaers, E. Cantatore, H. J. Wondergem, O. Werzer, R. Resel, M. Kemerink, S. Kirchmeyer, A. M. Muzafarov, S. A. Ponomarenko, B. de Boer, P. W. M. Blom, D. M. de Leeuw, *Nature*, **2008**, *16*, 956.

(54) O. P. Dimitriev, A. P. Dimitriyeva, A. I. Tolmachev, V. V. Kurdyukov, *J. Phys. Chem. B*. **2005**, *109*, 4561.
(55) http://wiki.answers.com/Q/What's_H_aggregate

Chapter 2
Manipulation of charge carrier injection into organic field-effect transistors by self-assembled monolayers

In this chapter charge injection of gold source and drain electrodes modified by self-assembled monolayers of alkanethiols and perfluorinated alkanethiols into poly(2-methoxy-5-(29-ethylhexyloxy)-1,4-phenylene vinylene) (MEH-PPV) and regio-regular poly(3-hexyl)thiophene (rr-P3HT) in bottom contact-bottom gate field-effect transistors is studied. The presence of an interfacial dipole associated with the molecular monolayer at the metal/semiconductor interface changes the work function of the electrodes, and, hence, the injection of the charge carriers. The FET characteristics are analysed with the transfer line method. The device parameters are corrected for the contact resistance of the electrodes and mobilities of the polymers are determined. It has been shown that the performance of the pentacene single layer in bottom contact-bottom gate field effect transistor is also improved by modified gold source and drain electrodes of self-assembled monolayers of alkanethiols and perfluorinated alkanethiols. In this case the dominating role on the performance is played by the morphology of the pentacene rather than the work function of the modified electrodes. Therefore, the alignment of the energy levels at the interface unrevealed from the morphology.

2.1 Introduction

Organic field-effect transistors (OFETs), being promising candidates for low-cost, low speed and large-area display applications, have gone through extensive improvements in recent years.[1] Although organic (opto)electronic devices are at the edge of commercialization there are still fundamental challenges concerning the formation of contacts, charge injection from the contacts and transport of the injected charges through the device .[2-4] These are key parameters for reliable operation of an organic (opto)electronic device. Charge injection into the device is efficiently achieved *via* Ohmic contacts by choosing a metal with a work function that matches the Highest Occupied Molecular Orbital (HOMO) or Lowest Unoccupied Molecular Orbital (LUMO) of the organic semiconductor (within a few tenths of an electronvolt), respectively. In general, however, there is a misalignment between the energy levels of the contacts and the semiconducting polymer and therefore a barrier exists for injection of the charges from the metal into the polymer. Consequently, the performance of OFETs can be severely affected by this injection barrier. Thus manipulation of the injection barrier at the metal/polymer interface is of interest. Changing the injection barrier will result in either facilitating charge injection and therefore improving the performance of the device or reducing the charge injection and degrading the performance.[5,6] Engineering of the injection barrier is achieved either through manipulation of the HOMO (or the LUMO) of the polymer, or by modifying the work function of the electrodes. The latter approach is realized by insertion of polar molecules at the metal/semiconducting (polymer) interface. This can be regarded as inserting a sheet of electric dipoles at the interface which in turn results in a charge redistribution on the metal surface. From classical electrostatics one can calculate the potential drop caused by this dipole sheet. Imposing a sheet of dipoles on metals can be done by molecules that are evaporated[7] on the electrodes or molecules that are adsorbed, physically or chemically, on the surface. A prime example of the latter is a self-assembled monolayer (SAM) that consists of thiols on gold (Au).[8-11] One can regard the work function of a metal as a measure of the extension of the wave function of the free electrons at the surface of the metal into vacuum. Exposing the metal to an electric field caused by the dipolar monomolecular layer results in a larger extension of the wave function of the free electron into the vacuum and, hence, the electron is easier to extract from the metal and the work function of the metal is reduced.

Alkanethiols are well known to self-assemble in a uniform and densely packed monolayer on metal surfaces like Au.[10] The presence of electric dipoles associated with the molecule and the gold–sulfur bond, at the metal/molecule interface, will result in a modification of the work function of Au.[11] Recently, the successful utilization of alkanethiols to tune the work function of Au and silver (Ag) electrodes was demonstrated.[12] Improvement of the charge injection and blocking in organic light-emitting diodes and photovoltaic cells was observed. By using alkanethiols or perfluorinated alkanethiols on Ag, the current density was modified by 6 orders of

magnitude.[12] Hamadani *et al.* applied conjugated thiols in a bottom contact geometry in OFETs to control the charge injection into regio-regular poly(3-hexyl)thiophene (rr-P3HT).[13] Besides using the SAMs for tuning the charge injection in (opto)-electronic devices, it is demonstrated that the interfacial layers formed by a SAM of hexamethyldisilazene (HMDS) on SiO_2 at the insulator/semiconductor interface of an OFET improves the wetting of the rr-P3HT solution on the surface and the mobility of the charge carriers is increased due to morphological changes.[14]

Thiol-based SAMs also have been used to modify the OFET characteristics of sexithiophene and pentacene as the semiconductor.[5,15] Recent studies on metal/SAM/pentacene systems have shown that SAMs not only alter the alignment of the electronic energy levels at the interface, but also influence the morphology of the evaporated pentacene layers.[16-19] The presence of the SAM on the metal reduces the surface free energy and promotes the growth of pentacene layers with a standing-up orientation.[20] In this respect, understanding of the SAM-modified electrodes in OFETs becomes complex when both interfacial energetics and morphology are simultaneously changed.

For pentacene ($C_{22}H_{14}$)-(or in general crystalline organic semiconductors) based OFETs with SAM-modified gate oxide and/or electrodes, however, changes in device current are accompanied by changes in the morphology of pentacene deposited onto the modified surface.[21-23] The charge transport properties strongly depend on the packing and orientation of the pentacene molecules,[24] which are governed in thin films as used in OFETs by the interaction between the pentacene molecules as well as their interaction with the substrate. When pentacene is deposited on SiO_2 the interaction between the pentacene molecules results in pentacene layers with an upstanding orientation, packed in a herringbone-like structure.[25] By direct evaporation of pentacene on top of metal surfaces, an interfacial dipole (*ID*) appears at the metal/pentacene interface[26] which shifts the metal's work function often to undesirable values and reflects itself in the deteriorated FET performance.[27,28]

In this work, the tuning of the work function of the Au electrodes from 5.6 eV to 4.0 eV with 1H,1H,2H,2H-perfluorodecanethiol (PFDT) and hexadecanethiol (HDT), respectively is demonstrated. The low work function electrodes (modified with hexadecanethiol) give rise to an injection barrier for holes, resulting in a larger threshold voltage and a suppression of the current in the OFETs. In contrast, the addition of the perfluorinated SAM to the Au electrodes increases the work function. Since Au creates already a nearly Ohmic contact with poly(2-methoxy-5-(29-ethylhexyloxy)-1,4-phenylene vinylene) (MEH-PPV, HOMO at 5.2 eV) and regio-regular poly(3-hexyl)thiophene (rr-P3HT, HOMO at 4.8 eV), devices modified with the perfluorinated SAM, which increase the work function to 5.6 eV, do not show significantly improved behavior. Moreover, The thermal stability of the SAM is investigated to elucidate the influence of annealing on the interfacial issues of the OFET.

Later, a single layer of pentacene was used to disentangle the alignment of the energy levels at the interface from the morphology. The morphology at the electrode/gate oxide interface was studied. The Au electrodes were modified with a monolayer of alkanethiols or perfluorinated alkanethiols, these having opposite dipoles moments. Then it will be addressed which of the two, *i.e.*, aligned energy levels or morphology, has a more pronounced influence on the OFET performance in a bottom contact-bottom gate (BC/BG) geometry. It has been demonstrated that the interfacial morphology between the SAM-modified contacts and the transistor channel dominates the FET performance rather than manipulation of the schottky barrier and charge injection. The SAM-modified electrodes can be used to control the morphology to such an extent that stable and reproducible BC/BG OFETs with only one monolayer of pentacene as the active semiconducting material were realized.

2.2 Experimental

2.2.1 Self-assembling molecules

Hexadecanethiol (HDT) ($CH_3(CH_2)_{15}$-SH) (Aldrich) was distilled prior to use. Perfluorinated decanethiol (PFDT) ($CF_3(CF_2)_7(CH_2)_2$-SH) was synthesized according to reference 1. 1H,1H,2H,2H-perfluoro octanethiol (PFOT) and decanethiol (DT) were used. These compounds are readily obtained in high yields.

2.2.2 Polymer TFTs

Poly (2-methoxy-5-(2'-ethylhexyloxy)-1,4-phenylene vinylene) (MEH-PPV) and regioregular poly(3-hexylthiophene) (rr-P3HT) was used as semiconducting polymer in the OFET. Polymers were spin-coated from solution. The solvents used were toluene and chloroform for MEH-PPV and rr-P3HT, respectively. In order to avoid contamination with water and oxygen, the polymers were spun in a glove box and then transported directly to the measurement setup. The layer thickness was typically 200 nm.

2.2.3 Deposition of pentacene

Pentacene ultra-thin film growth was carried out by a supersonic molecular beam deposition technique (SuMBD). Since the first few monolayers and their corresponding morphology in the proximity of the electrodes and on the gate insulator dominate the OFET performance, experiments were carried out with ultra-thin pentacene films of only one layer. High crystallinity in the pentacene was achieved by carrying out the SuMBD at a kinetic energy of 6.4 eV. More details can be found in ref 29.

2.2.4 Self-assembled monolayer formation on FET substrates

The FET substrates were rinsed thoroughly with acetone and 2-propanol, and blown dry with deionized N_2. The self-assembling molecules were dissolved in ethanol (~(1–3) × 10^{-3} M). The FET substrates with Au electrodes were immersed into the solution for 1 or 2 nights. After the self-assembly process, the substrates were thoroughly rinsed with ethanol, toluene, and 2-propanol, dried with a deionized N_2 flow, and used immediately for spin coating of the organic semiconductor or pentacene deposition.

2.2.5 Work function measurements

The Au substrates were used for work function measurements prepared by thermal evaporation of 150 nm of Au on SiO_2 substrate with 1 nm of chromium as adhesion layer. Prior to use, the substrates were cleaned by UV–ozone for five minutes and immediately immersed in the solution containing the thiols. HDT solutions were prepared with concentrations of 1 × 10^{-5} M and 3 × 10^{-3} M. The immersion time was varied from one minute to several days. The substrates were rinsed as described for FETs and the work function was measured in a glove box by a Kelvin probe. The Kelvin probe was calibrated with freshly cleaved highly oriented pyrolytic graphite (HOPG) under nitrogen atmosphere (glove box). Freshly cleaved HOPG is known to have a stable work function of 4.48 eV.[12]

2.2.6 Thermal stability measurements

For probing the thermal stability of SAMs, the substrates were first immersed in ~(1–3) × 10^{-3} M solution over night. After rinsing the substrates with ethanol, toluene and 2-propanol and drying with a deionized N_2 flow, SAM functionalized substrates were coated with a polymer layer by spin coating of polystyrene $(C_8H_8)_n$ from a 5 mg ml^{-1} solution in toluene. The samples (Au/SAM/PS) were annealed on a calibrated hotplate in the glove box for two hours at different temperatures. After cooling to room temperature the polystyrene layer was removed with acetone and the substrate was rinsed with ethanol, toluene and 2-propanol, and dried with a deionized N_2 flow. Finally, the work function was measured in the glove box.

2.2.7 Devices and electrical measurements

FETs were made using heavily doped silicon wafers as gate electrode, with 200 or 250 nm of thermally grown silicon dioxide (SiO_2) as the gate dielectric. A 5 or 10 nm layer of titanium was used as adhesion layer for the Au on SiO_2. By conventional photolithography, Au source and drain electrodes with finger or ring geometry were patterned on top of the SiO_2. The channel length varied from 1 to 40 μm

while the channel width was kept constant. Two FET configurations, shown in Fig. 2.1, were demonstrated: a finger configuration with typical length L=10 μm and width W=10000 μm; ring configuration with L=10–40 μm and W=1000 μm. For both transistors the capacitance of the gate insulator is 17 nF cm^{-2}. Electrical measurements were carried out in a probe station under high vacuum (10^{-6} mbar) with a Keithley 4200 Semiconductor Characterization System at room temperature.

Figure 2.1. Finger (left) and ring (right) geometries of FETs.

2.2.8 Atomic force microscopic characterization

The atomic force microscopy (AFM) height and amplitude images on the pentacene OFETs were simultaneously recorded at room temperature under ambient conditions after the electrical measurement. Reference morphology analysis was performed by examination of monolayers deposited on bare SiO_2 using tapping mode AFM. The first pentacene monolayer on SiO_2 was completed after 50 min of deposition. The morphology of the films was studied by using tapping mode AFM (Digital Instruments). The AFM images of 3μm × 3μm were recorded.

2.3 Modifying the work function: Magnitude and (thermal) stability

The effect of the PFDT and HDT SAMs on the work function of Au was examined. A complete monolayer of PFDT and HDT increases the work function to 5.6 eV and decreases the work function of Au to 4.0 eV, respectively (Fig. 2.2).[12] Both the magnitude and the stability of the work function of the SAM modified Au electrode are of great concern. A highly stable (tuned) work function in time is desired when applications are envisioned that use these molecular layers in electronic devices. To address the magnitude, a series of experiments with diluted SAM solutions were conducted with different immersion times.

The results presented in Fig. 2.2a indicate that the process of the monolayer formation is indeed very fast and even after reducing the concentration of the solution by a factor of 100, the shift in the work function approaches its maximum value after 100 minutes in solution. Reducing the concentration of the solution provides the possibility of tuning the work function of Au to preselected values by immersing the substrate for a short time in the solution. The explanation lies in the nature of the self-assembly process, since the monolayer does not fully cover the Au surface during short immersion time[30] and, therefore, the resulting work function is less than expected. Utilizing different immersion times of the Au-coated substrate in a 1×10^{-5} M solution of HDT, the work function of Au can be tuned between 4.5 and 4.0

eV. The utilization of SAMs in devices also requires a good stability of the SAM over longer periods of time. The stability measurements of the modified substrates, shown in the inset of Fig. 2.2a, clearly indicate that both monolayers (HDT and PFDT) are very stable when kept in N_2 atmosphere at room temperature and no degradation of the modified electrodes and their work functions is observed after 1 month.

To improve the performance of polymer-based FETs, post production treatments such as annealing of the polymer are often required to improve the properties of the polymer and/or the physical contacts between the polymers and the electrodes. SAMs are known to be less thermally stable than polymers[31] and, therefore, the thermal stability of the SAMs used is investigated in a configuration that mimics the actual device. To investigate the work function of SAM-modified Au electrode with the Kelvin probe at elevated temperatures, a series of experiment with large gold-coated glass substrates (3 × 3 cm) on which a SAM was applied and covered the SAM with a layer of polystyrene (PS), as described in the Experimental section were conducted.

After thermal annealing the Au/SAM/PS stack for 2 hrs on a hot plate in the glove box, the PS was removed by thoroughly rinsing with solvents; and the work function of the remaining Au/SAM was measured with the Kelvin probe (Fig. 2.2b). As the annealing temperature is increased, the work function increases steadily, and around 80 °C a total shift of 0.4 eV is observed.

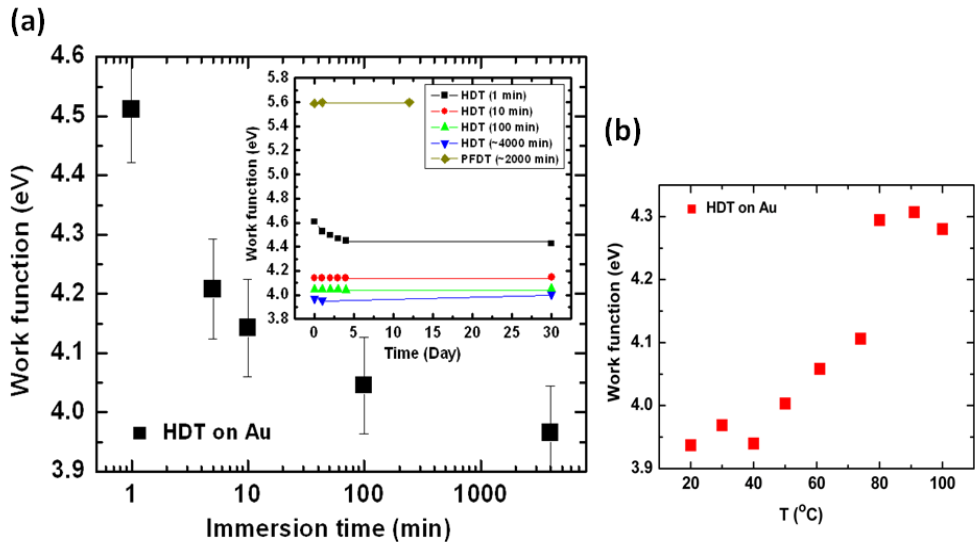**Figure 2.2.** (a) The work function measured with the Kelvin probe as function of the immersion time of the Au-coated substrate in the HDT SAM solution of 1 × 10^{-5} M. Inset: The stability of the work function for PFDT and for HDT (for different immersion times). (a) Stability of the HDT-modified Au substrates expressed by plotting the work function as measured with the Kelvin probe *versus* temperature.

This higher work function indicates less dipoles on the Au surface and, thus, a lower grafting density of the SAM on Au upon annealing. A decreasing grafting density can be correlated to phase transitions of the 2D packing of the SAM as was observed by Qian *et al*.[31] These authors demonstrate the appearance of low density phases upon annealing above 70 °C due to desorption of alkanethiol molecules from the Au surface.Obviously, a lower packing density of the dipoles on the Au surface results in a smaller potential shift of the work function of the annealed substrates. The SAM cannot freely desorb from the surface since a PS layer onto the SAM is spin coated. Therefore, the alkanethiols have to diffuse into the PS layer which is very likely at annealing temperatures above 70–80 °C. Thus annealing polymer-based electronic devices with SAM-modified electrodes at temperatures above ~60 °C can enhance the morphology of the polymer and its electronic properties, but will result in a reduced work function shift even if the monolayer is covered with a thin polymeric film. Both contrasting effects should be taken into account when electrical device parameters are extracted from such annealed field-effect devices.

2.4 Manipulation of charge injection in OFETs

Previously, the use of SAMs to tune the work functions of metal electrodes (Au, Ag) in organic electronic devices such as polymer (light-emitting) diodes and photovoltaic cells was reported.[12] For these diode geometries the effect of the electrode modification is obvious: one can block the injection of holes or electrons. In three terminal devices, this effect is less clear since high gating potentials result in a highly electrostatically doped semiconductor, which can give rise to strong band bending at the drain electrode/polymer interface. To evaluate the influence of the work function shift on the characteristics of the devices, a series of transistors were processed in which the Au electrodes were functionalized with two different SAMs with opposing dipole moments. The device was treated with the primer HMDS in order to make the surface hydrophobic.[32,33] Two different semiconducting polymers (MEH-PPV and rr-P3HT) were used in these SAM-modified FETs. Measurements were performed according to the procedures described in the experimental section.

2.4.1 Hole injection in MEH-PPV

Poly (2-methoxy-5-(29-ethylhexyloxy)-1,4-phenylene vinylene) (MEH-PPV) has its HOMO centered at 5.2 eV. Therefore a negligibly small injection barrier with Au is obtained, since the work function of vapor-deposited Au is ~ 4.9 eV (as measured with the Kelvin probe). The MEH-PPV/Au contact can be considered an Ohmic contact. Modifying the contacts with the HDT results in a work function of 4.0 eV and creates a large injection barrier of ~ 1 eV for the injection of holes. On the other hand, PFDT increases the work function of Au to 5.6 eV. In the latter case an Ohmic contact is expected. Output characteristics of the two sets of finger transistors with W/L = 10000(μm)/20(μm) are shown in Fig. 2.3 and demonstrate the effect of different SAMs on the charge injection.

The results show that HDT suppresses the current of the transistor, while in the case of PFDT the output characteristics are almost unaffected compared to the untreated transistor. As expected, PFDT-modified Au contacts form an Ohmic contact with MEH-PPV similar to untreated Au contacts. The small difference in the current between the PFDT treated and untreated transistor can be explained by the presence of the molecular monolayer at the metal/semiconductor interface, which can be regarded as a tunnel barrier at the interface that introduces an additional resistance at this interface.

The FET characteristics of MEH-PPV with the HDT modified Au electrodes demonstrate clearly that the large hole injection barrier suppresses the charge injection in these FETs. By investigating the transfer characteristics in the saturation regime, the threshold voltage from the intercept of the linear fit can be derived. From the slope, the mobility can be extracted.[1] As expected, both the untreated Au and Au modified with PFDT create an Ohmic contact, and, consequently, the slopes of the linear fits are similar, which implies similar apparent mobilities. Although the threshold voltage is mostly dominated by the properties of the gate dielectric and the dielectric/polymer interface, a small dependence on the electrodes is observed.[34] Further analysis of the transfer data in Fig. 2.4 shows that the mobilities obtained for untreated and for the PFDT-modified transistors are different than the mobility extracted for the HDT-modified transistor (slope of the linear fit).

From this analysis, one may deduce that the SAM affects the mobility of charge carriers in MEH-PPV. Since MEH-PPV is an amorphous material, its charge transport is isotropic and governed by the concentration of charge carriers.[3,35] Furthermore, the mobility of an amorphous material is an intrinsic property of the material which is dependent on the charge carrier density[3,35] and independent of the geometry and the contacts. Therefore, the mobility analysis mentioned above is not applicable for the SAM-modified transistors since the contacts of the transistors are playing a role in the charge injection process. A more correct method to extract mobilities from the data obtained is to perform an analysis using the transfer line method (TLM).[7,36,37] This method relies on measuring a series of transistors with the same channel width and different channel lengths. Via data analysis of the transfer characteristics, one can correct for the contact resistance and evaluate the true mobility of the organic semiconductor. Therefore, a series of finger transistors with channel lengths of 7.5, 10, 15, 20, 30 and 40 µm and a channel width of 10000 µm were measured and the TLM method was applied. These measurements were repeated for FETs with their Au contacts modified with HDT and PFDT. The analysis resulted in the same mobility for both SAM-modified and untreated FETs of 4×10^{-4} cm^{2}V^{-1}s^{-1} for MEH-PPV at low V_{DS} (V_{DS} = -2 V) and high V_G (where DS means drain and source and G means gate). Fig. 2.5 shows the calculated mobility and contact resistance of the transistors versus V_G. Fig. 2.5a demonstrates that the mobility is the same in all cases and independent of the contact modification. In this respect TLM is a good method to overcome the obstacles associated with the conventional analysis for OFETs at linear and saturation regimes.
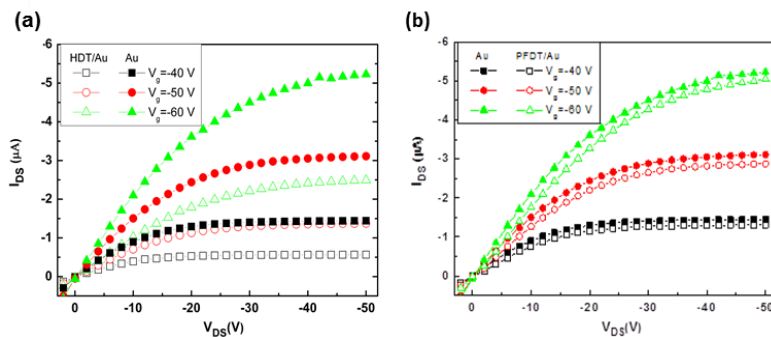
Figure 2.3. Output characteristics of a FET based on MEH-PPV with (a) untreated Au electrodes and HDT-modified electrodes and (b) untreated Au electrodes and PFDT- modified Au electrodes.
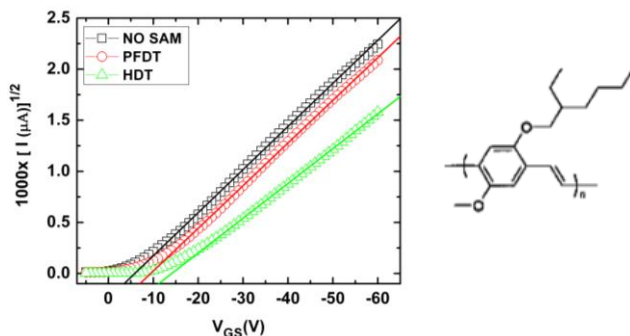
Figure 2.4. The transfer characteristics in the saturation regime and the increase of the threshold voltage for SAM-modified Au electrodes in MEH-PPV based transistors. On the right side the structure of MEH-PPV is shown.
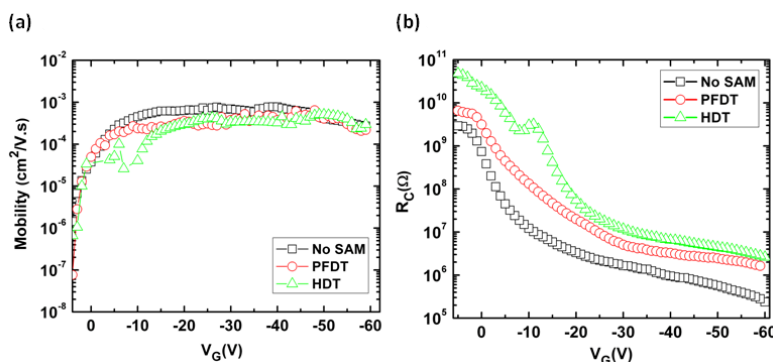
Figure 2.5. TLM analysis of the MEH-PPV-based transistors at V_{DS} = -2 V: (a) mobility and (b) contact resistance of the untreated and PFDT- and HDT-modified Au electrodes in OFETs.

Furthermore, the analysis for the contact resistances of the HDT-modified, PFDT-modified and untreated FET demonstrates an increasing contact resistance with the length of the SAM (Fig. 2.5b). The difference in the output characteristics of the transistors as demonstrated in Fig. 2.3 is well supported by TLM. HDT raises the contact resistance in the low gate voltage regime by more than two orders of magnitude compared to the untreated Au contacts. PFDT on the other hand increases the contact resistance by less than one order of magnitude. In general, the contact resistances decrease when the gate voltage is increased. For large contact resistances (larger than the bulk resistance of the semiconducting polymer in the transistor channel) most of the applied source and drain electrodes potential drops across the contacts instead of the channel. Therefore, the current that is extracted from the transistor decreases.

2.4.2   Hole injection in rr-P3HT

Regio-regular P3HT has been the subject of many studies in OFETs. Due to the presence of highly ordered crystalline phases at the semiconductor/dielectric interface, a higher mobility is obtained compared to other semiconducting polymers such as MEH-PPV. The on/off ratio of the transistor is increased upon annealing due to dedoping of the rr-P3HT.[38] In the case of using SAM-modified electrodes, one has to be careful using thermal treatment of the transistors since SAMs of alkanethiols, as shown in Fig. 2.2b, are thermally unstable at temperatures above 60 °C.[31] Therefore, annealing of rr-P3HT is unsuitable for experiments in which the Au electrodes are modified with SAMs of alkanethiols. Consequently, all the experiments with rr-P3HT were conducted at room temperature without any thermal treatment. Annealing of OFETs with rr-P3HT and SAM-modified Au electrodes[13] will also influence the anisotropic nature of the charge transport in rr-P3HT. Furthermore, a change of the interfacial morphology that P3HT adopts at the interface with the SAM has an impact on the mobility of the material and performance of the device.[39] Later, changes in the morphology changes for SAMs modified electrode FETs by changing the semiconductor to pentacene will be thoroughly addressed. The presence of a PFDT SAM with CF_3 end groups drastically alters the surface energy and CF_3 SAM results in a highly hydrophobic surface, which causes a poor wetting of the rr-P3HT on the contacts. Therefore, data based on PFDT-modified transistors were not used. However, the current–voltage characteristics of untreated transistors and transistors with HDT-modified Au electrodes are reliable and reproducible. The transfer characteristics of untreated and HDT-modified transistors with channel width of 10000 µm and channel lengths of 10, 15, 20, 30 and 40 µm were analysed with TLM and are plotted in Fig. 2.6. Since the HOMO level of rr-P3HT is located at 4.8 eV, an Ohmic contact is created with Au electrodes. For HDT treated Au contacts, the work function is changed to 4.0 eV. Consequently, an injection barrier for holes is expected. The mobility calculated from both transistor characteristics (untreated and HDT-treated) is $(1–2) \times 10^{-2}$ $cm^2V^{-1}s^{-1}$ at V_{DS} = -2 V and high V_G, which is similar to the reported mobility for rr-P3HT.[14,38,39] Even though the mobility in an OFET only depends on the temperature and charge carrier density,[3,35] analysis of the transfer and output characteristics with simplified models, such as the

gradual channel approximation, will result in mobilities which deviate from the accepted values. Such models are founded on Ohmic contacts between the semiconductor and the electrodes, which is not always applicable.
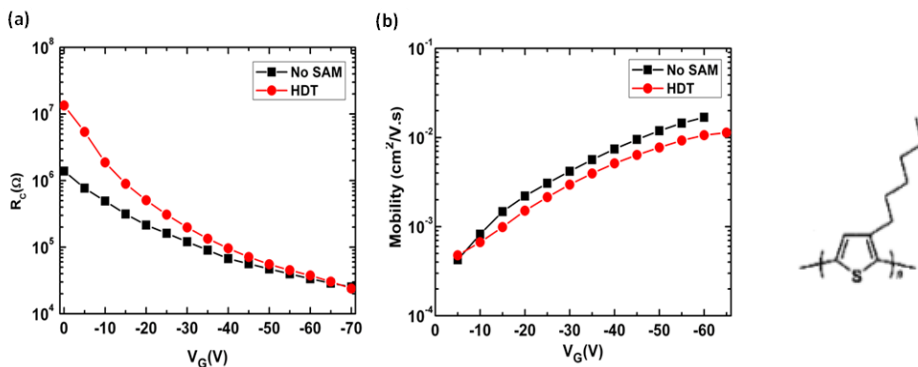
Figure 2.6. Comparison of (a) contact resistance and (b) mobility versus gate voltage for the HDT-modified and untreated transistor with rr-P3HT as the semiconductor at V_{DS} = -2 V. On the right side, the structure of rr-P3HT is shown.

The contact resistance for the SAM-modified Au electrodes is one order of magnitude larger than that of a transistor with bare Au electrodes. Taking the analysis of Burgi et al.[6] into account that the contact resistance is a combination of the resistances arising from the contact itself, the injection barrier and the bulk resistance at the interface, the difference in contact resistance can be attributed to the increase of the injection barrier due to the presence of the monolayer between the Au electrode and the semiconducting polymer, if the effect of morphology disregard. The morphology effect is addressed in the next section.
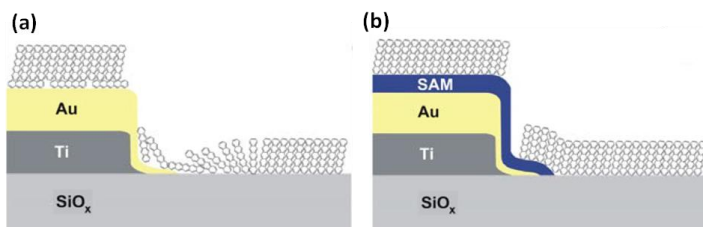
Figure 2.7. Schematic picture of pentacene packing (a) on top of bare gold electrodes (b) on top of the SAM modified gold electrode. The presence of the SAM on the metal reduces the surface free energy and promotes the growth of pentacene layers with a standing-up orientation.

2.5 Modified electrodes in single layer pentacene

For pentacene FETs with SAM-modified gate oxide and electrodes, changes in performance are accompanied by changes in the morphology of pentacene monolayer deposited onto the modified surface.[21-23] The presence of the SAM on the metal reduces the surface free energy and promotes the growth of pentacene layers with a standing-up orientation (Fig. 2.7).[20] In this respect, understanding of the SAM-modified electrodes in OFETs becomes complex when both interfacial energy and morphology are simultaneously changed. It has been demonstrated that the interfacial morphology between the SAM-modified contacts and the transistor channel dominates the FET performance rather than manipulation of the Schottky barrier and charge injection. The SAM-modified electrodes can enable to control the morphology to such an extent that stable and reproducible BC/BG OFETs with only one monolayer of pentacene as the active semiconducting material were realized.

For pentacene deposition, the FET substrates were dipped in a Piranha solution (demi water 100ml+ammonia (30%) 20ml+H_2O_2 20 ml) for 60 s at 70 °C to remove all organic impurities from the surface of the metal as well as from the oxide. Then the substrates were submerged in acetone in an ultrasonic bath for 5 min and spin dried. Next the substrates were exposed to UV–ozone for 20 min. To explore the role of the SAMs on aligned energy levels at the interface, the Au electrodes were treated with SAMs of opposite dipoles namely, 1H,1H,2H,2H-perfluoro octanethiol (PFOT) and decanethiol (DT). Kelvin probe measurement showed that PFOT and DT change the work function of Au from 4.8 eV to 5.5 and 4.2 eV, respectively.[12] From the work function measurement, it is expected that Au/PFOT/pentacene gives rise to an Ohmic contact, while the Au/DT/pentacene is expected to have a large energy offset with a charge injection barrier of ~ 0.7 eV.[40] The latter is anticipated to have a limited charge injection and, therefore, a poor performance. Hence, pentacene with only 1 ML thickness was deposited on the transistor substrates with bare Au electrodes and with PFOT-modified Au electrodes. AFM analysis of the pentacene monolayer growth is demonstrated in Fig. 2.8a. The difference in morphology at the electrode/semiconducting channel boundary is prominent between the untreated and PFOT modified Au electrodes. Remarkably, at the boundary between the Au/PFOT electrode and the SiO_2 the surface morphology of the pentacene monolayer is continuous and the large pentacene monolayer terraces extend from the edge of the electrodes into the channel and no morphological transition region is observed.

For the untreated Au electrode (Fig. 2.8), the morphological transition regime was formed at the boundary of the Au electrode/SiO_2 interface and no large pentacene monolayer terraces are observed. The electrical output characteristics of the two OFETs (Fig. 2.8b) show that the transistor with the unmodified Au electrodes hardly turns on and very low currents are observed (nA), while the PFOT-modified transistor illustrates very good field-effect characteristics with higher currents (μA). By modifying the Au electrode with PFOT SAM, the drain currents are more than three orders of magnitude higher over the complete bias range. Further investigation of the transfer characteristics of the FETs (Fig. 2.8c) demonstrates that the unmodified transistor displays a large switch-on voltage

of around -60 V, a low on/off ratio, and a very low saturated current. Consequently, the mobility amounts to values of only 10^{-5} cm^2 $V^{-1}s^{-1}$ in the saturation regime. However, the monolayer pentacene FETs with PFOT treated electrodes exhibit a superior performance compare to its untreated counterpart. The FET current in the saturated regime is three orders of magnitude higher with large on/off ratio and a charge carrier mobility that amounts to 0.015 $cm^2V^{-1}s^{-1}$. The current is free of hysteresis and the switch-on voltage is shifted to -10 V. PFOT treatment of the electrodes has a significant effect on the switch-on voltage and strongly reduces the hysteresis. These effects are usually attributed to trapped charges at the gate insulator/semiconductor interface. Nevertheless the occurrence of a discontinuous transition region and small pentacene islands can explain also the hysteresis in the transfer characteristics. Injected charges are trapped at the grain boundaries of the pentacene islands in the case of OFETs with untreated electrode leading to hysteresis and high switch-on voltage. In contrast, the monolayer pentacene OFETs with the SAM-modified electrode demonstrates a highly uniform morphology at the edge of the SAM-modified electrode/SiO_2. Therefore, the transition regime is eliminated and fewer traps are expected, hence a low switch-on voltage and less hysteresis.

2.6 Conclusion

It has been demonstrated that self-assembled monolayers can modify the work function of Au from 4.0 eV to 5.6 eV for HDT and PFDT, respectively. Both SAMs on Au and their corresponding work functions are stable in time. Adjusting processing parameters like the concentration of the SAM in solution and the immersion time provides the opportunity to tune the work function. The alkanethiol-based SAMs on Au are shown to be thermally unstable when annealed above 60 °C. The SAM modified Au electrodes are used in field-effect transistors to manipulate the injection of holes into polymeric semiconductors. Using the transfer line method (TLM), the mobility for MEH-PPV was found to be 4×10^{-4} $cm^2V^{-1}s^{-1}$ and that for rr-P3HT to be $(1-2) \times 10^{-2}$ $cm^2V^{-1}s^{-1}$ irrespective of the contacts treatment. The contact resistances extracted from the TLM are at least one order of magnitude larger for the SAM-modified Au contacts with respect to the untreated Au electrodes. The transfer line method used here is more generally applicable than the gradual channel approximation, especially when non-Ohmic contacts are formed in organic field-effect transistors.

Moreover, it has been presented that the performance of pentacene monolayer FETs is improved by modifying the metal electrodes with PFOT SAMs. With optimized growth condition of pentacene on the substrates via the supersonic molecular beam deposition, hysteresis-free transfer curves with very small switch-on voltages were obtained for only a single monolayer of pentacene. The realization of an efficient BC/BG transistor with only 1 ML of pentacene that has been elusive so far can be achieved by simply inserting a monolayer of PFOT on the Au electrode. The dominating role on the performance is played by the morphology of pentacene rather than the aligned energy levels at the contact. The preferred orientation of the pentacene on and next to the SAM-modified metal electrodes is identical to the orientation of the pentacene on SiO_2,[41] and,

therefore, no small crystalline domains are found near the SAM-modified electrodes. Due to the absence of small crystallites, pentacene grain boundaries are eliminated and charge trapping hardly occurs which led to good field-effect behavior of the transistors without a large switch-on voltage.
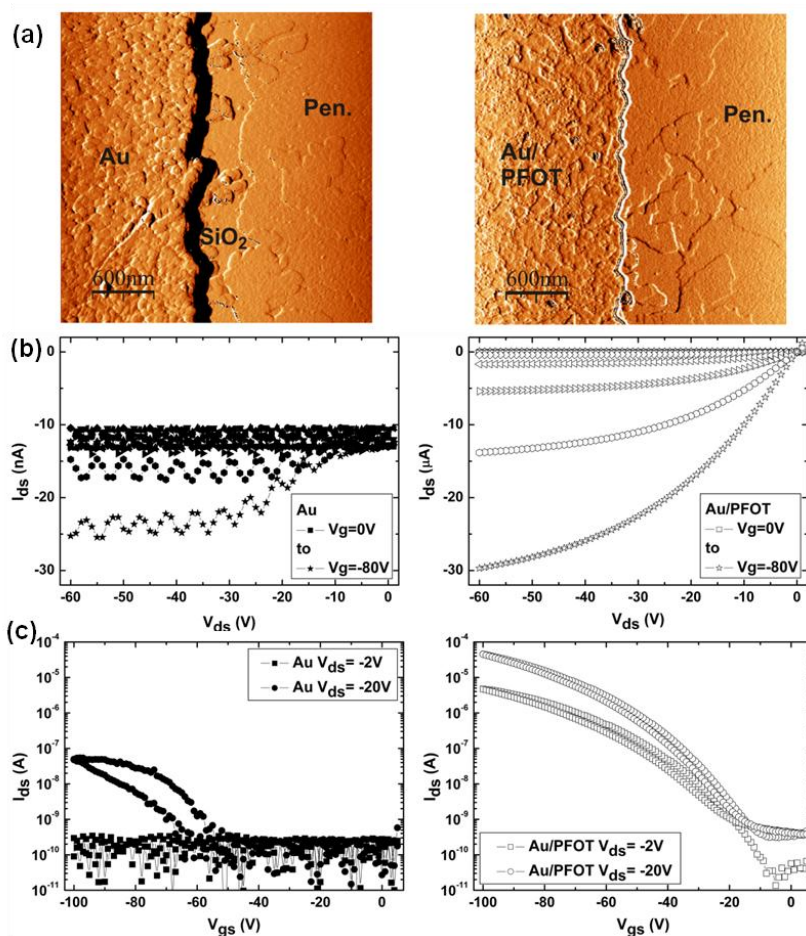
Figure 2.8. (a) AFM amplitude images (3µm×3µm) of a monolayer of pentacene at the interface between the gold electrode and the silicon oxide surface where the left image depicts a pentacene monolayer grown next to the bare gold electrode and the right image shows a pentacene monolayer grown next to PFOT-modified gold electrode. (b) Output characteristics of transistors with Au (left) and Au/PFOT (right) electrodes. Note that the y-axis is adjusted from nA to µA. (c) Transfer characteristics of the same transistors as in (a) with Au (left) and Au/PFOT (right) electrodes showing the superior performance of the Au/PFOT monolayer pentacene OFET. All the transistors have a channel length/channel width of 10/10000 and an oxide thickness of 250 nm.

References

(1) C. D. Dimitrakapoulos, P. R. L. Malenfant, *Adv. Mater.* **2002**, *14*, 99.

(2) B. de Boer, M. M. Frank, Y. J. Chabal, W. Jiang, E. Garfunkel, Z. Bao, *Langmuir* **2004**, *20*, 1539.

(3) C. Tanase, E. J. Meijer, P. W. M. Blom, D. M. de Leeuw, Phys. Rev. Lett. **2003**, *91*, 216601.

(4) T. van Woudenbergh, P. W. M. Blom, J. Huiberts, *Appl. Phys. Lett.* **2003**, *82*, 985.

(5) A. B. Chwang, C. D. Frisbie, *J. Phys. Chem. B* **2000**, *104*, 12202.

(6) L. Bürgi, T. J. Richards, R. H. Friend, H. Sirringhaus, *J. Appl. Phys*. **2003**, *94*, 6129.

(7) N. Koch, S. Duhm, J. P. Rabe, S. Rentenberger, R. L. Johnson, J. Klankermayer, F. Schreiber, *Appl. Phys. Lett.* **2005**, *87*, 101905.

(8) I. H. Campbell, S. Robin, T. A. Zawodzinski, J. D. Kress, R. L. Martin, D. L. Smith, N. N. Barashkov, J. P. Ferraris, *Phys. Rev. B* **1996**, *54*, 14321.

(9) L. Zuppiroli, L. Si-Ahmed, K. Kamaras, F. Nüesch, M. N. Bussac, D. Ades, A. Siove, E. Moons, M. Grätzel, *Eur. Phys. J.* **1999**, *11*, 505.

(10) J. C. Love, L. A. Estroff, J. K. Kriebel, R. G. Nuzzo, G. M. Whitesides, *Chem. Rev.* **2005**, *105*, 1103.

(11) R. W. Zehner, B. F. Parsons, R. P. Hsung, L. R. Sita, *Langmuir* **1999**, *15*, 1121.

(12) B. de Boer, A. Hadipour, M. M. Mandoc, T. van Woudenbergh, P. W. M. Blom, *Adv. Mater.* **2005**, *17*, 621.

(13) B. H. Hamadani, D. A. Corley, J. W. Ciszek, J. M. Tour, D. Natelson, *Nano Lett.* **2006**, *6*, 1303.

(14) H. Sirringhaus, N. Tessler, R. H. Friend, *Science* **1998**, *280*, 1741.

(15) D. J. Gundlach, L. Jia, T. N. Jackson, *IEEE Electr. Device L.* **2001**, *22, 571.*

(16) W. S. Hu, Y. T. Tao, Y. J. Hsu, D. H. Wei, Y. S. Wu, *Langmuir* **2005**, *25*, 2250.

(17) A. Kanjilal, L. Ottaviano, V. Di Castro, M. Beccari, M. Grazia, C. Mariani, *J. Phys. Chem. C* **2007**, *111*, 286.

(18) D. Kafer, L. Ruppel, G. Witte, *Phys. Rev. B* **2007**, *75*, 085309.

(19) Y. Ge, J. Whitten, *J. Phys. Chem. C* **2008**, *112*, 1174.

(20) M. Chiodi, L. Gavioli, M. Beccari, V. Di Castro, A. Cossaro, L. Floreano, A. Morgante, A. Kanjlal, C. Mariani, M. G. Betti, *Phys. Rev. B* **2008**, *77*, 115321.

(21) a) A. B. Chwang, C. D. Frisbie, *J. Phys. Chem. B* **2000**, *104*, 12202; b) D. J. Gundlach, L. Jia, T. N. Jackson, *IEEE Electr. Device Lett.* **2001**, *22*, 571; c) S. H. Kim, J. H. Lee, S. C. Lim, Y. S. Yang, T. Zyung, *Jpn. J. Appl. Phys.* **2004**, *43*, L60; d) N. Yoneya, M. Noda, N. Hirai, K. Nomoto, M. Wada, J. Kasahara, *Appl. Phys. Lett.* **2004**, *85*, 4663; e) C. Bock, D. V. Pham, U. Kunze, D. Kafer, G. Witte, Ch, Woll, *J. Appl. Phys.* **2006**, *100*, 114517; f) P. Stoliar, R. Kshirsagar, M. Massi, P. Annibale, C. Albonetti, D. M. de Leeuw, F. Biscarini, *J. Am. Chem. Soc.* **2007**, *129*, 6477; g) P. Marmont, N. Battaglini, P. Lang, G. Horowitz, J. Hwang, A. Kahn, C. Amato, P. Calas, *Org. Electron.* **2008**, *9*, 419.

(22) J. Kymissis, C. D. Dimitrakopoulos, S. Purushshothaman, *IEEE Trans. Electr. Dev.* **2001**, *48*, 1060.

(23) D. J. Gundlach, J. E. Royer, S. K. Park, S. Subramanian, O. D. Jurchescu, B. H. Hamadani, A. J. Moad, R. J. Kline, L. C. Teague, O. Kirillov, C. A. Richter, J. G. Kushmerick, L. J. Richter, S. R. Parkin, T. N. Jackson, J. E. Anthony, *Nat. Mater.* **2008**, *7*, 216.

(24) H. Sirringhaus, N. Tessler, R. H. Friend, *Science* **1998**, *280*, 1741.

(25) R. Ruiz, D. Choudhary, B. Nickel, T. Toccoli, K.-C. Chang, A. C. Mayer, P. Clancy, J. M. Blakely, R. L. Headrick, S. Iannotta, G. G. Malliaras, *Chem. Mater.* **2004**, *16*, 4497.

(26) A. Kahn, N. Koch, W. Gao, *Polym. Sci, Part B: Polym. Phys.* **2003**, *41*, 2529.

(27) A. Kanjilal, L. Ottaviano, V. Di Castro, M. Beccari, M. Grazia, C. Mariani, J. *Phys. Chem. C* **2007**, *111*, 286.

(28) D. Kafer, L. Ruppel, G. Witte, *Phys. Rev. B* **2007**, *75*, 085309.

(29) Y. Wu, T. Toccoli, N. Koch, E. Iacob, A. Pallaoro, P. Rudolf, S. Iannotta, *Phys. Rev. Lett. 2007, 98,* 076601.

(30) J. Noh and M. Hara, *Langmuir*, **2002**, *18*, 1953.

(31) (a) Y. Qian, G. Yang, J. Yu, T. A. Jung, G. Liu, *Langmuir*, **2003**, *19*, 6056; (b) P. Fenter, P. Eisenberg, K. S. Liang, *Phys. Rev. Lett.,* **1993**, *70*, 2447.

(32) The FET substrates with patterned gold electrodes were provided by Philips Research Laboratories Eindhoven.

(33) G. Ashkenasy, D. Cahen, R. Cohen, A. Shanzer, A. Vilan, *Acc. Chem. Res.* **2002**, *35*, 121.

(34) E. J. Meijer, C. Tanase, P. W. M. Blom, E. van Veenendaal, B.-H. Huisman, D. M. de Leeuw, T. M. Klapwijk, *Appl. Phys. Lett*. **2002**, *80*, 3838.

(35) (a) C. Tanase, E. J. Meijer, P. W. M. Blom, D. M. de Leeuw, *Org. Electron.* **2003**, *4*, 33; (b) C. Tanase, P. W. M. Blom, D. M. de Leeuw,E. J. Meijer, *Phys. Status Solidi A*, **2004**, *201*, 1236.

(36) N. Koch, *ChemPhysChem* **2007**, *8*, 1438.

(37) E. J. Meijer, G. H. Gelink, E. van Veenendaal, B.-H. Huisman, D. M. de Leeuw, T. M. Klapwijk, *Appl. Phys. Lett.*, **2003**, *82*, 4576.

(38) Z. Bao, A. Dodabalapur, A. J. Lovinger, *Appl. Phys. Lett*., **1996**, *69*, 6951.

(39) H. Sirringhaus, P. J. Brown, R. H. Friend, M. M. Nielsen, K. Bechgaard, B. M. W. Langeveld-Voss, A. J. H. Spiering, R. A. J. Janssen, E. W. Meijer, P. Herwig, D. M. de Leeuw, *Nature*, **1999**, *401*, 685.

(40) K. Hong, J. W. Lee, S. Y. Yang, K. Shin, H. Jeon, S. H. Kim, C. Yang, C. E. Park, *Org. Electr.* **2008**, *9*, 21.

(41) K. Asadi, Y. Wu, F. Gholamrezaie, P. Rudolf, P. W. M. Blom, *Adv. Mater.* **2009**, *21*, 4109.

Chapter 3

Controlling charge injection by self-assembled monolayers in bottom-gate and top-gate organic field-effect transistors

The modulation of the charge injection in organic field-effect transistors with self-assembled monolayers (SAMs) using both a bottom-gate and a top-gate geometry was investigated. The current modulation by using SAMs is more pronounced in the top-gate geometry due to the better defined upper surface of the bottom source and drain electrodes. By modifying Ag electrodes with a perfluorinated monolayer an injection barrier as high as 1.6 eV into poly(9,9-dioctylfluorene) (PFO) can be surmounted, enabling the measurement of the saturated field-effect mobility of $6\times10^{-5}\ cm^2V^{-1}s^{-1}$.

3.1 Introduction

In recent years organic materials, and especially conjugated polymers, have attracted considerable attention for application in polymeric and molecular electronic devices because of their unique mechanical and electrical properties. The solution processability provides the opportunity to produce on large area plastic substrates low-cost devices such as pixel engines in large-area active matrix displays and circuit components in radio frequency identification tags or smart cards.[1] The use of conjugated polymers in field-effect transistors (OFET)[2] and integrated circuits[3] requires a precise control of the key device parameters such as mobility, current modulation and threshold voltage. The device mobility of OFETs[4] depends, apart from sample preparation and deposition methods[1,3,5,6] on charge injection and transport.[7] The charge transport mechanism in OFETs is well-established,[8,9] whereas the physical understanding of charge injection is less developed.[10] The hole injection in organic electronic devices is affected by the energy difference between the Fermi level of the metal electrodes and the energy of Highest Occupied Molecular Orbital (HOMO) of the polymeric semiconductor.[11,12] Lowering this energy difference will improve the charge injection.[13–15] The injection barrier for a given polymer can be controllably tuned by changing the work function of the electrode through the use of self-assembled monolayers (SAMs). Alkanethiols are well-known to self-assemble into dense and uniform monolayers on metals like Au, Ag, Cu, Hg, and Pd. The macroscopic electric dipole moment of the ordered monolayer leads to a charge redistribution of the metal surface. The work function of the metal/SAM system is therefore substantially different than that of the bare metal.[16–18] SAMs have been used to modify the work function of source and drain electrodes, especially in FETs based on polycrystalline semiconductors like pentacene.[19–24] However, in that case the reported changes in current modulation can, next to modulation of the injection barrier, also be due to a different morphology of the deposited semiconductor at the contact. To unambiguously correlate a change in current modulation to a change in injection barrier due to application of a SAM, amorphous semiconductors were applied. Beside injection barriers also the geometry of the OFET can have a large effect on the device mobility.[25]

Three common geometries have been reported: the bottom contact/bottom-gate (BC/BG), bottom contact/top-gate (BC/TG) and top contact/bottom-gate (TC/BG) configuration, as shown in Fig. 3.1.[4] The top contact/bottom-gate (TC/BG) is similar to an inverted bottom contact/top-gate (BC/TG) and therefore disregarded. The difference between the bottom gate and top gate configuration is the position of the source and drain electrode with respect to both the gate electrode and the transport channel. In the bottom gate configuration, charges are directly injected from the electrode into the transport channel at the semiconductor/gate dielectric interface. In the top gate configuration the source and drain electrode are separated from the transport channel by a bulk semiconductor layer. The charges are then injected not only from the edge of the electrodes but also from those parts of the electrode that

overlap with the gate: the upper surface area of the electrodes.[26–29] The question is now whether a modification of the workfunction of the source and drain electrode by SAMs is equally effective in the different configurations. Here, the effect of modifying the injecting bottom contacts using SAMs in the bottom-gate and top-gate geometry is reported.

3.2   Fabrication of bottom gate and top gate OFETs

Organic field-effect transistors were made using heavily doped silicon wafers as bottom-gate electrode, with a 250 nm thick layer of thermally grown SiO_2 as a bottom-gate dielectric. 80 nm Ag source and drain electrodes were defined by photolithography on a 2 nm Cr adhesion layer. Two SAMs were investigated, hexadecanethiol (HDT) and 1H,1H,2H,2H-perfluorodecanethiol (PFDT). The substrates with Ag electrodes were immersed for two days into the ethanolic solution of the molecules of about $1–3 \times 10^{-3}$ M. After self-assembly, the substrates were thoroughly rinsed with ethanol, toluene, and 2-propanol, and dried with a deionized N_2 flow. Prior to the deposition of the organic semiconductor the substrate was treated with HMDS to passivate the surface. The semiconducting polymers poly(2-methoxy-5-(2_-ethylhexyloxy)-1,4-phenylene vinylene) (MEH-PPV) and poly(9,9-dioctylfluorene) (PFO) were spincoated from toluene in a glove box. The layer thickness was around 50 nm for MEH-PPV and 80 nm for PFO. For TG configuration, a 400 nm layer of poly(trifluoro-ethylene) (PTrFE) was used as a top-gate dielectric. The transistor was finished by evaporation through a shadow mask of 80 nm Ag as the top-gate. Electrical measurements were carried out in a probe station under high vacuum (10^{-6} mbar) with a Keithley 4200 Semiconductor Characterization System.

3.3   Results and discussions

The dipole moment of SAMs of alkanethiols and perfluorinatedalkanethiols exhibit a different sign.[13,16] Therefore they either increase or decrease the workfunction. The work function of Ag as measured with a Kelvin probe amounted to 4.3 eV. Application of a HDT SAM yields a workfunction of 3.8 eV and application of a PFDT SAM yields a workfunction of 5.5 eV. The values derived here are comparable to the values as measured and calculated in earlier works.[16,30]

The output characteristics of bottom-gate transistors with MEHPPV as the semiconductor (chemical structure as inset) and bare and SAM modified source and drain electrodes are presented in Fig. 3.2a. The current modulation using bare Ag electrodes is rather poor.
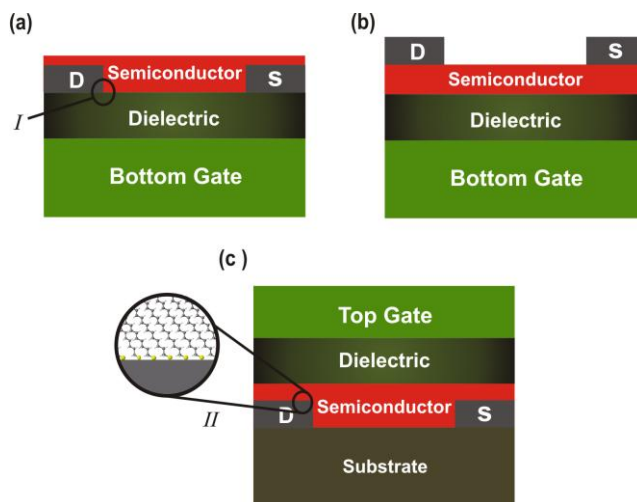
Figure 3.1. Field-effect transistors configurations:(a) bottom contact, bottom gate (BC/BG); (b) top contact, bottom gate (TC/BG); (c) bottom contact, top gate (BC/TG). The injection area at the ill-defined corner of the metal electrode in the bottom gate configuration (I) and the perpendicular injection area at the metal electrode in the top gate configuration (II) are highlighted.

The current modulation does not change using HDT modified electrodes. A small increase however is observed when using PFDT modified electrodes. The output characteristics of the corresponding top-gate transistors are presented in Fig. 3.2b. The current modulation is poor with bare Ag electrodes and even decreases using HDT treated electrodes. However, an enhanced current modulation is observed using PFDT modified electrodes. Note that the current enhancement using PFDT is larger in the top-gate configuration than in the bottom-gate configuration. The differences in current modulation correspond with the changes in injection barrier. The HOMO of MEH-PPV is situated at 5.2 eV. Hence the injection barriers are estimated as 0.9 eV for bare Ag electrodes, 1.4 eV for HDT modified electrodes and −0.3 eV for using PFDT modified electrodes. The current in the transistors with bare Ag electrodes is injection limited. The injection is worse using HDT modified electrodes and improves using PFDT modified electrodes. The current enhancement in the top-gate transistor is generally larger compared the bottom-gate configuration due to lower contact resistances.[31] Regardless of the FET configuration, both SAM layer affect the performance. PFDT increases the current in the output characteristics of the MEH-PPV OFET whereas HDT lowers the current output. However, the influence of both HDT and PFDT SAMs on charge injection in top-gate configuration is more pronounced than the bottom-gate. It can attribute these differences to the quality of the SAM. In a bottom-gate OFET, the conducting channel is directly in contact with the source and drain electrodes. The thickness of conducting channel in OFETs has been proven to be in the order of a few nanometers.[32–34] The rest of the semiconductor actually does not participate in the transport. Charge injection in OFETs

38

therefore takes places in very narrow region namely the corner of the electrode/dielectric interface as depicted with (*I*) in Fig. 3.1a. The side indicated with (*I*) of the deposited metal electrode may have an ill-defined crystal structure, and not clearly Ag(111).[35]

Highly ordered thiol SAMs however are formed on well-defined metallic surfaces such as Ag(111).[16] Due to ill-defined crystal structure at the corner of the electrode with the semiconductor/gate dielectric the monolayer is expected to be highly disordered. Subsequently the workfunction does not correspond to that measured for modified bulk electrodes *i.e.* Ag(111). The injection barrier in the corner therefore is larger than expected from the Kelvin probe measurement.[36–40] Measuring the actual value of the work function however is hampered by experimental limitations. In the top-gate geometry however the whole top surface, Ag(111) of the electrode that overlaps with the gate electrode is injecting. The Kelvin probe measurement shows that the SAM is macroscopically ordered as pointed in Fig. 3.1c.[41] Hence the injection barrier in the top-gate configuration is effectively lowered and the current is enhanced.
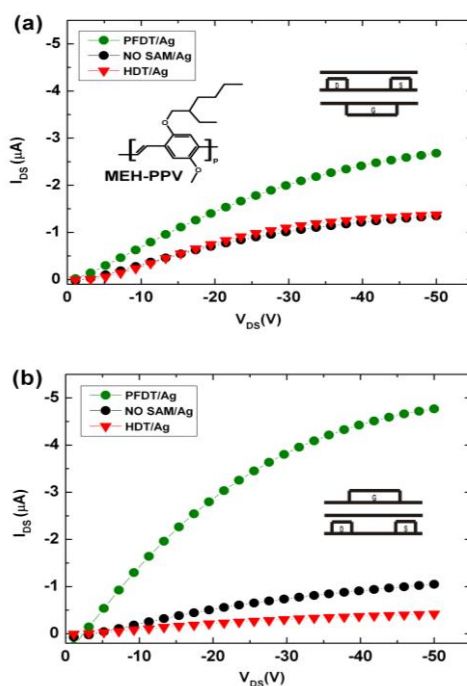
Figure 3.2. Output characteristics of a MEH-PPV bottom-gate field-effect transistor (a) and of a top-gate field-effect transistor (b). Black circles represent bare Ag source and drain electrodes; red triangles HDT modified Ag electrodes and green circles PFDT modified Ag electrodes. The channel widths and channel lengths are 20 mm and 20 µm. The gate bias is −50 V. The inset shows the chemical structure of MEH-PPV.

   In order to estimate the injection barrier that can be surmounted by a SAM, a semiconducting polymer with a deeper lying HOMO, *viz*. PFO, the chemical structure of which is shown as inset in Fig. 3.3a, was used. The HOMO of PFO is located at 5.9 eV leading to an injection barrier with bare Ag of 1.6 eV. The output characteristics of bottom gate transistors using both bare and SAM modified source and drain electrodes are presented in Fig. 3.3a. As inset, the current modulation by applying SAMs is shown on a semi-logarithmic scale. When using bare Ag or HDT modified electrodes, there is no current modulation. The injection is completely blocked due to the large injection barriers estimated as 1.6 eV and 2.1 eV respectively. Only when using PFDT modified electrodes charge can be injected and current modulation is observed, which agrees with the estimated small injection barrier of only 0.4 eV.
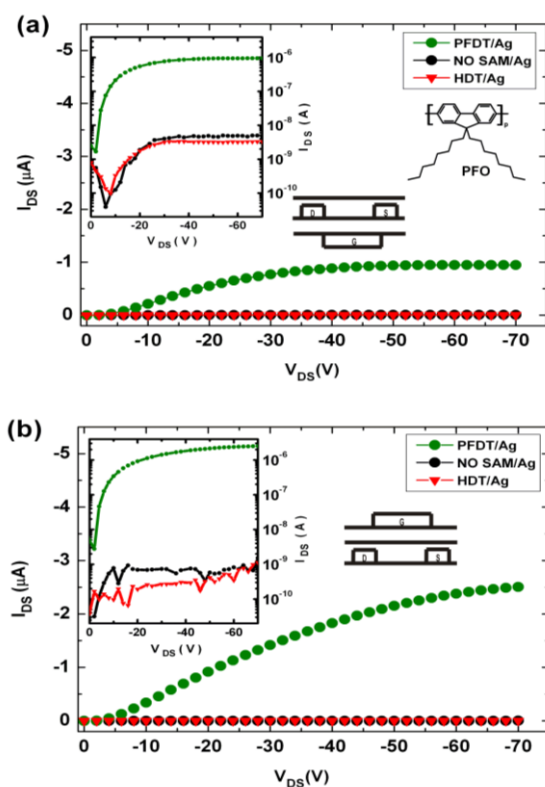
Figure 3.3. Output characteristics of a PFO bottom-gate field-effect transistor (a) and of a top-gate field-effect transistor (b) Black circles represent bare Ag source and drain electrodes; red triangles HDT modified Ag electrodes and green circles PFDT modified Ag electrodes. The insets present the current on a semi-logarithmic scale. The channel widths and channel lengths are 10 mm and 20 µm. The gate bias is −40 V. The inset shows the chemical structure of PFO.

The output curves of the corresponding PFO top-gate transistors are presented on a linear scale in Fig. 3.3b. For comparison the inset shows the output curves on a semi-logarithmic scale. Similarly as in Fig. 3.3a, when using either bare Ag or HDT modified electrodes there is no charge injection and no current modulation. With PFDT modified electrodes current modulation is observed, which indicates that the use of SAMs can surmount an injection barrier of 1.6 eV. The current in the top-gate configuration is slightly larger than that in the bottom gate configuration. The saturated device mobility is calculated as 6×10^{-5} $cm^2V^{-1}s^{-1}$. The slightly larger device mobility in the top gate configuration as compared to the bottom configuration can be due to the microscopic order in the SAM, as explained above for the MEH-PPV transistors.

3.4 Conclusion

In summary, the injection barriers in field-effect transistors can be tuned by using SAM modified source and drain electrodes. It has been demonstrated that barriers up to 1.6 eV can be surmounted. For such barriers hardly any FET characteristics is observed for bare electrodes. The modification is more effective in a top-gate configuration than in a bottom-gate configuration, which is due to a better ordering of the molecules in the SAM on top of the electrodes as compared to the side and corner of the electrode.

References

(1) C. D. Dimitrakopoulos, P. R. L. Malenfant, *Adv. Mater.* **2002**, *14,* 99.
(2) B. Crone, A. Dodabalapur, Y.-Y. Lin, R. W. Filas, Z. Bao, A. LaDuca, R. Sarpeshkar, H. E. Katz, W. Li, *Nature* **2000**, *403*, 521.
(3) H. Sirringhaus, N. Tessler, R. H. Friend, *Science* **1998**, *280*, 1741.
(4) P. V. Necliudov, M. S. Shur, D. J. Gundlach, T. N. Jackson, *J. Appl. Phys.* **2000**, *88*, 6594.
(5) D. M. DeLongchamp, S. Sambasivan, D. A. Fischer, E. K. Lin, P. Chang, A. R. Murphy, J. M. Frechet, V. Subramanian, *Adv. Mater.* **2005**, *17*, 2340.
(6) A. R. Murphy, J. M. J. Frechet, *Chem. Rev.* **2007**, *107*, 1066.
(7) L. Burgi, T. J. Richards, R. H. Friend, H. Sirringhaus, *J. Appl. Phys.* **2003**, *94*, 6129.
(8) (a) C. Tanase, E. J. Meijer, P. W. M. Blom, D. M. de Leeuw, *Phys. Rev. Lett.* **2003**, *91,* 216601; (b) M. C. J. M. Vissenberg, M. Matters, *Phys. Rev. B* **1998***, 57,* 12964; (c) W. F. Pasveer, J. Cottaar, C. Tanase, R. Coehoorn, P. A. Bobbert, P. W. M. Blom, D. M. de Leeuw, M. A. J. Michels, *Phys. Rev. Lett.* **2005**, *94*, 206601.
(9) H. Sirringhaus, *Adv. Mater.* **2005**, *17*, 2411.
(10) T. van Woudenbergh, P. W. M. Blom, M. C. J. M. Vissenberg, J. N. Huiberts, *Appl. Phys. Lett.* **2001**, *79*, 1697.
(11) G. Horowitz, P. Lang, M. Mottaghi, H. Aubin, *Adv. Funct. Mater.* **2004***, 14*, 1069.
(12) N. Koch, *Chem. Phys.* **2007**, *8*, 1438.

(13) K. Asadi, F. Gholamrezaie, E. C. P. Smits, P. W. M. Blom, B. de Boer, *J. Mater. Chem.* **2007**, *17*, 1947.

(14) (a) I. H. Campbell, J. D. Kress, R. L. Martin, D. L. Smith, N. N. Barashkov, J. P. Ferraris, *Appl. Phys. Lett.* **1997**, *71*, 3528; (b) S. Khodabakhsh, D. Poplavskyy, S. Heutz, J. Nelson, D. D. C. Bradley, H. Murata, T. S. Jones, *Adv. Funct. Mater.* **2004**, *14*, 1205.

(15) B. H. Hamadani, D. A. Corley, J. W. Ciszek, J. M. Tour, D. Natelson, *Nano Lett.* **2006**, *6*, 1303.

(16) B. de Boer, A. Hadipour, M. M. Mandoc, T. van Woudenbergh, P. W. M. Blom, *Adv. Mater.* **2005**, *17*, 621.

(17) I. H. Cambell, S. Rubin, T. A. Zawodzinski, J. D. Kress, R. L. Martin, D. L. Smith, N. N. Barashkov, J. P. Ferraris, *Phys. Rev. B* **1996**, *554,* 14321.

(18) R. W. Zehner, B. F. Parsons, R. P. Hsung, L. R. Sita, *Langmuir* **1999***, 15*, 1121.

(19) Z. Jia, V. W. Lee, I. Kymissis, L. Floreano, A. Verdini, A. Cossaro, A. Morgante, *Phys. Rev. B* **2010**, *82*, 125457.

(20) D. Boudinet, M. Benwadih, Y. Qi, S. Altazin, J. Verilhac, M. Kroger, C. Serbutoviez, R. Gwoziecki, R. Coppard, G. Le Blevennec, A. Kahn, G. Horowitz, *Org. Electron.* **2010**, *11*, 227.

(21) D. Yun, S. W. Rhee, *J. Mater. Chem.* **2010***, 20*, 9754.

(22) K. Asadi, Y. Wu, F. Gholamrezaie, P. Rudolf, P. W. M. Blom, *Adv. Mater.* **2009***, 21*, 4109.

(23) J. Hong, A. Park, S. Lee, J. Kang, N. Shin, D. Y. Yoon, *Appl. Phys. Lett.* **2008***, 92*, 143311.

(24) P. Marmont, N. Battaglini, P. Lang, G. Horowitz, J. Hwang, A. Kahn, C. Amato, P. Calas, *Org. Electron.* **2008**, *9*, 419.

(25) Y. Roichman, N. Tessler, *Appl. Phys. Lett.* **2002***, 80*, 151.

(26) I. G. Hill, *Appl. Phys. Lett*. **2005**, *87*, 163505.

(27) T. J. Richards, H. Sirringhaus, *J. Appl. Phys.* **2007**, *102*, 094510.

(28) T. van Woudenbergh, J. Wildeman, P. W. M. Blom, J. J. A. M. Bastiaansen, B. M. W. Langeveld-Voss, *Adv. Funct. Mater.* **2004**, *14*, 667.

(29) C. Chiang, S. Martin, J. Kanicki, Y. Ugai, T. Yukawa, S. Takeuchi, *Jpn. J. Appl. Phys.* **1998**, *37*, 5914.

(30) S. G. J. Mathijssen, P. A. van Hal, T. J. M. van den Biggelaar, E. C. P. Smits, B. de Boer, M. Kemerink, R. A. J. Janssen, D. M. de Leeuw, *Adv. Mater.* **2008**, *20*, 2703.

(31) K. P. Puntambekar, P. V. Pesavento, C. D. Frisbiea, *Appl. Phys. Lett.* **2003**, *83*, 5539.

(32) B. Crone, A. Dodabalapur, A. Gelperin, L. Torsi, H. E. Katz, A. J. Lovinger, Z. Bao, *Appl. Phys. Lett.* **2001**, *78*, 2229.

(33) M. Mottaghi, G. Horowitz, *Org. Electron*. **2006**, *7*, 528.

(34) M. A. Alam, A. Dodabalapur, M. R. Pinto, *IEEE Trans. Electron. Dev.* **1997**, *44*, 1332.

(35) N. A. Pangarov, *Electrochim. Acta.* **1962***, 7*, 139.

(36) E. Orgiu, N. Crivillers, J. Rotzler, M. Mayor, P. Samor, *J. Mater. Chem.* **2010***, 20*, 10798.

(37) A. Kahn, N. Koch, W. Gao, *Polym. Sci. B: Polym. Phys*. **2003**, *41*, 2529.

(38) D. M. Alloway, M. Hofmann, D. L. Smith, N. E. Gruhn, A. L. Graham, R. Colorado, V. H. Wycoski, T. R. Lee, P. A. Lee, N. R. Armstrong, *J. Phys. Chem. B.* **2003**, *107*, 11690.

(39) G. Ashkenasy, D. Cahen, R. Cohen, A. Shanzer, A. Vilan, *Acc. Chem. Res.* **2002**, *35*, 121.

(40) A. Vilan, D. Cahen, *Trend Biotechnol*. **2002**, *20*, 22.

(41) E. Ito, T. Arai, M. Hara, J. Noh, B. Korean, *Chem. Soc.* **2009**, *30*, 1309.

Chapter 4

Charge trapping by self-assembled monolayers as the origin of the threshold voltage shift in organic field-effect transistors

Crucial for organic transistors is the threshold voltage. The value has been tuned by applying self-assembled monolayers (SAMs) on the gate dielectric. The microscopic origin however is under debate. In this chapter, the semiconductor is delaminated after electrical characterization. The surface potentials of the revealed SAM perfectly agree with the threshold voltages, which demonstrate that the shift is not due to the dipolar contribution but due to charge trapping by the SAM.

4.1 Introduction

Application of organic thin film transistors (TFTs) is envisioned in pixel engines in active matrix displays and in integrated circuits for contactless RF identification transponders.[1,2,3] A key device parameter of a transistor is the threshold voltage, V_{th}. This voltage should be set at a given value and, furthermore, be identical for all devices in a circuit. Any deviation yields a reduced gain of logic gates, a decreased noise margin of integrated circuits or an inhomogeneously emitting display.[4,5] For standard Si transistors, the threshold voltage can be accurately set by the amount of doping applied by ion implantation.[6,7] In organic transistors, however, local doping of individual transistors is not an option. To get around this constraint and to externally set V_{th}, several options have been published, such as the incorporation of level shifters in integrated circuits,[8] the use of a gate metal with a specific work function[9,10] or the use of dual-gate transistors.[11] As an alternative method the application of a self-assembled monolayer (SAM) at the gate dielectric interface has been reported.[12-16] The threshold voltage can be set by varying the chemical composition of the SAM. The change in V_{th} has tentatively been explained as being due to the dipole moment of the composing molecules. Device simulations, however, have indicated that the dipolar contribution is too small.[17] Alternatively, trapped interface charges have been suggested. The mechanism is under debate; as mentioned in a recent publication direct experimental evidence to accurately explain the voltage shifts is still lacking.[16] Here organic field-effect transistors with various self-assembled monolayers on the gate dielectric were fabricated. The value of the threshold voltage varies over tens of volts, depending on the nature of the SAM. To elucidate the origin of the significant differences, the semiconductor was peeled off and the surface potential of the SAM modified gate dielectric was measured by scanning Kelvin probe microscopy (SKPM).[18,19] It was unambiguously showen that the origin of the voltage shifts is a result of charge trapping induced by the SAM. The temporal behaviour of the surface potential after removing the semiconductor is discussed.

4.2 Experimental

Transistor test devices were fabricated with heavily doped n^{++} Si monitor wafers acting as a common gate electrode with 200 nm thermally grown SiO$_2$ as gate dielectric. Au source and drain electrodes were defined using conventional photolithography. Ti was used as an adhesion layer. The test devices were treated for 10 min with UV-ozone to remove all organic compounds. Three types of organosilane molecules with ethoxy end groups were used, viz. $(CF_3)(CF_2)_7(CH_2)_2Si(OC_2H_5)_3$, $(CH_3)(CH_2)_9Si(OC_2H_5)_3$ and $(NH_2)(CH_2)_3Si(OC_2H_5)_3$. The chemical structures are presented as inset in Fig. 4.1. The SAMs were grown by vapour deposition at 120 °C for the NH$_2$-SAM and 150 °C for the CH$_3$-SAM and the F-SAM. The treated test devices were rinsed with iso-propanol to remove non-covalently bound molecules. Polytriarylamine (PTAA)

was used as a *p*-type amorphous semiconductor. The chemical structure is presented in Fig. 4.3. Thin films were spincoated from a toluene solution.

Specular X-ray reflectivity measurements were performed using a X'Pert MRD pro diffractometer in the Bragg Brentano geometry. The calculated fit to the XRR results is based on the recursive algorithm of Parratt and the roughness model of Nevot and Croce. X-ray photoelectron spectroscopy (XPS) measurements were carried out using monochromatic Al Kα-radiation in a Quantera SXM from Ulvac-PHI. Atomic Force Microscopy (AFM) measurements were conducted with a Veeco Dimension 3100 atomic force microscope equipped with a Nanoscope IV control unit. Scanning Kelvin Probe Microscopy (SKPM) measurements were performed in ambient atmosphere. The height profile was recorded in tapping mode. The potential profiles were scanned in non-contact lift mode 20 nm above the surface. Water contact angles were measured with a Contact Angle System OCA 30. The electrical transport was characterized using a HP 4155C semiconductor parameter analyzer.

4.3 Delamination of semiconductor

The microstructure of the SAMs was investigated with X-ray reflectivity, contact angle and AFM measurements. Fig. 4.1 shows the reflected X-ray intensity as a function of incidence angle. The fully drawn curves are a fit to the data. The calculated and measured values of the SAM thickness are presented in Table 4.1. The values agree with the calculated lengths of the molecules. Only in case of the NH_2-SAM the numbers deviate which could be due to formation of a double layer. The hydrophobicity of the SAMs was investigated by water contact angle measurements. The static contact angles presented in Table 4.1 corresponds to literature values.[12,20,21]

	F-SAM	CH$_3$-SAM	NH$_2$-SAM
SAM thickness [nm]	1.3	1.1	0.88
SAM thickness [nm] calculated	1.2	1.2	0.36
Water contact angle	108°	91°	67°
Water contact angle after exfoliation	105°	90°	64°

Table 4.1. Thickness of the SAMs derived from X-ray reflectivity measurements. Calculated length of the molecules. Static contact angles of the SAMs before and after exfoliation of the PTAA semiconductor.

The morphology of the SAMs was investigated with AFM. A typical topographical image is presented in the inset of Fig. 4.1. The monolayer is homogeneous without microscopic defects. Saturated transfer curves of the PTAA transistors with three different SAMs are presented in Fig. 4.2a. The charge carrier mobility is in the

order of 10^{-4}-10^{-3} cm^{2}V^{-1}s^{-1}. The major difference between the transistors is the value of the threshold voltage, here approximated by the pinch-off voltage. The offset between the pinch-off voltage and the threshold voltage can be disregarded for the discussion. The threshold voltage of transistors with a CH$_3$-SAM is around 0 V, with a NH$_2$-SAM the threshold voltage is negative and with a F-SAM the threshold voltage is positive. For the example of Fig. 4.2a, the numbers are about 0 V, -16 V and +20 V, respectively, in agreement with threshold voltages reported for corresponding pentacene transistors.[12] The change in threshold voltage can be the result of the following mechanisms: the macroscopic dipole moment of the SAM, charge trapping at the gate dielectric semiconductor interface or doping of the semiconductor. To disentangle the mechanisms, the local potential is probed with SKPM.
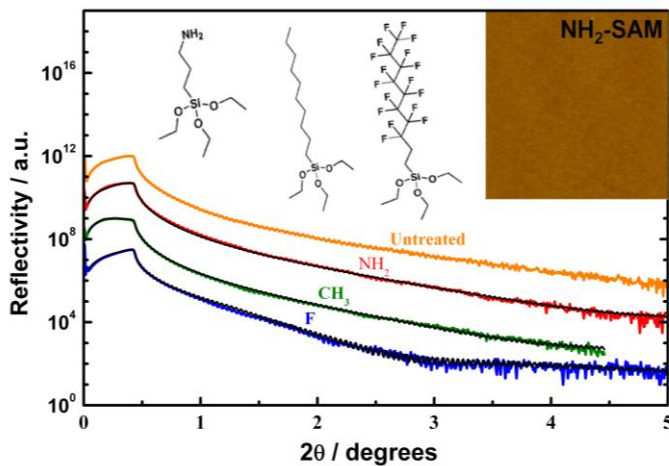
Figure 4.1. SAM characterization. X-ray reflection as a function of incident angle for the SAMs. The solid black lines are fits to the experimental data. Inset: Chemical structures of the SAM molecules (topleft). AFM topography image of 20 μm x 20 μm of NH$_2$-SAM (topright).

The bulk semiconductor however electrically shields the buried SAM, which prevents the SAM from being probed directly. Therefore the semiconductor has to be removed. With a piece of adhesive tape the PTAA semiconductor layer is completely removed as a continuous film from the gate dielectric. After peeling off the polymer, the source and drain current is zero.

The exfoliation is facilitated by the SAM which lowers the interfacial energy. The complete removal is supported by XPS measurements, a well-established technique to identify the chemical composition of the topmost surface layers. Nitrogen is a marker for the presence of the semiconductor PTAA. Fig. 4.3 presents the N1s peak with binding energy around 399 eV before and after exfoliation of the PTAA. For the F-SAM and the CH$_3$-SAM the signal has completely disappeared as checked on various spots on the

surface, indicating the complete removal of PTAA. For the NH_2-SAM, XPS is not an appropriate technique because nitrogen is present in both polymer and monolayer. Contact angle measurements confirm that the SAM itself is not affected by exfoliation. Table 4.1 shows that the static contact angles after peeling off resemble the contact angles before peeling off. A photograph of the CH_3-SAM contact angle after exfoliation is presented as inset in Fig. 4.3.

4.4   Results and discussion

The surface potential of the area between the source and drain, *i.e.* the channel region, was measured as quickly as possible after measuring the transfer curve (Fig. 4.2a) and peeling off the PTAA layer. During the SKPM measurement, all electrodes were grounded. The local surface potentials are presented in Fig. 4.2b.

The offset at the source and drain contacts is due to the capacitive coupling between the AFM cantilever and the transistor channel region. The surface potential in the channel region depends on the type of SAM. For the CH_3-SAM the surface potential is zero. In the case of the F-SAM, a negative surface potential of -18 V is observed while the NH_2-SAM shows a positive surface potential of +14 V. The surface potentials have been measured as fast as possible after peeling off because their amplitude decreases with time. As an example the temporal behaviour of the F-SAM is presented in Fig. 4.4a. The value of the maximum potential is plotted as a function of time in Fig. 4.4b. The potential decreases about exponentially with time.

The time constant depends on the relative humidity of the air. At 60 % relative humidity the decay constant is a factor of five smaller than in dry air. The temporal behaviour is not well understood. The trapped charges in the channel region get compensated which might be caused by surface conduction of absorbed water.[22]

The threshold voltage of a field-effect transistor is equal to the flat band voltage, V_{FB}, corrected for fixed oxide charges, Q_f, trapped interface charges, Q_i [23] and the dipolar contribution due to SAM, V_{SAM} :

$$V_{th} = V_{FB} + V_{SAM} - \frac{Q_f + Q_i}{C}$$

Flat band voltages are typically in the order of 0.1 V. The dipolar potential follows from the Helmholtz equation:

$$V_{SAM} = \frac{\mu_{zSAM}}{A\varepsilon_r\varepsilon_0}$$

where μ_{zSAM} is the net vertical component of the molecular dipole moment, A is the lateral area per molecule, ε_r is the relative permittivity of the molecule and ε_0 is the vacuum permittivity.[24]
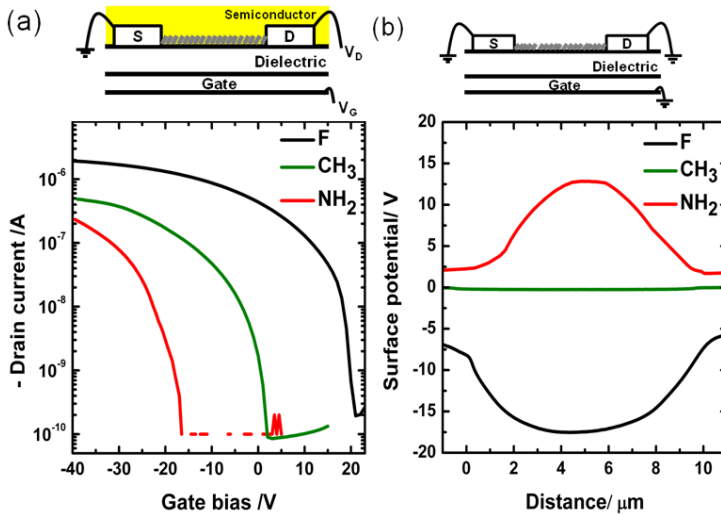
Figure 4.2. (a) Saturated transfer characteristics of field-effect transistors with the three different SAMs on the gate dielectric. The black, green and red lines correspond to the F-SAM, the CH_3-SAM and the NH_2-SAM, respectively. The channel length and width are 10 µm and 10000 µm respectively and the source and drain bias is -30 V. The transistor layout is schematically presented at the top. (b) Local surface potentials of the SAMs after peeling off the PTAA semiconductor. The black, green and red lines correspond to the F-SAM, the CH_3-SAM and the NH_2-SAM, respectively. The transistor layout after delamination is schematically presented at the top.

      The surface potentials were measured directly after applying the SAM on the gate dielectric prior to applying the PTAA semiconductor. The local potentials as a function of position in the channel region are presented in Fig. 4.5. The surface potentials are the order of about 1 V and might be due a dipolar contribution of the ordered molecules. The values of the observed threshold voltages are too big to be a result of the dipole moment of the SAM. Reported device simulations confirm the small dipolar contribution of less than 1 V for molecules with comparable dipole moments.[17] All SAMs bind in the same manner to the SiO_2 surface. The transfer curve of the CH_3-SAM exhibits a threshold voltage around 0 V. Therefore, it is extremely unlikely that the observed variations in threshold voltage are due to fixed oxide charges. Hence the changes in threshold voltage of the NH_2-SAM and F-SAM are due to trapped interface charges. This assignment is confirmed by the SKPM measurements. The contributions to the surface potential of the dipole moment of the molecules, the flat band voltage and the fixed charges can be neglected with respect to the contribution of the interface charges. Therefore the surface potential when using grounded electrodes is given by, $V_{SKPM} \approx Q_i/C$ *i.e.* it is largely dominated by trapped interface charges.
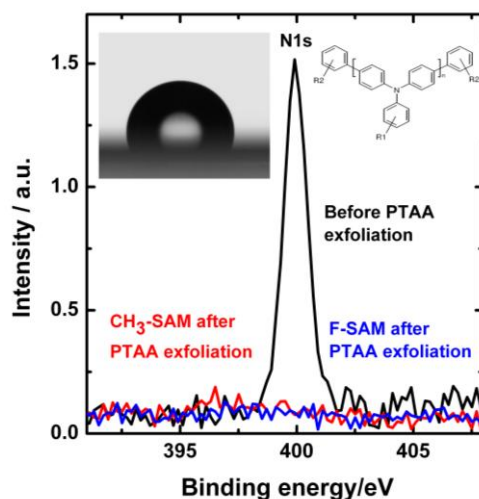
Figure 4.3. X-ray photoelectron spectra before and after peeling off the PTAA semiconductor. The black line shows the PTAA N1s peak before peeling off. The red line and blue line are measured after peeling off the PTAA semiconductor from the CH$_3$-SAM and the F-SAM. The insets show the chemical structure of the PTAA semiconductor and a picture of a water droplet on the CH$_3$-SAM after exfoliation.

In dry air the maximum surface potential of the stripped device extrapolated back to time zero perfectly matches with the corresponding threshold voltages (Fig. 4.4b). In humid air the changes are too fast to reliably estimate the extrapolated starting potential. The agreement between extrapolated potential and threshold voltage unambiguously shows that the threshold voltage shift originates from trapped charges by the SAM. The CH$_3$-SAM is inactive while the NH$_2$-SAM traps positive charges and the F-SAM traps negative charges. The presence of the negative charges could be due to surface conduction of the SiO$_2$[22] but it is not completely clear yet. Note that it is well-known that exfoliation of two insulating materials can yield static charges by contact electrification or tribo-charging. A review on space-charge electrets that exhibit a net macroscopic electrostatic charge is presented in ref 25.

The classical example is charging of adhesive tape by unrolling. Peeling off ordinary sticky tape in vacuum can even yield individual X-ray pulses, typically a few nanoseconds long, of up to 15 kV.[26] However, the potentials measured here are not generated by the peeling process.

Firstly, the one to one correspondence between the threshold voltage shifts due to application of SAMs on the gate dielectric, with the surface potentials as measured by SKPM would be a rare coincidence. The measured surface potentials are highly reproducible. That is not expected when the charges are generated by peeling off. Then a large spread in the amount of static charges is expected.
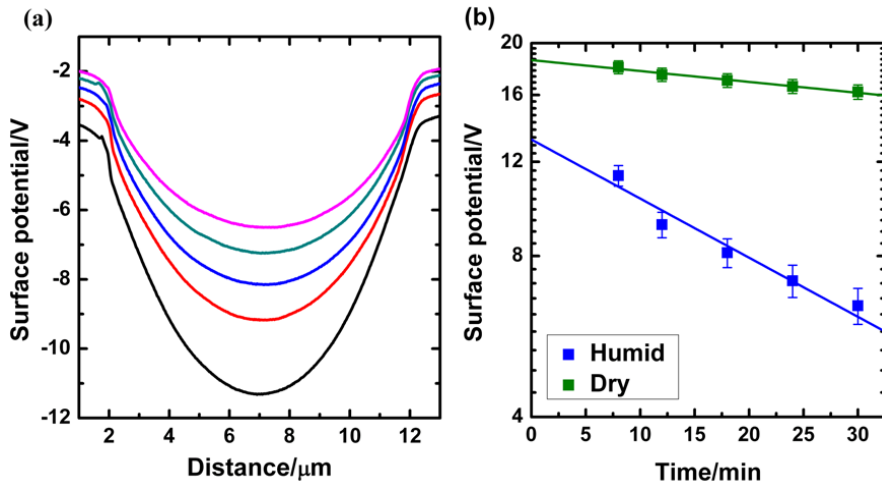
51

Figure 4.4. Temporal behavior of potential. (a) Surface potential profiles measured with SKPM on the F-SAM after peeling off the PTAA semiconductor. The potentials decrease with time. The time interval between the measurements amounted to 6 min. The relative humidity was 60%. (b) Maximum local surface potentials as a function of time. The green and blue points were measured in a relative humidity of 30% and 60%. The solid lines are an exponential fit to the data**.**

Secondly, in separate series of experiments, the surface potentials were measured with KPM before and after peeling off adhesive tape from a variety of substrates. Unrolling tape itself yields potentials higher than experimentally could be measured. Peeling off tape from a bare metal substrate does not lead to any static charges, as expected. Repetitive experiments on bare back-gated SiO_2 transistor substrates showed potential differences before and after exfoliation of at most 0.5 V. The measurements agree with literature data. Surface potentials of only 0.95 V were measured during peeling off Alq_3 with adhesive tape.[27]

Thirdly, the exact same exfoliation procedure has been used previously to locate trapped charges in PTAA field-effect transistors generated upon prolonged application of the gate bias.[19] After stressing the threshold voltage was measured. Subsequently the semiconductor was peeled off with adhesive tape and the surface potential of the revealed interface was measured using SKPM. A one to one correlation of the threshold voltage shift with the measured surface potential was found, ruling out that the static charges are generated in the peeling process.

Finally, depending on the nature of the SAM the transistor is either normally-on or normally-off, meaning that at 0 V bias the semiconductor is either conducting or insulating. In a normally-on transistor exfoliation cannot generate stable static charges and, therefore, the experimental procedure cannot be the cause of the negative threshold voltage shift. In short, generation of static charges

by the exfoliation process can be disregarded. The measured threshold voltage shifts are due to charges trapped by the SAM.
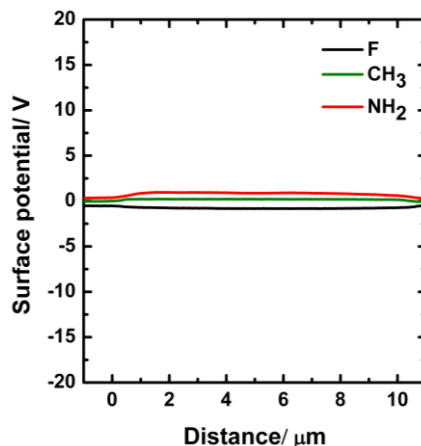
Figure 4.5. Local surface potentials as a function of position in the channel region after applying SAMs on the gate dielectric but prior to depositing the PTAA semiconductor. The black, green and red lines correspond to the F-SAM, the CH_3-SAM and the NH_2-SAM, respectively.

4.5 Conclusion

In summary, organic field-effect transistors with different self-assembled monolayers on the gate dielectric were fabricated. The threshold voltage depends on the type of SAM. In agreement with literature data, the threshold voltage of CH_3-SAM is about 0 V, while that for F-SAM and NH_2-SAM are at 20 V and -16 V, respectively. To elucidate the origin of the large differences, the semiconductor was peeled off after electrical characterization and the surface potential of the SAM modified gate dielectric was measured by SKPM. The surface potentials agree with the corresponding threshold voltage, which unambiguously shows that the surface potential shift is due to the charge trapping by the SAM.

References

(1) G. H. Gelinck, H. E. A. Huitema, E. Van Veenendaal, E. Cantatore, L. Schrijnemakers, J. B. P. H. Van der Putten, T. C. T. Geuns, M. Beenhakkers, J. B. Giesbers, B. H. Huisman, E. J. Meijer, E. M. Benito, F. J. Touwslager, A. W. Marsman, B. J. E. Van Rens, D. M. de Leeuw, *Nat. Mater.* **2004***, 3,* 106*.*

(2) E. Cantatore, T. C. T. Geuns, G. H. Gelinck, E. van Veenendaal, A. F. A. Gruijthuijsen, L. Schrijnemakers, S. Drews, D. M. de Leeuw, *IEEE J. Solid-St. Circ.* **2007**, *42*, 84.

(3) K. Myny, S. Steudel, P. Vicca, M. J. Beenhakkers, N. van Aerle, G. H. Gelinck, J. Genoe, W. Dehaene, P. Heremans, *Solid-St. Elect.* **2009**, *53,* 1220.

(4) S. de Vusser, J. Genoe, P. Heremans, *IEEE Trans. Elect. Dev.* **2006**, *53,* 601.

(5) J. R. Hauser, *IEEE Trans. Educ.* **1993**, *36*, 363.

(6) M. R. MacPherson, *Appl. Phys. Lett.* **1971**, *18,* 502.

(7) T. Mizuno, J. Okamura, A. Toriumi, *IEEE Trans. Elect. Dev.* **1994**, *41,* 2216.

(8) E. Cantatore, T. C. T. Geuns, G. H. Gelinck, E. van Veenendaal, A. F. A. Gruijthuijsen, L. Schrijnemakers, S. Drews, D. M. de Leeuw, *IEEE J. Solid-St. Circ.* **2007**, *42*, 84.

(9) I. Nausieda, K. K. Ryu, D. Da He, A. I. Akinwande, V. Bulovic, C. G. Sodini, IEEE. *Trans. Elect. Dev.* **2010***, 57, 1003.*

(10) H. W. Zan, W. T. Chen, C. C. Yeh, H. W. Hsueh, C. C. Tsai, H.F. Meng, *Appl. Phys. Lett.* **2011**, *98,* 153506.

(11) M. Spijkman, E. C. P. Smits, P. W. M. Blom, D. M. de Leeuw, Y. B. S. Côme, S. Setayesh, E. Cantatore, *Appl. Phys. Lett.* **2008**, *92,* 143304.

(12) S. Kobayashi, T. Nishikawa, T. Takenobu, S. Mori, T. Shimoda, T. Mitani, H. Shimotani, N. Yoshimoto, S. Ogaw, Y. Iwasa, *Nature Mater.* **2004**, *3,* 317.

(13) K. P. Pernstich, S. Haas, D. Oberhoff, C. Goldmann, D. J. Gundlach, B. Batlogg, A. N. Rashid, G. Schitter, *J. Appl. Phys.* **2004**, *96,* 6431.

(14) Y. Jang, J. H. Cho, D. H. Kim, Y. D. Park, M. Hwang, K. Cho, *Appl. Phys. Lett.* **2007**, *90,* 132104.

(15) J. Takeya, T. Nishikawa, T. Takenobu, S. Kobayashi, Y. Iwasa, T. Minani, C. Goldmann, C. Krellner, B. Batlogg, *Appl. Phys.Lett*. **2004**, *85,* 5078.

(16) Y. Chung, E. Verploegen, A. Vailionis, Y. Sun, Y. Nishi, B. Murmann, Z. Bao, *Nano Lett.* **2011**, *11,* 1161.

(17) S. K. Possanner, K. Zojer, P. Pacher, E. Zojer, F. Schürrer, *Adv. Funct. Mater*. **2009**, *19,* 958.

(18) V. Palermo, M. Palma, P. Samori, *Adv. Mater.* **2006**, *18,* 145.

(19) S. G. J. Mathijssen, M. J. Spijkman, A. M. Andringa , P. A. van Hal , I. McCulloch , M. Kemerink , R. A. J. Janssen , D. M. de Leeuw, *Adv. Mater.* **2010**, *22,* 5105.

(20) H. Sugimura, K. Ushiyama, A. Hozumi, O. Takai*, Langmuir* **2000***,16,* 885.

(21) A. Hozumi, Y. Yokogawa, T. Kameyama, H. Sugimura, K. Hayashi, H. Shirayama, O. Takai *J. Vac. Sci. Technol. A* **2001**, *19,* 1812.

(22) S. G. J. Mathijssen, M. Kemerink, A. Sharma, M. Cölle, P. A. Bobbert, R. A. J. Janssen, D. M. de Leeuw, *Adv. Mater.* **2008**, *20,* 975.

(23) S. M. Sze, *Physiscs of Semiconductor Devices*, *Wiley-Interscience, New York* **1981.**

(24) D. J. Ellison, B. Lee, V. Podzorvo, C. D. Frisbie, *Adv. Mater.* **2011**, *23,* 502.

(25) L. S. McCarty, G. M. Whitesides, *Angew. Chem. Int. Ed.* **2008**, 47, *2188.*

(26) C. G. Camara, J. V. Escobar, J. R., Hird, S. J. Putterman, *Nature* **2008**, *455*, 1089*.*

(27) Y. Okabayashi, E. Ito, T. Isoshima, H. Ito, M. Haraet, *Thin Solid Films*, **2009**, *512*, 839.

Chapter 5
Solution-processabale septithiophene monolayer transistors

Liquid crystalline septithiophene FETs is obtained by spin coating. The bulkiness of the end groups enhances the solubility and allows for solution processing. By controlling the concentration, monolayer FETs have been fabricated. In this chapter the electrical characterization and the spectroscopic properties of the monolayer are studied.

5.1 Introduction

Current efforts towards conjugated organic materials and (opto)electronic devices thereof, strive for the development of efficient photovoltaic cells, bright/multicolour organic light-emitting diodes (OLED), or organic light emitting transistors (OLETs), which combine in a single device the electrical switching functionality of a field-effect transistor and the capacity of light generation.[1] In all of these applications, the efficiency of charge transport within the organic layers plays a key role. In an organic thin film field effect transistor (OFET), transport of carriers in the channel between the source and drain electrodes occurs in the first layers of the semiconductor, close to the dielectric layer adjacent to the gate electrode.[2,3] Thus, the transport property in such a device is very sensitive to molecular packing to the same extent as the interfacial interactions between the three electrode terminals. Down scaling the semiconducting film to a monolayer reduces the electrical transport to two dimensions. Therefore, any structural imperfection or deficient electrical contacts lead to potential barriers and, hence, to a deteriorated charge carrier mobility.[4] Often, the mobility in monolayer transistors is orders of magnitude lower than in the corresponding multilayer film.[5,6] The major problems of polycrystalline films, as obtained usually, is the existence of structural defects and grain boundaries, which act as traps for the charge carriers and therefore considerably reduce mobilities.[5-7] Liquid crystalline (LC) π-conjugated molecules may improve these restrictions.[8,9] Their capability to self-heal structural defects and form large structurally homogeneous domains is well documented.

Oligothiophenes are a promising class of organic semiconductors, and their derivatives have been employed as active layers in OFETs. Significant research efforts have been devoted to the exploitation of oligothiophene derivatives but only a few examples of oligomers with more than six thiophene rings without solubilizing substituents in the β-position have been reported,[10-12] in particular because of their extremely low solubility. Examples of LC phases are described in the literature, wherein flexible peripheral substituents are combined with a rigid thiophene core.[11-13] In this chapter, the crystal structure of α,ω-substituted septithiophenes is reported and it is demonstrated that this material is an excellent candidate for the realization of monolayer OFETs. The presence of several high temperature transitions between the crystalline and LC phases of 2-octyldodecyl-disubstituted septithiophene (7T) is revealed. The high solubility of these substituted septithiophenes was used for accurate control of the surface coverage by a simple spin coating process. The structure of the monolayer was assessed with atomic force microscopy (AFM) and X-ray reflectivity measurements. The process enabled fabrication of monolayer OFETs which exhibit mobilities comparable to or even better than OFETs with vacuum deposited multilayer films. In addition, the orientation and packing of 7T within the (sub) monolayer was probed with time-resolved fluorescence spectroscopy. The 2D packing of the molecules in the monolayer differs from the 3D crystal structure.

5.2   Experimental

5.2.1   Design and synthesis of oligothiophene

The introduction of branched alkyl side chains in the α- and ω-positions and the use of a soluble precursor opened synthetic access to long oligothiophenes by the combination of ring-closure and metal catalyzed coupling reactions described in ref 12b. The 2-octyldodecyl end groups provide good solubility of 7T (see Fig. 5.1) and have a strong impact on the packing properties of the molecules in bulk and thin film as will be described below.

5.2.2   Film preparation and microscopy

Molecules were dissolved in dry toluene. The mixture was stirred under room temperature overnight, a transparent yellow solution was obtained, and it was filtered through a 0.2 μm PTFE filter. Spin-coated monolayers of 7T molecules were prepared on heavily doped silicon wafers acting as the common bottom gate covered with a 200 nm layer of thermally grown SiO_2. The gold source and drain contacts were defined by conventional photolithography. Ti (10 nm) was used as an adhesion layer. Normally HMDS was applied to passivate the SiO_2 gate dielectric. However, the presence of HMDS led to crystallization of the 7T molecules. Therefore, prior to spin-coating the monolayer, any HMDS and all organic contaminants were removed by 10 min UV-Ozone treatment. The monolayer could be applied by spin-coating 7T molecules from a dry toluene solution of 1 mg/ml at 2000 rpm for 30s with an acceleration of 600 rpm s^{-1}. The surface coverage was controlled by concentration. The morphology of the 7T thin films was investigated by AFM (NanoScope V, Digital Instruments Veeco Instruments) under ambient conditions. AFM experiments have shown that the morphology of the monolayer on the patterned SiO_2 is similar to that on bare silicon.

5.2.3   Differential Scanning Calorimetry (DSC)

DSC measurements were performed on a Netzsch DSC 404 instrument under the protection of a N_2 flow. About 1 mg of 7T was sealed in an Al pan, heated to 200 °C and kept at that temperature for 2 min to erase the thermal history, and then cooled to −70 °C at a rate of 10 °C min^{-1}. Afterwards the sample was heated to 200 °C at a rate of 10 °C min^{-1} again to determine the melting behavior of the compound.

5.2.4   X-ray reflectivity (XRR)

XRR measurements were performed at the W1 beamline at the synchrotron radiation source HASYLAB (Hamburg, Germany) using a wavelength of λ = 0.118 nm. The

samples were measured under a helium atmosphere to avoid radiation damage. The XRR data was fitted with the software package GenX.[15]

5.2.5 Electrical and optical characterization

The electrical transport was measured using a HP 4155C semiconductor parameter analyzer in a vacuum of 10^{-6} mbar. Fluorescence spectra were recorded using a continuous wave spectrophotometer (Edinburg Instruments F900). Measurements at room temperature were performed in inert atmosphere (N_2), low temperature spectra were taken using a cryostat. Spectra were corrected for the wavelength dependence of the sensitivity of the detection channel. Fluorescence lifetimes were obtained through single photon counting.

5.3 Results and discussion

5.3.1 Analysis of 7T molecules

Strong π–π interactions and separation between the rigid conjugated backbone and the long flexible chains in the periphery result in the presence of a LC phase. This was corroborated by measuring the specific heat (DSC).[12a] Indeed, the DSC thermogram of septithiophene depicted in Fig. 5.1 shows three reversible transitions: a low temperature thermal event at 65 °C ($\Delta H = 9$ J g^{-1}) followed by two consecutive transitions, one at 166 °C ($\Delta H = 39$ J g^{-1}) and a clearing transition at 171 °C ($\Delta H = 9.4$ J g^{-1}). The enthalpy of transition gives a hint to the existence of a LC phase prior to the isotropic phase. The temperature dependent by X-ray diffraction (XRD) pattern was also investigated in ref 13. In summary, the first thermal event at 65 °C corresponds to a crystal–crystal transition. Between 166 and 171 °C, the compound is in the LC state. Moreover the thiophene core is tilted by 15° with respect to the layer plane. The presence of the bulky alkyl chains makes packing of the thiophene cores less dense than in compounds with linear alkyl chains.

5.3.2 Film characterization

Because of the bulky alkyl substituents, the solubility of the septithiophene is relatively high compared to the unsubstituted one, with a saturation concentration of 3 g L^{-1} in toluene. This concentration is largely sufficient to cast several nanometer thick films. Characterized by AFM, the film's morphology is very homogeneous even on a large scale. In addition, the molecules form a layered structure with a 34 Å step height. This value is similar to bulk material as inferred from XRD pattern in ref 13. And in a thick film, the material organizes in layers with the molecules close to the substrate normal according to XRD studies in ref 13. To form a physisorbed monolayer it is essential to accurately control the surface coverage.
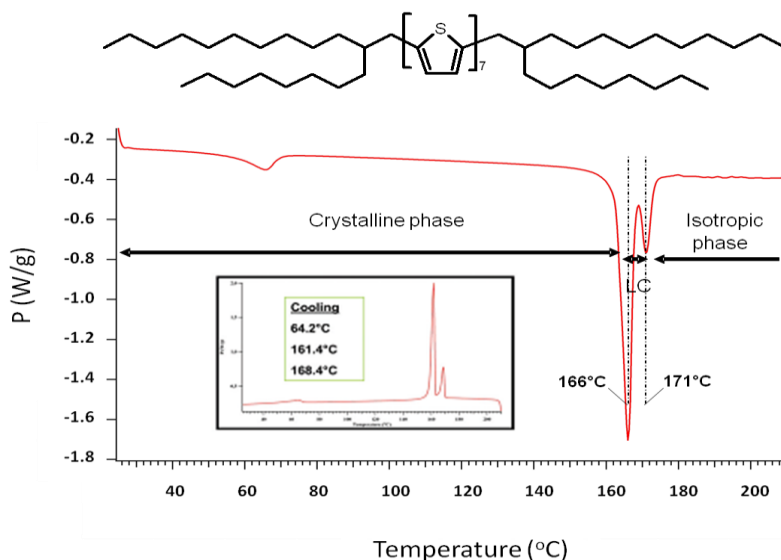
Figure 5.1. Molecular structure of 7T and DSC trace recorded during heating of 7T; the inset shows the corresponding cooling curve and the thermal transition temperatures.

The low nucleation density with pronounced growth rate is a prerequisite to reduce the density of the grain boundaries and to obtain large 2D single crystals. Often non-substituted oligothiophenes exhibit a marked tendency to form 3D layered islands before the monolayer is completed. Only in rare cases is the formation of islands without a closed monolayer observed; in most cases the monolayer is formed followed by the formation of islands. Here, it is demonstrated that septithiophene behaves remarkably different. Essentially, the surface density of monolayer islands increase linearly with the solution concentration (Fig. 5.2), while the growth is sensitive to the surface energy and processing conditions (*e.g.*, spinning velocity). On a SiO_2 surface, a complete monolayer was achieved from toluene containing 0.9 g L^{-1} septithiophene. The average island size was 1–2 µm. Above this concentration, the molecules have a tendency to form multilayer stacks with a well defined thickness of 34 Å. Remarkable is the rectangular symmetry of the islands which infer their crystalline nature. High resolution AFM imaging allows resolution of the inner superstructure with a 250 Å periodicity (Fig. 5.2). This shape becomes difficult to resolve once the monolayer coverage is reached, likely a result of coarsening of the domains. The superstructure may be the result of 2D organization of the molecules. Indeed, in 3D, 7T crystallizes in multilayer stacks with partial interdigitation of the alkyl chains while the thiophene cores are inclined relative to the layer plane. However, it will be shown that in a monolayer, the molecules are tilted at an angle greater than in the 3D crystal. Apparently, the surface force (the confining interface) and lack of interdigitation lead to a large tilt angle, which would weaken the π–π interactions. Thus, a balance between geometrical requirements and intermolecular interaction could be the cause of this superstructure.[15-14a]
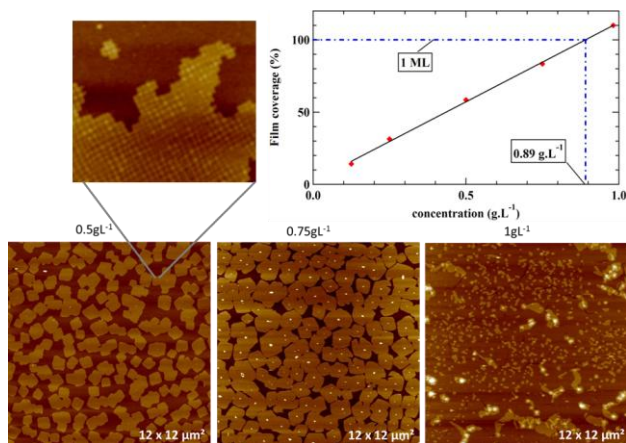
59

Figure 5.2. The diagram shows the solution concentration versus the surface coverage (top right); the film coverage was estimated from the AFM data 100% coverage is achieved at 0.89 g L^{-1} in toluene with 3000 rpm. The AFM micrographs (bottom) show the morphology of the monolayer depending on the solution concentration. In addition, in submonolayer coverage the islands are square shaped and in the upper image the internal sub-structure of the islands with a periodic length of 250 Å is resolved.

5.3.3 X-Ray reflectivity (XRR)

The molecular packing and the position of the long axes of the thiophene core relative to the dielectric surface plane are important for optoelectronic properties of the septithiophene monolayers. For this purpose the layer structure of the monolayer perpendicular to the substrate surface was investigated by XRR.

XRR experiments were executed for three films spun from solutions with concentrations of 0.5, 0.9, and 1.0 g L^{-1} and for a fourth sample, spun from a 0.9 g L^{-1} solution and subsequently solvent annealed. The XRR data were fitted to determine the structure of the monolayer.[16] A three-layer model was used to account for the different electron densities of the alkyl chains and the thiophene backbone (Fig. 5.3). The XRR fits confirm that the films are monolayers and reveal the thicknesses of the individual sublayers. The best fit was obtained for the solvent annealed 0.9 g L^{-1} sample showing that the three-layer model is the right choice. A thickness of 20.5 Å was obtained for the thiophene layer and 9.3 or 11.3 Å for the alkyl layers; the roughnesses between the layers are around 2 Å. An estimation of the tilt angles of the thiophene backbone and alkyl chains with respect to the substrate surface normal (Fig. 5.3) can be calculated from the sub-layer thicknesses and the length of the molecular building blocks. For the solvent annealed sample the long molecular axis of the 7T is tilted with an angle of approximately 40° with respect to the substrate surface.
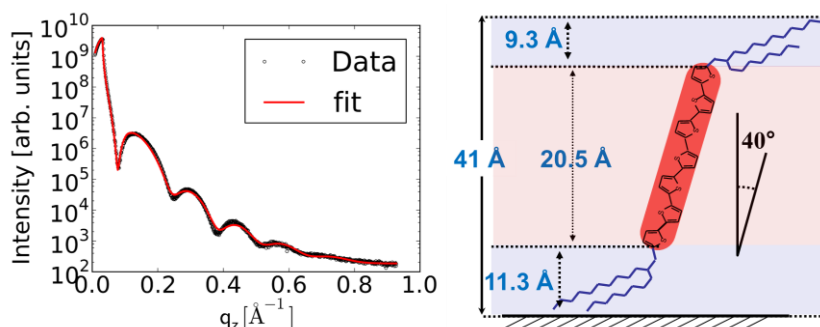
Figure 5.3. X-ray reflectivity data for monolayer. The data (symbols) are presented together with the best fit to a three-layer model (line). The scheme depicts the sub-layers structure and the results of the XRR- fit.

5.3.4 Electrical and optical characterization

The microstructure of thin films and single crystals of conjugated oligomers such as oligothiophenes, oligophenylenes, and oligophenilene-vinylenes is based on stacked layers in which the long molecular axes are parallel to each other with a herringbone configuration. The overlap between the π-orbitals favors charge transport. Here the electrical transport in monolayer field-effect transistors and the molecular packing by optical spectroscopy were investigated.
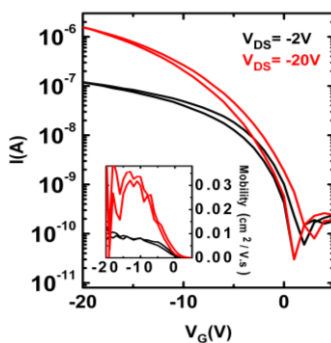
Figure 5.4. Linear and saturated transfer characteristic of a 7T spin-coated monolayer field-effect transistor. The channel length is 40 μm and channel width is 1000 μm. To prevent parasitic leakage currents, a ring geometry was used. The inset shows the linear and saturated mobility.

In general, transistors are annealed prior to the measurements at 130 °C to remove any residual water and solvent. However, the 7T molecules exhibit a transition at 65 °C, limiting the annealing temperature to 60 °C. As a result, a small hysteresis at high

source and drain bias and a relatively large parameter spread is observed. In Fig. 5.4, a typical transfer characteristic for a ring transistor with a channel length of 40 μm and a channel width of 1000 μm are presented. The transfer curve shows a current modulation of five decades. The inset shows that the linear mobility is about 1×10^{-2} cm^{2}V^{-1}s^{-1} which is an order higher than the mobility of the bulk drop-cast films (~2×10^{-3} cm^{2}V^{-1}s^{-1}). The mobility, however, is comparable to that measured in quinquethiophene (5T) self assembled monolayer field-effect transistors (SAMFETs) (2×10^{-2} cm^{2}V^{-1}s^{-1}).[7] The mobility is thermally activated. The activation energy as obtained from temperature dependent mobility measurements $\mu_{FET} = \mu_0 \exp(-E_a/kT)$ amounted to 60 to 90 meV, in good agreement with the activation energy obtained for 5T SAMFETs of 80 meV. The value of the activation energy indicates that the transport could still be trap limited by, for example, grain boundaries.

To investigate the molecular packing in the 7T monolayer fluorescence, excitation and extinction, and time-resolved fluorescence spectra were measured. The fluorescence and the fluorescence excitation of a dilute solution (10^{-5} M) of the 7T molecules dissolved in 2-MeTHF is shown in Fig. 5.5a. The spectra were measured at room temperature (solid lines) and at a low temperature of about 80 K (dashed line) in the glassy state of the solvent. The dilute solution shows a very bright fluorescence with an onset at 2.35 eV. The spectrum at room temperature shows a characteristic vibronic fine structure that becomes more pronounced at low temperature in frozen 2-MeTHF. The excitation spectrum shows an onset at 2.4 eV. At room temperature the vibronic fine structure is hardly resolved, only a broad structure remains with a maximum near 2.6 eV. Fig. 5.5a shows a pronounced vibronic fine structure at low temperature, 80 K. The difference originates from the torsional flexibility around the single bonds joining the thiophene rings. The significant thermal population of the non-planar conformation of the 7T moiety causes the loss of fine structure at room temperature.

The fluorescence, excitation, and extinction spectra of the fully covered 7T monolayer, spin-coated on a quartz substrate, are shown in Fig. 5.5b. The film obtained with 0.9 g L^{-1}, corresponding to 100% coverage, shows the onset of fluorescence at 2.2 eV with a maximum intensity at about 2.0 eV. The excitation spectrum displays an onset at 2.3 eV with a maximum intensity near 2.66 eV. The extinction spectra do not show a strong dependence on the angle of incidence. The spectra exhibit the same shape as the excitation spectrum. The transition dipole moment for the lowest energetically allowed optical transition of the 7T moiety, S$_0$–S$_1$, is oriented along the long axis of the molecule. The substantial extinction measured under a zero degree angle of incidence indicates that the thiophene core is not perpendicular to the surface but tilted. It is well-known that, in first approximation, the dipole strength of an absorption band is conserved when comparing isolated and interacting molecules.[17] An estimate of the tilt angle of molecules can be obtained by evaluating the area under the absorption curve and comparing this with the isotropically averaged dipole strength of the isolated molecules as observed in 2-MeTHF solution. For compound 7T in 2-MeTHF a dipole strength of 120 D^2 obtained and hence a transition dipole moment of 9.5 D when including a correction for the Lorentz local field in the solvent (n = 1.49) cage around the molecule.[18] For the fully covered film

the projection of the transition dipole moment in the plane of the film along the surface direction amounts to 10.85 D were found. This implies an angle between the transition dipole moment of the molecule and direction perpendicular to the surface of approximately 60°. The tilt is different to that derived from XRR measurement as discussed above. Note that the excitation spectra at low temperature are similar to those at room temperature. Small changes, however, are observed in the emission spectra. The intensity ratio of the vibronic bands slightly depends on temperature. The appearance of new peaks that may indicate temperature induced reorganization.[19]

The spectra of the isolated molecules are different from that of a fully covered monolayer. The maximum in the excitation of the film is blue-shifted with respect to that of a single molecule. Furthermore the onset of the 0–0 fluorescence is red-shifted, and the ratio of the 0–0 and 0–1 vibronic bands is larger in the film than for the single molecule. The differences indicate that the 7T molecules in the film are packed into *H*-aggregates.[20] The 0–0 transition then is partially forbidden and the fluorescence is red-shifted and dominated by the 0–1 vibronic transition. Similarly, the extinction is blue-shifted.

The *H*-aggregate packing is supported by the intensity of the fluorescence. Single molecules exhibit a bright fluorescence. The emission in thin films is optically forbidden and, therefore, the intensity of thin films is orders of magnitude lower than expected from the fluorescence quantum efficiency of single molecules. Note that the fluorescence intensity scales with coverage. Fig. 5.5c shows that the fluorescent intensity of a 0.5 g L^{-1} (50% coverage) film is almost half of that of the fully covered film. This clearly shows that the fluorescence originates from the monolayer islands and that a contribution from single molecules in between the islands to the fluorescence can be disregarded.

The fluorescence decay was measured at room temperature for isolated molecules and thin films. The fluorescence of single molecules decays exponentially with time irrespective of emission wavelength. The decay time is 1.3 ns. The decay of thin films does not depend on the coverage. The decay time is about 0.5 ns, ruling out the presence of isolated molecules in the films. The shorter decay time in the film indicates the presence of additional photophysical decay pathways, possibly involving intermolecular charge transfer interactions. The decay time does not depend on the emission wavelength. Hence the emission in the partially and fully covered films originates from the same type of *H*-aggregates.

5.4. Conclusion

In summary, it has been demonstrated that 2-octyldodecyl-disubstituted septithiophene is capable of forming crystalline and liquid crystalline phases. In 3D, 7T crystallizes in multilayer stacks with partial interdigitation of alkyl chains while the thiophene cores are inclined relative to the layer plane. However, in a monolayer, the molecules are tilted at an angle greater than in the 3D crystal. The bulkiness of the end groups enhances the solubility and allows for solution deposition and self-assembly of an electrically connected monolayer. The process resulted in monolayers with high mobility and on–off current modulation in a field-effect transistor. Moreover, spectroscopic

signatures of the monolayer could be recorded and are consistent with those expected from a closely packed layer of tilted molecules. Differences in spectroscopic properties of the monolayer and isolated molecules in solution provide evidence for delocalization of the excitation through intermolecular interactions within the layer.
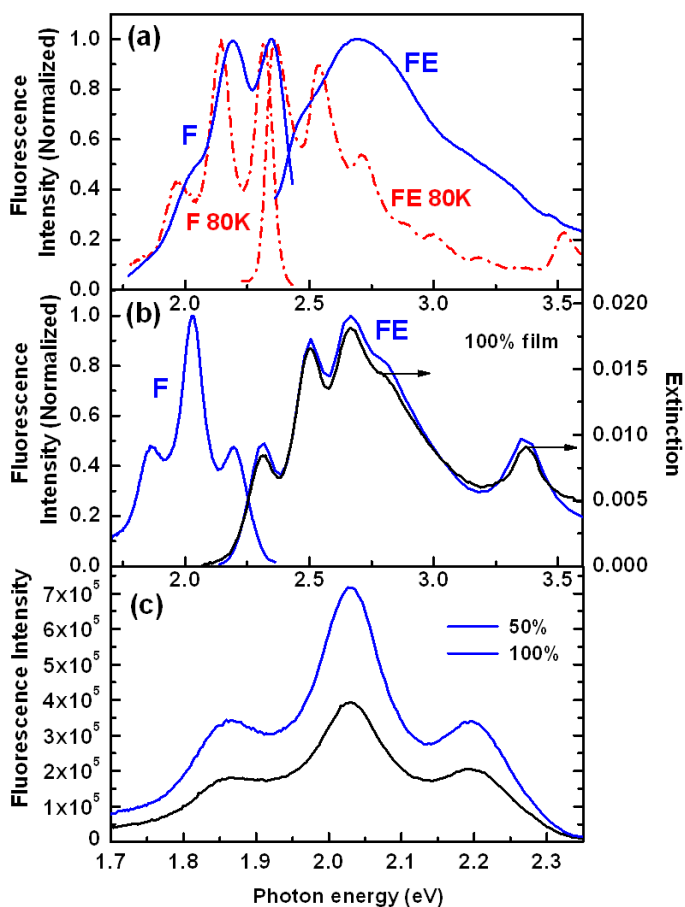
Figure 5.5. (a) Fluorescence (F) and fluorescent excitation (FE) spectra of 7T molecules in MeTHF. The blue lines represent measurements in solution at 293 K; the red dashed curves at 80K. (b) Fluorescence and excitation spectra of a fully covered (0.9 g/l = 100% film) 7T monolayer on quartz (blue solid lines). The black line shows the extinction of the 100% film measured at zero angle of incidence (c) Fluorescence intensity of partially covered, 0.5 g/l = 50% film and fully covered 100% 7T monolayers on quartz.

References

(1) a) M. Pope, C. E. Swenberg, *Electronic Processes in Organic Crystals and Polymers*, 2nd ed., Oxford University Press, New York **1999**; b) F. A. Hegmann, *Phys. Canada* **2003**, *59*, 127; c) M. E. Gershenson, V. Podzorov, A. F. Morpurgo, *Rev. Mod. Phys.* **2006**, *78*, 973; d) B. Oregan, M. Grätzel, *Nature* **1991**, *353*, 737; e) R. F. Service, *Science* **2004**, *306*, 2034; f) J. H. Burroughes, D. D. C. Bradley, A. R. Brown, R. N. Marks, K. Mackay, R. H. Friend, P. L. Burns, A. B. Holmes, *Nature* **1990**, *347*, 539; g) J. Godlewski, M. Obarowska, *Opto-Electron. Rev.* **2007**, *15*, 179; h) M. Muccini, *Nat. Mater.* **2006**, *5*, 605.

(2) G. Horowitz, R Hajlaoui, H. Bouchriha, R. Borguiga, M. Hajlaoui, *Adv. Mater.* **1998**, *10*, 923.

(3) F. Dinelli, M. Murgia, P. Levy, M. Cavallini, F. Biscarini, D. M. De Leeuw, *Phys. Rev. Lett.* **2004**, *92*, 116802.

(4) a) X. Guo, M. Myers, S. Xiao, M. Lefenfeld, R. Steiner, G. S. Tulevski, J. Tang, J. Baumert, F. Leibfarth, J. T. Yardley, M. L. Steigerwald, P. Kim, C. Nuckolls, *Proc. Natl. Acad. Sci. U.S.A.* **2006**, *103*, 11452; b) G. S. Tulevski, Q. Miao, M. Fukuto, R. Abram, B. Ocko, R. Pindak, M. L. Steigerwald, C. R. Kagan, C. Nuckolls, *J. Am. Chem. Soc.* **2004**, *126*, 15048; c) M. Mottaghi, P. Lang, F. Rodriguez, A. Rumyantseva, A. Yassar, G. Horowitz, S. Lenfant, D. Tondelier, D. Vuillaume, *Adv. Funct. Mater.* **2007**, *17*, 597.

(5) R. Ruiz, A. Papadimitratos, A. C. Mayer, G. G. Malliaras, *Adv. Mater.* **2005**, *17*, 1795.

(6) B. -N. Park, S. Seo, P. G. Evans, *J. Phys. D* **2007**, *40*, 3506.

(7) E. C. P. Smits, S. G. J. Mathijssen, P. A. van Hal, S. Setayesh, T. C. T. Geuns, K. A. H. A. Mutsaers, E. Cantatore, H. J. Wondergem, O. Werzer, R. Resel, M. Kemerink, S. Kirchmeyer, A. M. Muzafarov, S. A. Ponomarenko, B. de Boer, P. W. M. Blom, D. M. de Leeuw, *Nature* **2008**, *455*, 956.

(8) a) A. J. J. M. van Breemen, P. T. Herwig, C. H. T. Chlon, J. Sweelssen, H. F. M. Schoo, S. Setayesh, W. M. Hardeman, C. A. Martin, D. M. de Leeuw, J. J. P. Valeton, C. W. M. Bastiaansen, D. J. Broer, A. R. Popa-Merticaru, S. C. J. Meskers, *J. Am. Chem. Soc.* **2006**, *128*, 2336; b) S. A. Ponomarenko, E. A. Tatarinova, A. M. Muzafarov, S. Kirchmeyer, L. Brassat, A. Mourran, M. Moeller, S. Setayesh, D. M. de Leeuw, *Chem. Mater.* **2006**, *18*, 4101.

(9) I. McCulloch, M. Heeney, C. Bailey, K. Genevicius, L. MacDonald, M. Shkunov, D. Sparrowe, S. Tierney, R. Wagner, W. Zhang, M. L. Chabinyc, R. J. Kline, M. D. McGehee, M. F. Toney, *Nat. Mater.* **2006**, *5*, 328.

(10) a) D. J. Gundlach, *Nat. Mater.* **2007**, *6*, 173; b) F. Garnier, A. Yassar, R. Hajlaoui, G. Horowitz, F. Deloffre, B. Servet, S. Ries, P. Alnot, *J. Am. Chem. Soc.* **1993**, *115*, 8716; c) M. Berggren, D. Nilsson, N. D. Robinson, *Nat. Mater.* **2007**, *6*, 3.

(11) S. Westenhoff, A. Abrusci, W. J. Feast, O. Henze, A. F. M. Kilbinger, A. P. H. J. Schenning, C. Silva, *Adv. Mater.* **2006**, *18*, 1281.

(12) a) A. Kreyes, M. Amirkhani, I. Lieberwirth, R. Mauer, F. Laquai, K. Landfester, U. Ziener, *Chem. Mater.* **2010**, *22*, 2079; b) S. Ellinger, U. Ziener, U. Thewalt, K. Landfester, M. Moeller, *Chem. Mater.* **2007**, *19*, 1070; c) A. Kreyes, M. Amirkhani, I. Lieberwirth, R. Mauer, F. Laquai, K. Landfester, U. Ziener, *Chem. Mater.* **2010**, *22*, 6453.

(13) M. Defaux , F. Gholamrezaie, J. Wang, A. Kreyes, U. Ziener, D. V. Anokhin, D. A. Ivanov, A. Moser, A. Neuhold, I. Salzmann, R. Resel, D. M. de Leeuw, S. C. J. Meskers, M. Moeller, A. Mourran, *Adv. Mater.* **2012**, *24*, 973.

(14) a) T. Yasuda, H. Ooi, J. Morita, Y. Akama, K. Minoura, M. Funahashi, T. Shimomura, T. Kato, *Adv. Funct. Mater.* **2009**, *19*, 411; b) M. A. Hempenius, B. M. W. Langeveld-Voss, J. A. E. H. van Haare, R. A. J. Janssen, S. S. Sheiko, J. P. Spatz, M. Möller, E. W. Meijer, *J. Am. Chem. Soc.* **1998**, *120*, 2798; c) S. Ellinger, A. Kreyes, U. Ziener, C. H-Richter, K. Landfester, M. Moeller, *Eur. J. Org. Chem.* **2007**, *34*, 5686; d) O. Lengyel, W. M. Hardeman, H. J. Wondergem, D. M. de Leeuw, A. J. J. M. van Breemen, R. Resel, *Adv. Mater.* **2006**, *18*, 896; e) H. Wada, T. Taguchi, M. Goto, T. Kambayashi, T. Mori, K. Ishikawa, H. Takezoe, *Chem. Lett.* **2006**, *35*, 280; f) S. Ponomarenko, S. Kirchmeyer, *J. Mater. Chem.* **2003**, *13*, 197.

(15) A. Mourran, B. Tartsch, M. Gallyamov, S. Magonov, D. Lambreva, B. I. Ostrovskii, I. P. Dolbnya, W. H. de Jeu, M. Moeller, *Langmuir* **2005**, *21*, 2308.

(16) M. Björck, G. Andersson, *J. Appl. Crystallogr.* **2007**, *40*, 1174.

(17) N. Harada, K. Nakanishi, *Circular Dichroic Spectroscopy: Exciton Coupling in Organic Stereochemistry; University Science Books: Mill Valley, CA,* Oxford University Press, Oxford, UK **1983.**

(18) J. Michl, E. W. Thulstrup, *Spectroscopy with Polarized Light*, VCH Publishers, New York **1986.**

(19) R. N. Marks, R. H. Michel, W. Gebauer, R. Zamboni, C. Taliani, R. F. Mahrt, M. Hopmeier, *J. Phys. Chem. B* **1998**, *102*, 7563.

(20) E. Da Como, M. A. Loi, M. Murgia, R. Zamboni, M. Muccini, *J. Am. Chem. Soc.* **2006**, *128*, 4277.

Chapter 6
Preparation of quinquethiophene monolayers

In this chapter the preparation of monolayers using chloro [11-(5''''-ethyl-2,2':5',2'':5'',2''':5''',2''''-quinquethien-5-yl)undecyl]dimethyl-silane is presented. The molecule contains a dimethylchlorosilyl anchoring group, a quinquethiophene core connected with an undecane spacer. The material used consists of a mixture of the active compound with a non-active compound that cannot bind to the surface. The ratio between the active and non-active compound has been varied and the monolayer formation and the electrical transport in self-assembled monolayer field-effect transistors has been investigated. A tentative model for the monolayer formation is presented. The inactive compound is required to obtain smooth fully covered monolayers. The process window depends on the composition.

6.1 Introduction

Oligothiophenes are well-known organic semiconductors applied in organic field-effect transistors (OFETs). Numerous different derivatives *i.e.* with improved solubility have been investigated. The layer thickness in OFETs is usually 30-100 nm. A monolayer field-effect transistor is attractive as the charge transport in OFETs occurs in the first few nanometers[1,2] and the use of only a monolayer can significantly decrease the amount of materials used. A spin-coated monolayer field-effect transistor of septithiophene (7T) was discussed in Chapter 5. In this chapter, self-assembled monolayer field-effect transistors (SAMFET) of quinquethiophene (5T) are introduced. Here the monolayer is made directly from solution. Molecules with an anchoring group react with the activated substrate. The advantage of the strong covalent binding between the substrate and the layer is a higher robustness to temperature treatment.

6.2 Monolayer preparation

Monolayers were grown from chloro [11- (5''''-ethyl-2,2':5',2'':5'',2''':5''',2''''- quinquethien-5-yl) undecyl] dimethylsilane, compound 1 in Fig. 6.1. The chemical structure presented in Fig. 6.1. contains a dimethylchlorosilyl group anchoring group. And quinquethiophene core connected with an undecane spacer. The anchoring group after hydrolysis can chemically bind to the SiO_2 surface. The last step in the synthesis, as presented in Fig 6.1, leads to the formation of a byproduct, compound 3. This molecule does not have a chlorosilane anchoring group. Therefore it cannot form a covalent bond with a SiO_2 surface and is regarded as "inactive". The mixture cannot be purified. Monolayers were formed with two compositions *viz*. 50%-50% and 90%-10%. SAM formation and electrical transport was investigated as a function of composition.
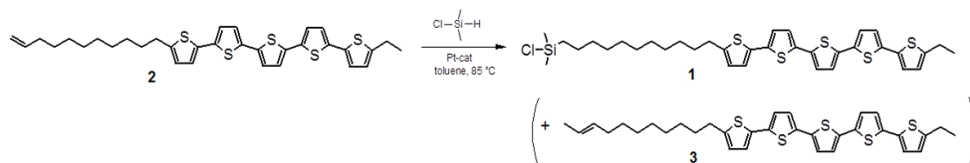
Figure 6.1: Synthesis of the molecule **1** (chloro[11-(5''''-ethyl-2,2':5',2'':5'',2'''-quinquethien-5-yl)undecyl]-dimethylsilane). Compound **1** is obtained by a hydrosilylation reaction of compound **2**. Compound **3** which cannot adhere to Si-OH groups as a byproduct is produced. It is not possible to completely separate compounds **1** and **3**.

The standard procedure to make monolayers is as follows. First the substrates (silicon dioxide substrates or quartz) were rinsed with ethanol and iso-propanol. The surface was cleaned in 600 W O_2 plasma for 2 minutes at 25 °C. Next, the substrates were activated by dipping them for 30 seconds in hydrofluoric acid, rinsed thoroughly with

water and blow dried with nitrogen. The substrates were transferred to an N_2 flow box. A solution of the compound was made by dissolving 10 mg in 10 ml dry toluene for an hour in an N_2 flow box. The solution was filtered through a 0.2 μm PVDF filter (Whatman). For more diluted solutions, *e.g.* 10 mg in 20 ml, after filtering, extra solvent was added. The substrates were immerged in the solution for various incubation times at room temperature. Subsequently the samples were transferred to a bottle containing clean toluene, taken out of the flow box, thoroughly rinsed with toluene, and blow dried.

6.3 Results

6.3.1 Characterization of the SAM

A schematic picture of the ideal monolayer formation is presented in Fig. 6.2. Surface treatment by UV-ozone produces OH-groups on the SiO_2 substrates. The active compound 1 has a mono-chloro anchoring group that covalently can attach to the SiO_2 surface. We note that the anchoring group can hydrolyse with water present in the solution yielding dimers and larger aggregates in the solution. To prevent the formation of dimers, the monolayers were fabricated in a flow box and used purified dried solvents. SAMFETs using a mixture of 50% active and 50% non-active compounds have been reported previously.[3] A summary is presented below. The SAMFETs were made using the standard procedure as described above. XPS, X-ray reflectivity, and AFM measurements confirmed the presence of a single monolayer. The AFM topography image of a fully covered monolayer is reproduced in Fig. 6.3a. Furthermore brag rods were observed in grazing incidence X-ray diffraction measurements. The rods are due to the absence of periodicity perpendicular to the ordered SAM layer, which therefore unambiguously showed that the SAM layer is a dense smooth monolayer. Scanning Kelvin probe microscopy (SKPM) measurements have shown that electrical conduction only occurs in those parts of the SAM that are electrically connected to the source or drain electrode.[4] Typical linear and saturated transfer curve are reproduced in Fig 6.3b. The SAMFET exhibits a bulk-like carrier mobility of about 0.02 $cm^2V^{-1}s^{-1}$, a large current modulation and a high reproducibility.[3,5]

Below, fabrication of SAMFETs using a different composition, not 50%-50% but 90%-10% active-inactive is presented. The experimental procedure was similar as for the 50%-50% composition. Optical photographs of transistor test substrates are shown in Fig. 6.4. A concentration of 1 mg/ml was used. The incubation time was either 1 or 2 nights. Fig. 6.4 shows crystallization especially on the contacts. The crystallization can even be observed by the naked eye. The large amount of active molecules in the solution causes dimerization, which prevents SAM formation on the SiO_2 surface. Presumably the thiophene groups in the semiconducting core of the SAM molecules react with the Au electrodes.
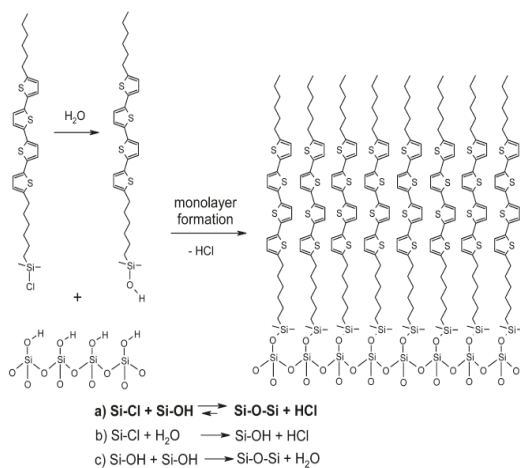
Figure 6.2. Schematic picture of the ideal formation of a self-assembled monolayer on SiO_2. The reaction steps (a,b,c) all happen during self-assembly.
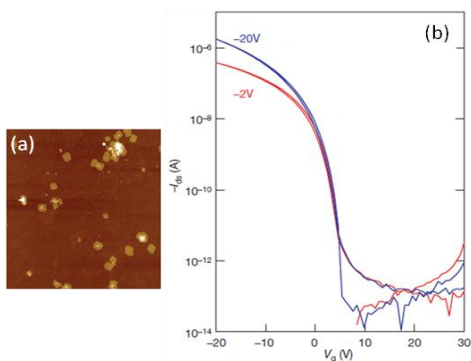
Figure 6.3. (a) Reproduced AFM image of a quionquethiophene SAMFETs measured on a 20 μm by 20 μm surface area. The SAM was made from a 50%-50% mixture of compounds 1 and 3.[4] (b) A typical linear and saturated transfer curve reproduced from ref 3.
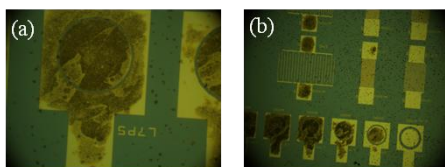
Figure 6.4. Optical photograph of a transistor test substrate covered by 90%-10% SAM molecules (a) substrate incubated for 1 night in 1mg/ml solution (b) substrate incubated for 2 nights in 1mg/ml solution. The crystallization is clearly visible, especially on the gold electrode contact areas.

In an attempt to decrease the amount of crystallization shorter incubation times were used. The concentration was kept the same 1 mg/ml. AFM pictures are presented in Fig. 6.5a. The pictures show island growth of partially covered SAMs. The field-effect mobilities are presented as a function of channel length in right side of Fig. 6.5b. For short incubation times, in the order of minutes, the mobility scales inversely with channel length, which has been explained by percolation theory.[2,6] Islands only contribute to the charge transport, or mobility, when they are part of a percolating path connecting both electrodes. Only after an incubation time of 1 night a fully covered SAMFET is obtained. The mobility then is constant and does not depend on channel length. However, the optical micrograph in Fig. 6.4a confirms crystallization, clearly showing there is more than one layer present.
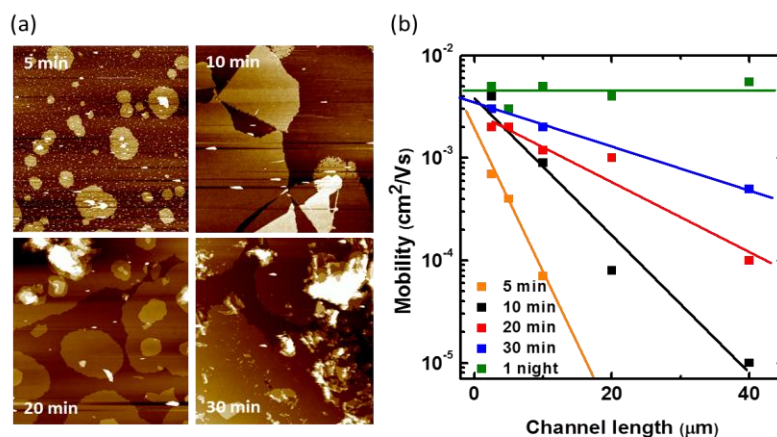
Figure 6.5. (a) AFM images of 1 mg/ml SAM of 90%-10% composition with incubation time of 5, 10, 20 and 30 min. The scan area amounted to 20 μm by 20 μm. (b) Mobility versus channel length for varies incubation times; 5, 10, 20, 30 min and 1night.

In an attempt to reduce the crystallization, the concentration of the compound in the solution was reduced. Layers made with 0.5 mg/ml and an incubation time of 2 days did not show crystallization by naked eye. The surface was characterized by AFM. A typical topography image is presented in Fig. 6.6a. The layers contain lots of holes. The cross section of one of the holes depicted in Fig. 6.6a allows determining of the SAM thickness. The thickness of about 3.9 nm corresponds to the calculated length of the molecule, which is 3.8 nm.

However the monolayer is not perfectly smooth; crystallization is still observed especially on the gold electrodes. Hence to stop the fast crystallization, the solution was further diluted to 0.3 mg/ml. A typical optical image is presented in Fig 6.7a. When using a concentration of 0.3 mg/ml there is no more crystallization on the contacts. The AFM image in Fig 6.7b shows that the layer is homogenous except for some minor double layers.
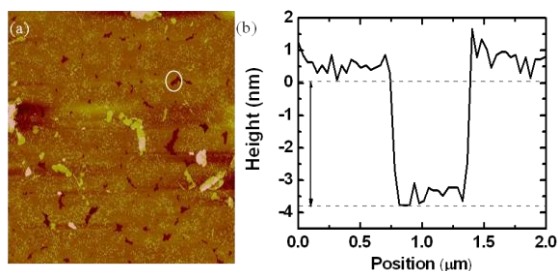
Figure 6.6. (a) Topography image of 90%-10% SAM with 0.5 mg/ml concentration incubated for 2 nights in solution, measured on a surface area of 20 μm by 20 μm. The white circle indicated a hole in the film.(b) A cross section along the hole.

The corresponding typical linear and saturated transfer curve as measured in vacuum are presented in Fig. 6.7c. The curves show no hysteresis, a high on/off ratio and a threshold voltage at 0 V. The linear mobility is comparable to the saturated mobility and amounts about 0.003 to 0.009 $cm^2V^{-1}s^{-1}$. The mobility is slightly lower than the bulk mobility of 0.02 $cm^2V^{-1}s^{-1}$ and lower than the mobility of SAMFETs using a 50%-50% composition.
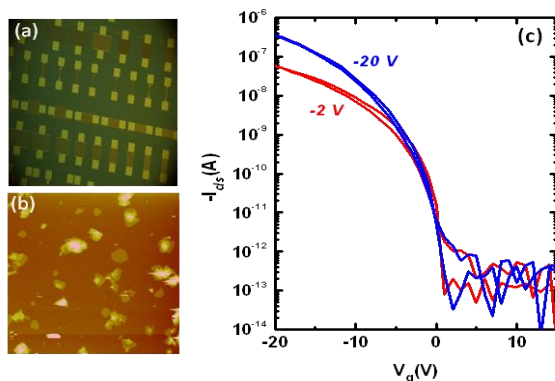
Figure 6.7. (a) Optical image of transistor substrate incubated for 1 night in solution of 90%-10% of 0.3 mg/ml concentration. (b) AFM image of the corresponding monolayer measured on a surface area of 20 μm by 20 μm. (c) Linear and saturated transfer curve of the corresponding SAMFET.

In order to demonstrate that a monolayer is present and that the electrical conductivity only occurs through connected molecules, partially covered SAMFETs were fabricated by decreasing the incubation time. The mobility versus channel length for 15 min and 2 hrs incubation time is presented in Fig 6.8. The mobility is inversely proportional to channel length for partially covered monolayers. For a fully covered SAMFET the mobility is constant.

72
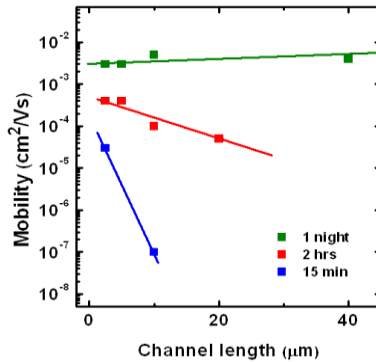
Figure 6.8. Mobility versus channel length for SAMFETs prepared 15 min, 2 hrs and 1 night.

Fig. 6.9. present the mobility on a semi-logarithmic scale of SAMFETs made using various concentrations. The inset shows the data replotted on a linear scale. The channel length was 40 μm and the incubation time was 1 night. The mobility is constant at high concentration and decreases below 0.3 mg/ml. There is hardly any current below 0.2 mg/ml and the mobility cannot be reliably extracted. The microstructure changes as well. At high concentration strong crystallization on the electrodes is observed. A monolayer is formed with double and triple layers on top. Upon decreasing the concentration the crystallization decreases. At 0.3 mg/ml as smooth monolayer with only a small amount of bilayers observed as in Fig 6.7b. However the process window is limited and reproducible SAMFETs can hardly be achieved.
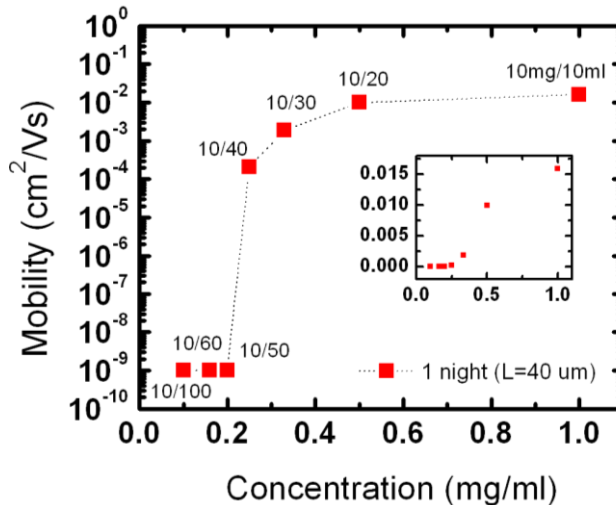
Figure 6.9. Mobility versus concentration (mg/ml) of 90%-10% SAMFETs for L=40 μm. The incubation time was 1 night. The inset shows the data replotted on a linear scale.

73

6.4 Discussion

The two compositions investigated *viz* 50%-50% and 90%-10% show differences in morphology and electrical characteristics which might be due to differences in growing mechanism as elucidated in Fig. 6.10. The active compound 1 can covalently bind to the hydrolyzed SiO_2 surface. The by-product compound 3 is not functionalized and, in theory, this inactive compound cannot bind to the surface.
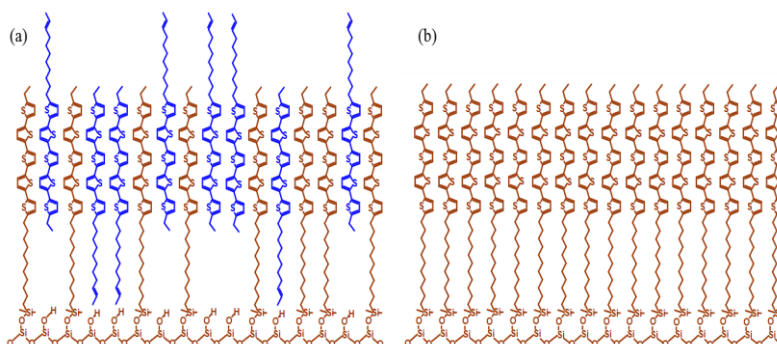
Figure 6.10. Possible structures of the self-assembled monolayer (a) formed by co-crystallization of the mixture of active and non-active molecules and (b) formed only by the active molecules.

However, π-π stacking of the oligothiophene cores can be a driving force for co-crystallization of compound 1 and 3. For the 50%-50% SAM layers, the X-Ray reflectivity measurements, AFM measurements, and grazing incidence synchrotron measurements as reported in ref 3 unambiguously demonstrate the presence of a fully ordered monolayer. There are no indications for layer-by-layer growth.
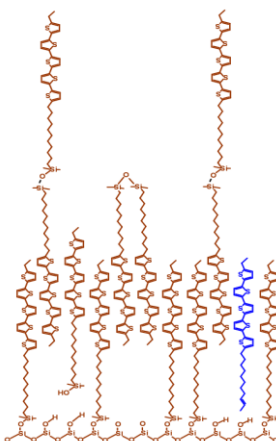
Figure 6.11. Schematic representation of the formation of an "imperfect" layer.

However, in case of the 90%-10% composition we expect a perfectly ordered monolayer as depicted in Fig. 6.10b, but there is a high degree of co-crystallisation. A reason might be that some of the functional molecules can be upside down, *i.e.* Si-Cl up. This would lead to formation of a second layer by hydrolysis of the upper Si-Cl bond followed by self-condensation with the excess functional molecules in solution. This mechanism is shown in Fig. 6.11.

Moreover, the amount of water turned out to be crucial for the 90%-10% composition. Because the amount of active molecules is higher as compared to the 50%-50% mixture, the probability for molecules to already react in solution, producing aggregates, is higher. In the last step of the pre-treatment the substrates were washed with water. The substrates were then immersed in the solution. Although dry toluene was used as a solvent, the amount of absorbed water is enough for the reaction of the molecules and the SiO_2 substrate. Excess water in the solution might lead to aggregation. Hence the water content on the surface and in the solution drives the growing kinetics. The layer formation is difficult to control hampering comparison between different experiments. To stop aggregation of the molecules in solution, self-assembly at 80°C temperature was attempted. Not much differences were observed.

Apparently the presence of the inactive compound 3 is crucial to obtain smooth monolayers. It might inhibit the formation of aggregates and double layers. The inactive molecules participate in the monolayer formation process without diminishing the semiconducting properties of the oligothiophene SAMs.

6.5 Conclusion

Fully and partially covered monolayers of quinquethiophene with two different compositions of active and non-active molecules have been investigated. Two compositions were used, *viz.* 50%-50% and 90%-10%. The processing for each system has been optimized. In short, the use of a solution with a concentration of 1 mg/ml for 50%-50% and 0.3 mg/ml for 90%-10% yields a complete smooth layer. There are only a limited number of defects such as absorbed aggregates formed in the solution and some second and third layers. The SAMFETs made with 50%-50% are highly reproducible. However SAMFETs made with 90%-10% exhibit a small process window. Small variations in concentration around the optimum concentration of 0.3 mg/ml lead to either a low mobility or to excessive crystallization. Furthermore the mobility of the 50%-50% SAMFETs is slightly higher than that of 90%-10% SAMFETs.

The island growth of the partially covered SAM can be explained as follows; a few reactive molecules covalently attach to the hydrolysed surface forming anchoring points. The monodentate molecules in the solution then physisorb on the hydrated surface where they can covalently bind and subsequently grow into a compact SAM. The amount of the non-active molecule is crucial for SAM formation. The low amount of non-active molecules in the 90%-10% composition does not impede dimerization in solution and on the surface layer. Smooth fully covered SAMs can be made but the process

window is limited. Therefore, all the 5T monolayers in the following chapters are produced using the 50%-50% composition.

References

(1) G. Horowitz, R Hajlaoui, H. Bouchriha, R. Borguiga, M. Hajlaoui, *Adv. Mater.* **1998**, *10*, 923.

(2) F. Dinelli, M. Murgia, P. Levy, M. Cavallini, F. Biscarini, D. M. De Leeuw, *Phys. Rev. Lett.* **2004**, *92*, 116802.

(3) E. C. P. Smits, S. G. J. Mathijssen, P. A. van Hal, S. Setayesh, T. C. T. Geuns, K. A. H. A. Mutsaers, E. Cantatore, H. J. Wondergem, O. Werzer, R. Resel, M. Kemerink, S. Kirchmeyer, A. M. Muzafarov, S. A. Ponomarenko, B. de Boer, P. W. M. Blom, D. M. de Leeuw, *Nature*, **2008**, *455*, 956.

(4) S. G. J. Mathijssen, E. C. P. Smits, P. A. van Hal1, H. J. Wondergem, S. A. Ponomarenko, A. Moser, R. Resel, P. A. Bobbert, M. Kemerink, R. A. J. Janssen, D. M. de Leeuw, *Nature Nanotechnol*. **2009**, *4*, 674.

(5) F. Gholamrezaie, S. G. J. Mathijssen, E. C. P. Smits, T. C. T. Geuns, P. A. van Hal, S. A. Ponomarenko, H-G Flesch, R. Resel, E. Cantatore, P. W. M. Blom, D. M. de Leeuw.

(6) P. Stallinga, *Adv. Mater.* **2011**, *23*, 3356.

Chapter 7

Microstructure and phase behavior of a quinquethiophene based self-assembled monolayer as a function of temperature

The self-assembly of monolayers is a highly promising approach in organic electronics, but most systems show weak device performances, probably because of a lack of long-range order of the molecules. The present self-assembled monolayer was formed by a molecule that contains a dimethylchlorosilyl group combined with a quinquethiophene unit through an undecane spacer. This system is the first reported self-assembled monolayer on silicon oxide surfaces that forms two-dimensional crystals. A detailed structural characterization is presented based on grazing-incidence X-ray scattering experiments. By transverse shear microscopy, the shape and size of the crystallites were determined: polygonal shapes with lateral sizes of several micrometers were observed. In situ temperature studies revealed gradual changes of the molecular packing that were irreversible. Melting of the crystal structure was found at 520 K, whereas the self-assembled monolayer remained stable up to 620 K. This chapter presents unknown structural properties of a self-assembled monolayer revealing insights into layer formation and irreversible evolution upon temperature treatment.

7.1 Introduction

Self-assembly of monolayers represents a key technology in organic electronics. An established technique, known since the 1980s, is monolayer formation from solution on silicon dioxide.[1] The field of self-assembled monolayers (SAMs) in general[2,3] and of SAMs on silicon dioxide[4-6] in particular has been reviewed several times. It has been demonstrated that transport in organic field-effect transistors is determined by the first monolayer of the organic semiconductor and its interface properties.[7,8] The thickness of the accumulation layer is at most a few nanometers, and the charge transport occurs solely at the gate dielectric-semiconductor interface.[9-11] Therefore, the concept of SAMs as semiconductors in field-effect transistors (FETs) has attracted much attention in the field of organic electronics, as SAMFETs could be used as basic building blocks of self-assembled electronics.[12,13] A quinquethiophene-based SAMFET was recently reported, and it was shown that its key device parameters were identical to those of bulk thin-film transistors.[12,14] The molecule (Fig. 7.1) has a dimethylchlorosilane anchoring group that can be grafted onto a hydroxylated silicon dioxide substrate.[15] An undecane spacer is incorporated to provide flexibility for the arrangement of the semiconducting quinquethiophene backbone. The molecule is end-capped with an ethyl group. It is well-known that, for efficient charge transport, a highly ordered system with overlapping π orbitals is required,[16] as demonstrated, for example, for pentacene monolayers[7] and oligothiophenes.[17] The morphology and crystallographic packing as a function of temperature for the first reported crystalline SAM on silicon dioxide will be determined. This is an important step toward technological realization of SAM-based electronics as practical applications of such devices require a large temperature budget. It has been found that two-dimensional crystals are generated during layer formation and that a gradual crystalline phase transition occurs upon temperature treatment.

7.2 Experimental

Monolayer preparation using chloro[11-(5''''-ethyl-2,2':5',2'':5'',2''':5''',2''''-quinquethien-5-yl)undecyl]dimethyl-silane on Si wafers with 200 nm thermal dioxide has been described previously.[12,14] To obtain full coverage, the substrate was immersed for 1 night in a solution of dissolved molecules. Lower immersion times resulted in submonolayer coverages of the substrate, whereas longer immersion times did not result in the formation of multilayers. Samples with both submonolayer and full monolayer coverages were investigated in their pristine state (*i.e.*, directly after being removed from solution) and additionally after 400 K temperature treatment in a vacuum for 1 h, as was done for the reported SAMFETs.[12]

The microstructure was investigated with AFM measurements. Transverse shear microscopy (TSM)[23,24] was employed to investigate the morphology, shape, and crystallographic orientation of grains in the layers. In TSM, the probe is scanned in contact mode parallel to the cantilever's long axis. The torsion of the cantilever induced by the different crystallographic alignment of tilted molecules can be recorded by the four

quadrant photodiode. An isotropic surface, such as one formed from molecules standing exactly upright, will yield no contrast in TSM mode. The information obtained by TSM is supported by topographic images. To determine the height of submonolayer islands, topographic images in tapping mode were also recorded. To avoid any deformation of the SAM, these measurements were performed with the smallest forces possible to still guarantee stable imaging conditions.

X-ray scattering experiments were performed under grazing-incidence conditions at the ID10B at the European Synchrotron Radiation Facility (ESRF) in Grenoble, France.[18] Detailed experimental procedures have been reported in ref 18. In situ temperature studies were performed using a specifically designed heater stage for grazing-incidence X-ray diffraction (GIXD) experiments. Samples were mounted horizontally and tilted with respect to the incident beam to adjust the angle of incidence. X-ray reflectivity (XRR) measurements were performed using Cu K_α radiation. Simulations of the XRR data were based on a two-layer model for the SAM layer with two different mean electron densities (see an earlier work on the same system[12]). One layer represented the alkyl spacer groups, and the second represented the top layer of the thiophene backbones. Details of the calculations can be found in ref 18. The total layer thickness was always found to be above the theoretically expected value of 36 Å.

7.3 Results and discussion

7.3.1 Pristine Layers

The structure of the SAM in the pristine state as derived from XRD measuremtns,[18] that is, after removal of the sample from solution without temperature treatment, shows a homogeneous, smooth, and densely packed monolayer of molecules standing fully upright with unitcell parameters of a = 5.6 Å, b = 7.2 Å, and γ = 90° (Table 7.1). These values are comparable to those reported previously for the same system.[12,14] Formation of the crystalline structure does not yield a unique unit cell; the variation of the unit-cell parameters is reported in Table 7.1. Although the size of the unit cell varied [average volume per molecule = (456 ±7) Å^3], the packing of the molecules demonstrated a herringbone motif, as generally found in oligothiophenes.[19] Because the alkyl spacer groups do not provide a detectable structural scattering signal, it has not been possible to judge their ordering, although long-range order has already been detected in alkyl-based SAMs.[20]

Fig. 7.1a shows the morphology of a film with submonolayer coverage recorded in tapping mode. It shows polygonal-shaped islands with a lateral size in the range of 10 μm. The corresponding height histogram reveals an average island height of 42 Å, which is close to the length of the stretched molecule (36 Å). The submonolayer was built from molecules standing exactly upright, as confirmed by the appearance of Bragg rods[21] observed by GIXD (Fig. 7.2a). Consequently, no contrast between individual domains was obtained by TSM, as can be seen from the shear

force contrast image presented in Fig. 7.1f. Fig. 7.1e presents the simultaneously recorded topography image.

state	a [Å]	b [Å]	γ [°]	tilt angle θ [°]	tilt dir. Ω [°]	packing angle ß [°]	volume [Å⁻³]
pristine state	5.6± 0.2	7.2± 0.2	90±2	0	--	63	456±7
annealed at 400K	5.6± 0.2	8.1± 0.2	90±2	13±2	0±3	60	462±11

Table 7.1. Unit-cell parameters (a, b, γ), Molecular packing parameters (Tilt angle θ, Tilt direction Ω, Herringbone angle β), and Unit-cell volume given for the phase of upright-standing molecules (Pristine) and the phase of tilted molecules (Annealed at 400 K).

7.3.2 Layers annealed at 400 K

Heat-treated samples were investigated by AFM, which showed smooth layers. Crystalline domains with rims of approximately 0.5 Å heights at the grain boundaries were found. TSM images (Fig. 7.1c) show polygonal domains of different contrast (similar in shape and size to the islands in the submonolayer in Fig. 7.1 (a,e). This contrast is the result of different azimuthal orientations of the tilted quinquethiophene units of the molecule. Panels c and d of Fig. 7.1 show the same image but with the domain boundaries emphasized by black lines, as guides for the eye, in Fig. 7.1d. The thin lines represent domain boundaries that were inserted based on additional TSM and topography images recorded with different forces providing different contrasts. GIXD was employed to verify the molecular tilt found by TSM and to evaluate its magnitude. Fig. 7.2b shows an indexed reciprocal-space map of a SAM annealed at 400 K.
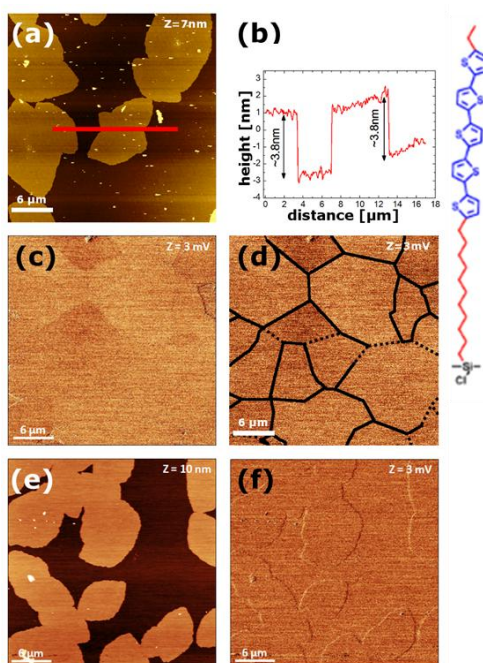
Figure 7.1. (a) Atomic force microscopy topography image (recorded in tapping mode) of a pristine submonolayer SAM showing a polygonal shaped island. (b) The height profile along the red line. (c) TSM image of a SAM annealed at 400 K. (d) Image c with additionally drawn clear domain boundaries (thick lines) and proposed boundaries (thin lines). The scale bars correspond to 6 μm. (e) Topography image (recorded in contact mode) of a pristine submonolayer SAM and (f) corresponding TSM image showing no shear force contrast (apart from morphology-induced artifacts at the islands' edges).
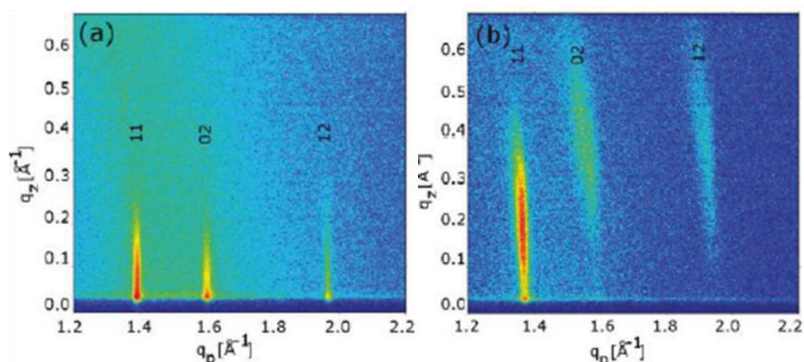
Figure 7.2. Reciprocal-space maps of (a) a pristine SAM of uprightstanding molecules and (b) a SAM annealed at 400 K showing the footprint of tilted molecules.

The intensity of the Bragg rods has been analyzed in detail in ref 18. It has been shown that upon annealing, a transition from a phase with upright-standing molecules (Bragg rods, Fig. 7.2a) to a phase of tilted molecules occurred.[22] Even within one sample, the tilt of the molecules, and hence the size of the unit cell varied slightly causing the Bragg rods to have an arc-like shape in GIXD. The packing of the molecules has been derived from Density functional theory (DFT) calculations.[18] They support the existence of two crystal packing motives. The reported packing[18] is reproduced in Fig. 7.3.
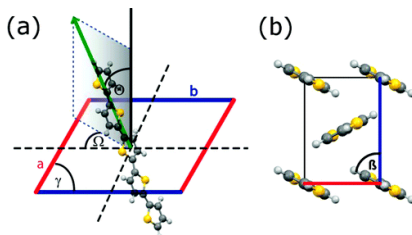
Figure 7.3. (a) Schematic view of the orientation of an individual molecule (tilt angle θ, tilt azimuth Ω) within the two-dimensional unit cell (a, b, γ). (b) View along the long molecular axes giving the location of the herringbone angle β. β defined as angle between the aromatic plane of the molecule and the b lattice vector.

7.3.3 In situ studies

Investigations on the thermal stability of the microstructure were performed in situ by GIXD and XRR. GIXD investigations gave the tilt angle of the molecules as a function of temperature (Fig. 7.4a).
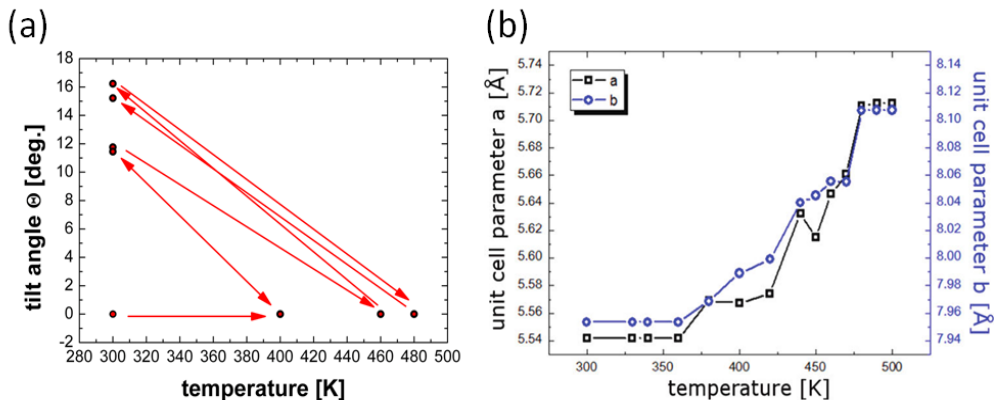
Figure 7.4. (a) Evolution of the molecular tilt angle θ during in situ temperature cycling of the sample. Arrows indicate the chronology of the experiment. (b) Evolution of the unit-cell parameters a (left scale) and b (right scale) as a function of temperature of a SAM pretreated by annealing at 400 K.

The in situ studies revealed that the quinquethiophene units were always standing upright at elevated temperatures ($\theta = 0°$). However, after thermal treatment, distinct tilt angles were observed at room temperature (T = 300 K). The tilt angle increased with the temperature of heat treatment to a value of 17°. These changes in the molecular tilt angle were irreversible. Similar temperature induced changes of the tilt angle have been observed in SAMs of phosphonic acids.[23]

The unit-cell parameters as a function of temperature (Fig. 7.4b) show that the enlargement of the unit cell was isotropic. The lattice constants expanded by about 0.2 Å in the temperature range from 300 to 500 K. The observed thermal expansion is comparable to that of other SAMs on silicon oxide surfaces.[24] The crystalline structure was lost at 520 K, in excellent agreement with the melting temperature of 526 K reported for quinquethiophene.[25] Several heating and cooling steps in the range between 300 and 520 K showed that the crystalline order could not be improved or recovered by temperature; hence, it can be concluded that the crystalline order is induced during the formation of the layer and, therefore, depends strongly on the preparation of the substrate. The thermal expansion of the unit cell was not fully reversible, so that a slightly expanded lattice remained after the heat treatment. Considering the change in the molecular tilt angle together with the irreversible lattice expansion, a volume of the unit cell of (470 ± 13) $Å^3$ was observed after heat treatment at 500 K (compare Table 7.1).

The XRR results (Fig. 7.5) revealed a constant layer thickness up to 620 K that was satisfactorily described with a two-layer model assuming two different electron densities for the thiophenes and the alkyl groups. Above 620 K, a single-layer model with an average electron density described the experimental data well, indicating a transition from a layered structure to a disordered layer with a heat-induced decrease in layer thickness. The layer thickness remained stable even when the film was cooled; constant layer thickness of 16 Å upon cooling from 780 to 300 K; Fig. 7.5b. It can be expected that, at elevated temperatures, cracking of the molecules occurs so that the layer partially decomposes.[38] The complete desorption of the SAM was observed above 880 K. Because temperature treatment did not show any impact on the domain size, it can be concluded that the morphology and size of the crystalline domains of the SAM are determined during layer formation. This is supported by the correspondence in shape between the submonolayer islands and the crystalline domains (Fig. 7.1) and by diffraction experiments in which no healing or recovery effects of the crystalline order by the influence of temperature were observed. Annealing below 520 K always yielded a phase of tilted molecules, in contrast to the upright standing molecules in the pristine films. The almost reversible increase of the unit cell during the temperature treatment can be considered a result of thermal expansion, whereas the irreversible expansion of approximately 10% suggests partial desorption of less strongly bound (physisorbed) molecules. This irreversibility within the sample is also reflected in the irreversible increase of the tilt angle of the molecules after temperature treatment. A schematic picture of tilted molecules after annealing is presented in Fig. 7.6.

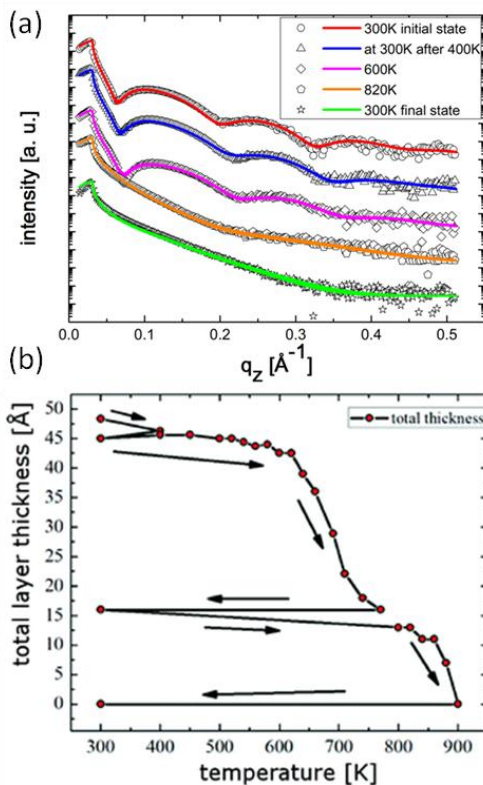**Figure 7.5.** (a) X-ray reflectivity measurements during the temperature treatment of a SAM. The data (symbols) are presented together with the simulations (lines). The curves are shifted for clarity. (b) Evolution of the total layer thickness due to heating and cooling of the sample, where the arrows indicate the sequence of the experiment.
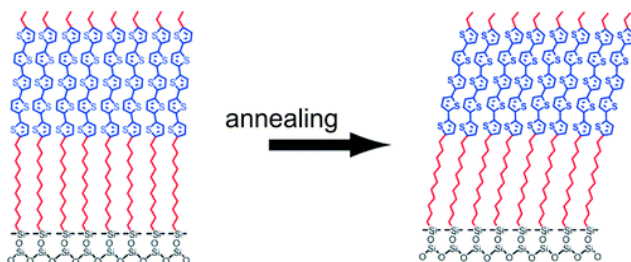

Figure 7.6. Schematic picture of tilted molecules after annealing.

7.4 Conclusion

Detailed structural and morphological investigations of the two-dimensional crystal structure of a quinquethiophene-based SAM have shown that different phases can be found depending on the sample thermal history. In the pristine state and at elevated temperature, the molecules stand exactly upright on the surface. Upon temperature treatment, the molecules tilt toward the b axis of the unit cell, but no impact of temperature on the domain size was found. In situ investigations at temperatures up to 520 K revealed an almost reversible isotropic expansion of the unit cell, and melting of the crystal was observed above 520 K. Between 520 and 620 K, a layered SAM with amorphous quinquethiophene units was present. The layered order was lost above 620 K, and a disordered state formed that desorbed completely at 880 K. The two-dimensional ordering in this SAM is induced by the layer formation process, during which single-crystalline domains with polygonal shapes are formed with a lateral size in the micrometer range. The crystal structure shows a certain variation of both the lattice constants and the molecular packing that is related to the specific nature of self-assembled monolayers formed by partial covalent bonding of the molecules to the substrate.

References

(1) J. Sagiv, *J. Am. Chem. Soc.* **1980**, *102*, 92.

(2) F. Schreiber, *Prog. Surf. Sci.* **2000**, *65*, 151.

(3) G. Heimel, F. Rissner, E. Zojer, *Adv. Mater.* **2010**, *22*, 2494.

(4) S. Onclin, B. J. Ravoo, D. N. Reinhoudt, *Angew Chem Int Ed.* **2005**, *44*, 6282.

(5) K. Wen, R. Mao, H. Cohen, J. Sagiv, A. Gibaud, A. Desert, B. M. Ocko, *ACS Nano.* **2008**, *2*, 579.

(6) C. Haensch, S. Hoeppener, U. S. Schubert, *Chem. Soc. Rev*. **2010**, *39*, 2323.

(7) S. C. B. Mannsfeld, A. Virkar, C. Reese, M. F. Toney, Z. Bao, *Adv. Mater.* **2009**, *21*, 2294.

(8) H. S. Lee, D. H. Kim, J. H. Cho, M. Hwang, Y. Jang, K. Cho, *J. Am. Chem. Soc* **2008**, *130*, 10556.

(9) F. Dinelli, M. Murgia, P. Levy, M. Cavallini, F. Biscarini, D. M. de Leeuw, *Phys. Rev. Lett.* **2004**, *92*, 116802.

(10) T. Muck, J. Fritz, V. Wagner, *Appl. Phys. Lett*. **2005**, *86*, 232101.

(11) S. D. Quiroga, A. Shehu, C. Albonetti, M. Murgia, P. Stoliar, F. Borgatti, F. Biscarini, *Rev. Sci. Instrum*. **2011**, *82,* 025110.

(12) E. C. P. Smits, S. G. J. Mathijssen, P. A. van Hal, S. Setayesh, T. C. T. Geuns, K. A. H. A. Mutsaers, E. Cantatore, H. J. Wondergem, O. Werzer, R. Resel, M. Kemerink, S. Kirchmeyer, A. M. Muzafarov, S. A. Ponomarenko, B. de Boer, P. W. M. Blom, D. M. de Leeuw, *Nature* **2008**, *455*, 956.

(13) M. Novak, A. Ebel, T. Meyer-Friedrichsen, A. Jedaa, B. F. Vieweg, G. Yang, K. Voitchovsky, F. Stellacci, E. Spiecker, A. Hirsch, M. Halik, *Nano Lett.* **2011**, *11*, 156.

(14) S. G. J. Mathijssen, E. C. P. Smits, P. A. van Hal, H. J. Wondergem, S. A. Ponomarenko, A. Moser, R. Resel, P. A. Bobbert, M. Kemerink, R. A. J. Janssen, D. M. de Leeuw, *Nat Nanotechnol.* **2009**, *4*, 674.

(15) S. A. Ponomarenko, O. V. Borshchev, T. Meyer-Friedrichsen, A. P. Pleshkova, S. Setayesh, E. C. P. Smits, S. G. J. Mathijssen, D. M. de Leeuw, S. Kirchmeyer, A. M. Muzafarov, *Organometallics* **2010**, *29*, 4213.

(16) M. Mottaghi, G. Horowitz, *Org. Electron* **2006**, *7*, 528.

(17) G. R. Dholakia, M. Meyyappan, A. Facchetti, T. J. Marks, *Nano Lett.* **2006**, *6*, 2447.

(18) H. G. Flesch, S. G. J. Mathijssen, F. Gholamrezaie, A. Moser, A. Neuhold, J. Nov, S. A. Ponomarenko, Q. Shen, C. Teichert, G. Hlawacek, P. Puschnig, C. Ambrosch-Draxl, R. Resel, D. M. de Leeuw, *J. Phys. Chem. C* **2011**, *115*, 22925.

(19) D. Fichou, *Handbook of Oligo- and Polythiophenes*; Wiley-VCH, **1999**.

(20) T. Koga, M. Morita, H. Ishida, H. Yakabe, S. Sasaki, O. Sakata, H. Otsuka, A. Takahara, *Langmuir* **2005**, *21*, 905.

(21) Y. Yoneda, *Phys. Rev.* **1963**, *131*, 2010.

(22) K. Kjaer, *Physica B: Cond Mat.* **1994**, *198*, 100.

(23) M. De Pauli, C. A. Perez, M. C. Prado, D. H. C. Araujo, B. R. A. Neves, A. Malachias, *Synth. Met*. **2012**, *161*, 2521.

(24) I. M. Tidswell, T. A. Rabedeau, P. S. Pershan, S. D. Kosowsky, J. P. Folkers, G. M. Whitesides, *J. Chem. Phys.* **1991**, *95*, 2854.

(25) P. Wolfer, C. Muller, P. Smith, M. A. Baklar, N. StingelinStutzmann, *Synth. Met.* **2007**, *157*, 827.

Chapter 8
Photophysics of self-assembled monolayers of π-conjugated quinquethiophene derivative

The photophysics of fully and partially covered self-assembled monolayers (SAMs) of a quinquethiophene (5T) derivative have been investigated. The monolayers behave as H-aggregates. The fluorescence of fully covered SAMs is weak and red shifted and the extinction is blue shifted as compared to that of single molecules. The fluorescence of partially covered SAMs is dominated by that of single molecules on the surface. The extinction spectra are similar for fully and partially covered monolayers, which show that even the smallest islands are H-aggregates. The extinction spectra are furthermore closely resemble those for 5T single crystals which demonstrates that in oligothiophene crystals the intermolecular interactions within one layer molecules are stronger than the interlayer electronic coupling.

8.1   Introduction

Conjugated organic molecules are applied in a broad array of opto-electronic devices such as solar cells, field-effect transistors and light emitting diodes.[1] Their photophysics have been widely investigated.[2-4] Emphasis has been on oligothiophenes as they are soluble in common organic solvents, environmentally stable and synthetically accessible. Comprehensive investigations of the photophysics of oligothiophenes of up to seven thiophene units in solution have been performed.[5-8] The photophysics of single crystals is more complicated. Optical excitation in single crystals yields a bound electron hole pair or exciton, introduced by Frenkel in 1931.[9] In organic molecular crystals the dielectric constant is small. The Coulomb interaction between the electron and hole leads to a large binding energy on the order of 0.1 to 1 eV. Frenkel excitons thus tend to be small, of the same order as the size of the unit cell.

Oligothiophenes usually crystallize in structures with two or four molecules in the unit cell. Optical properties of oligothiophene crystals have been studied in considerable detail, both experimentally[10,11] and theoretically.[12-17] Complete understanding is complicated by the three dimensional molecular packing with more than one molecule in the unit cell and the electronic coupling between molecules being different in all three directions.
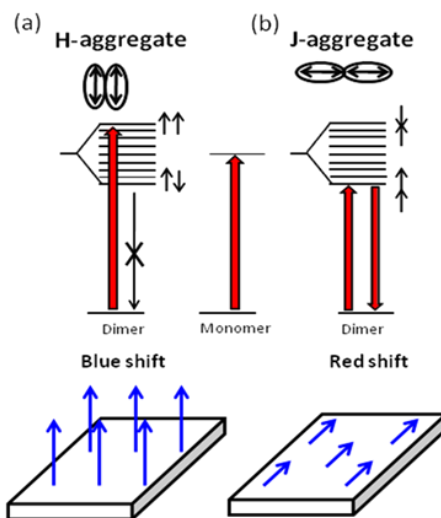
Figure 8.1. Schematic exciton bandstructure in (a) *H*-aggregate with cofacial arrangement of molecular transition dipole moments (b) *J*-aggregate with in-line alignment of molecular transition dipole moments. Allowed optical transitions are shown with red arrows and forbidden transitions with a black line. Lower part shows two dimensional arrays of transition dipoles for which *H*-aggregate and *J*-aggregate characteristics may be expected.

The exciton can couple to both intermolecular vibrations and photon states, yielding polaritons. Furthermore the optical response of the crystals could be affected by the presence of surface states, defects and disorder.[18-21] The problem may be simplified by studying two dimensional layers of oligothiophene molecules rather than the three dimensional crystals, however, the optical properties of oligothiophene SAMs have so far not been reported.

Closely packed, two dimensional, self-assembled monolayers of a quinquethiophene (5T) derivative have recently been reported.[22] The observation of Bragg-rods in grazing incidence X-ray diffraction measurements indicates a high degree of in-plane order. Not surprisingly, corresponding self-assembled monolayer field-effect transistors exhibit a bulk-like carrier mobility, large current modulation and high reproducibility.[23,24] The oligothiophene moieties are oriented with their long axis perpendicular to the surface.[25]

Intermolecular interactions in a monolayer of chromophoric molecules gives rise to formation of an exciton band.[26-29] In a first order approximation, the electronic structure of the exciton band can be understood by treating the excited state intermolecular interactions as a coupling between transition dipole moments of the individual constituent molecules. For oligothiophene, the transition dipole moment for the allowed transition from ground state to the first excited singlet state S_1 is oriented along the long axis of the oligothiophene. For arrays of oscillating transition dipoles oriented perpendicular to the surface, all dipole-dipole interaction energies are positive. For this arrangement there will be only one allowed transition that is blue shifted (*i.e.* occurring at higher frequency) with respect to the transition in the single molecules. The two dimensional array of perpendicularly oriented molecules is thus expected to behave as an *H*-aggregate, see Fig. 8.1. In an *H*-aggregate the lowest optical transition is forbidden. Nevertheless, fluorescent emission is possible due to perturbation by molecule vibrations and disorder. The residual fluorescence from *H*-aggregates has an extremely low quantum yield and it is red-shifted in comparison with the single molecules.

In contrast for a two dimensional lattice of transition dipoles oriented in plane and arranged in a brickwork pattern (see. Fig. 8.1) a red shifted absorption is predicted provided that the head-to-tail inline interaction is stronger than the co-facial lateral coupling. This is typical for *J*-aggregates.[28] In a *J*-aggregate only the optical transition to the lowest energy state is allowed. Consequently, *J*-aggregates show a small Stokes shift and fluorescence with a high quantum yield. Although for dense SAMs, *J*-aggregation may not be expected, we note that *J*-type aggregation on a surface has been reported for sexithiophene[19] and is a common type of 2-dimensional molecular arrangement for cyanine dyes.[27]

The photophysics of partially and fully covered monolayers were investigated. By comparing optical properties as a function of aggregate size, the length scale of in-plane interactions was studied. From a comparison of the measured spectra with those reported for single crystals the importance of out-of-plane interlayer interactions can be estimated.

8.2 Experimental

Self-assembled monolayers (SAM) were prepared on silicon monitor wafers covered with a 200-nm layer of thermally grown SiO_2 to study the morphology and on quartz to measure the extinction spectra. Quartz was chosen as an optically silent substrate. The chemical structure of the self-assembling molecule, chloro[11-(5''''-ethyl-2,2':5',2'':5'',2''':5''',2''''-quinquethien-5-yl)undecyl]-dimethylsilane (1) is shown in Fig. 8.2a. The molecule consists of a conjugated quinquethiophene core. To bind the molecules to the SiO_2 surface, a monochlorosilane anchoring group was attached via an undecane spacer. The compound contains an inactive impurity (2) that cannot bind to the SiO_2 surface. The chemical structure is presented in Fig. 8.2b. Co-crystallization is reported to be unlikely but could not be excluded.[24,30] As model compound to study the behaviour of single molecules in solution with no possibility to dimerize, 5-ethyl-5''''-(undec-10-enyl)-2,2':5',2'':5'',2''':5''',2''''-quinquethiophene (3) was used. This molecule is an isomer of 2 with the double bound between the primary and secondary carbon atom of the alkenyl substituent.

To grow the SAM, the surface was activated by an oxygen plasma treatment followed by acid hydrolysis. The SAM was formed by submerging the activated substrate into a 1 mM solution of the molecule in dry toluene. The coverage was varied by changing the incubation time from 5 minutes to 2 weeks. After monolayer formation the substrates were rinsed with dry toluene and dried with N_2.

The morphology was investigated by Atomic Force Microscopy (AFM) measurements using a Veeco Dimension 3100 atomic force microscope. The profile measurements were performed in non-contact tapping mode. Typical topography images (20 μm × 20 μm) of partially and fully covered SAMs on SiO_2 are presented in Fig. 8.2c. The AFM images show that the SAM grows in the form of islands.[25] The height differences in the topography are 3.5 nm, in perfect agreement with the calculated length of the molecule. A small fraction of the islands shows a bilayer, most likely due to the presence of dimers in the solution.[25] Fig. 8.2c shows that after two weeks of exposure a uniform fully covered monolayer is obtained.

Fluorescence spectra were recorded on an Edinburg F900 fluorescence spectrometer. The sample compartment was flushed with nitrogen. Fluorescence spectra were corrected for the wavelength dependence of the sensitivity of the detection channel and for a small dark count rate of the thermoelectrically cooled photomultiplier tube. Extinction spectra were recorded on a Perkin Elmer lambda 900 spectrophotometer. Fluorescence decay times were obtained using a time correlated single photon counter using a Edinburgh FS 920 spectrophotometer.

X-ray Photoelectron Spectroscopy (XPS) measurements were carried out using a Quantera SXM from Ulvac-PHI, employing monochromatic Al Kα radiation with a spot of 100 μm, scanning across an area of 1200 μm x 500 μm. The chemical state and the atomic concentrations of the elements present on the surface were determined from narrow-scan measurements. Measurements were done at a take-off angle of 60°. The information depth is then approximately 6 nm.
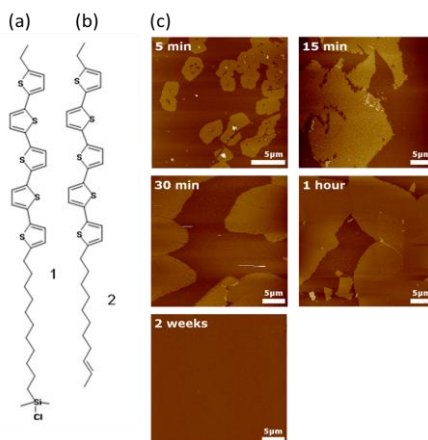
Figure 8.2. (a) The chemical structure of the self-assembling molecule, chloro[11-(5''''-ethyl-2,2':5',2'':5'',2''':5''',2''''-quinquethien-5-yl)undecyl]-dimethylsilane. The molecule consists of a conjugated quinquethiophene core and a monochlorosilane anchoring group attached via an undecane spacer. (b) The corresponding inactive compound without anchoring group is presented as well. (c) Typical AFM topography images of self-assembled monolayers on SiO_2 monitor wafers as a function of incubation time in the solution ranging from 5, 15, 30 min, 1 hr and 2 weeks.

8.3 Optical characterization of quinquethiophene self-assembled monolayers

To analyse the photophysics of the monolayers, first the optical properties of the single molecule as a function of temperature were measured.
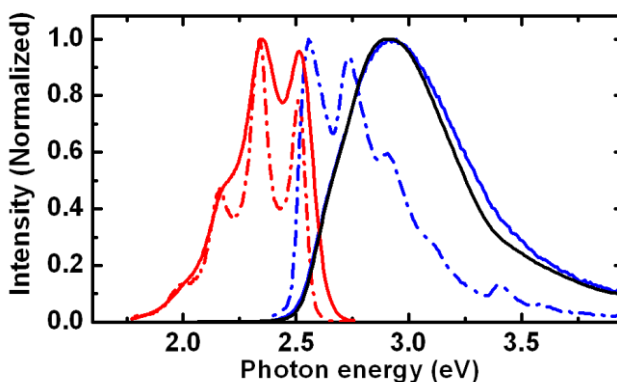
Figure 8.3. Normalized fluorescence (red), fluorescence excitation (blue) and extinction (black) spectra of the compound 3. The solid lines represent spectra measured of toluene solutions at 293 K. The dashed lines were measured in a glassy 2-MeTHF matrix at 80 K.

The active molecule is not stable in solution; the compound is prone to dimerization. Hence a non-active model compound that has the same π-conjugated

quinquethiophene (5T) core was used. Fig. 8.3 shows the normalized fluorescence (red), fluorescence excitation (blue) and extinction spectra (black). The solid lines represent spectra measured of toluene solutions at 293 K. The dashed lines were measured in a glassy 2-MeTHF matrix at 80 K. The fluorescence is due to the optically allowed S_1-S_0 transition and exhibits a maximum at about 2.3 eV. The vibronic fine structure is based on a 1400 cm^{-1} fully symmetric vibrational mode which is typical for the 5T-moiety and which is associated with changes in the bond length alternation upon optical excitation. The vibronic fine structure gets more pronounced at low temperature. Previous studies have shown that the loss of resolution at room temperature is due to the torsional flexibility around the single bonds joining the thiophene units that leads to a significant thermal population of non-planar conformers of the 5T moiety.[31] The same vibrational progression is observed in the excitation spectrum. From the extinction spectra a Stokes shift of 0.5 eV is determined. The maximum extinction coefficient amounts to 4×10^4 M^{-1}cm^{-1}.

From integration of the molar extinction coefficient for the molecule in toluene solution over the photon energy range corresponding to the S_0-S_1 transition and correcting for the local Lorentz-field in the solvent, a transition dipole moment μ for the S_0-S_1 transition with a magnitude of 8.1 Debye was determined. The transition dipole moment is oriented along the long axis of the molecule.[32]

Extinction spectra of self assembled monolayers on quartz are presented in Fig. 8.4a. The normalized spectra are identical. The spectra were measured with the incident beam under an angle of 57 degrees with the substrate normal. The extinction increases with incubation time due to changes in the monolayer coverage. XPS measurements were performed to derive the coverage. The sulfur 2p peak with binding energy of 163.7 eV was used as a marker for the thiophene units. The peak intensity is presented in Fig. 8.5 together with the maximum extinction at 3.45 eV as a function of incubation time. The coverage increases with incubation time. A full monolayer is obtained after about 4 hrs. A quantitative analysis of the XPS data showed that the layer thickness of the SAM is 4.2 nm assuming a densely packed monolayer which is in agreement with the calculated length of the molecule and the AFM data.[33] The good agreement between XPS and extinction measurements show that self-assembly growth ends upon formation of a fully covered monolayer.

The extinction spectra for a fully covered SAM as a function of angle of incidence are presented in Fig. 8.4b. Two extinction bands with maxima at 3.5 and 4.5eV are observed. The dependence of extinction on the orientation is clearly different for the two bands: the band at 4.5 remains almost constant when changing the angle of incidence while the band at 3.5 eV increases in intensity for large angles of incidence. Assuming a dipole model and including a correction for the local electric field at the quartz-air interface based on the Fresnel coefficients one predicts that transitions with transition dipole moment in the plane of the monolayer (so perpendicular to the surface normal) do not depend strongly on angle of incidence. In contrast transition dipole moments parallel to the surface normal are predicted to give zero extinction at normal incidence with the extinction rising steeply for angles of incidence going away from normal.
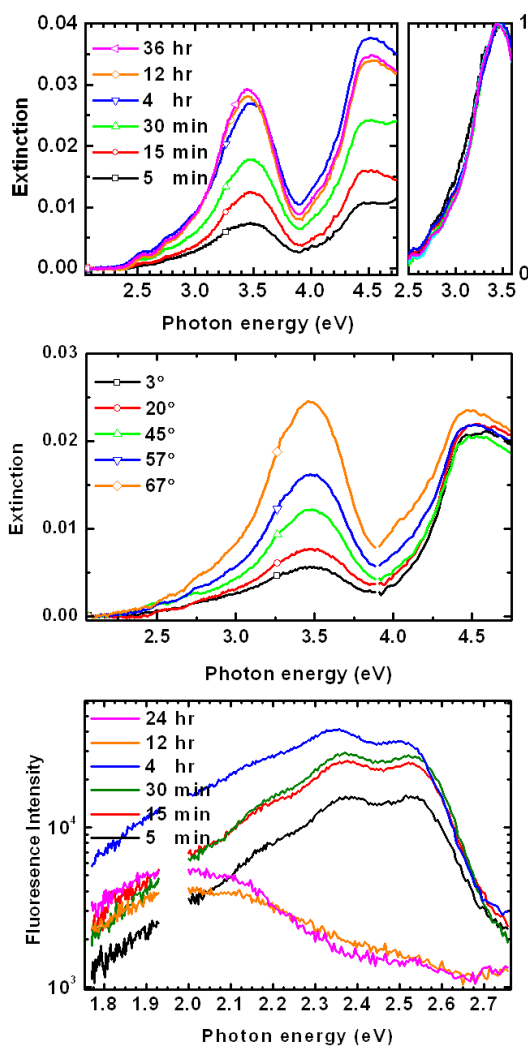
Figure 8.4. (a) Extinction spectra of monolayers. The coverage was varied by varying the incubation time between 6 min and 24 hours. The spectra were measured under excitation under an angle of 57 degrees with the substrate normal. The right hand side shows the spectra normalized for unit extinction at 3.45 eV. (b) Extinction spectra of a fully covered monolayer as a function of angle of incidence. (c) Fluorescence spectra of the corresponding monolayers of Fig. 8.4a.

Therefore, the 4.5 eV band to a transition polarized in the plane of the layer can be assigned. This assignment is compatible with the large *b*-polarized component of the corresponding transition for the 5T single crystal[32] and compatible with substantial charge transfer character for this transition.
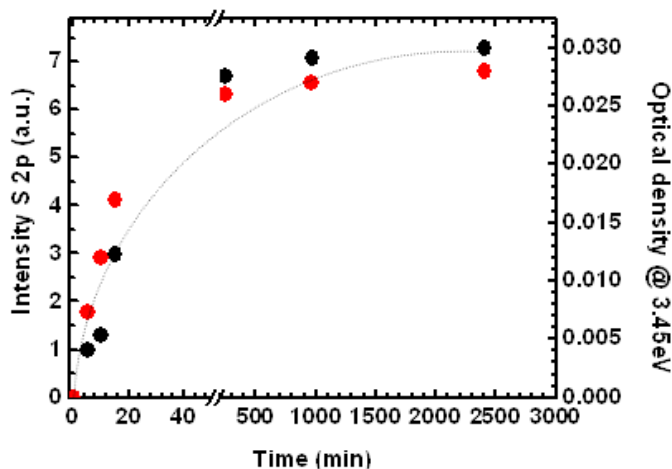
Figure 8.5. Monolayer coverage from XPS and extinction measurements. The sulfur 2p peak intensity at 163.7 eV binding energy (black circles) and optical density at 3.45 eV (red circle) as a function of incubation time. The line is a guide to the eye.

The rise of the extinction of the 3.5 eV band with angle of incidence shows that this transition is polarized primarily along the surface normal. This is in agreement with an almost upright orientation of the molecules as derived from grazing incidence X-ray diffraction measurements.[25] The substantial extinction near normal incidence indicates a considerable component of the transition dipole moment in the plane of the film which most likely arises from a charge transfer contribution to the transition.[34]

In comparison to the isolated molecule, the maximum of the first optical extinction band at 3.5 eV of the monolayer has shifted to higher frequency. The blue shift of about 0.5 eV matches very closely to optical data reported for a thin layer (95 nm) of quinquethiophene molecules deposited by vacuum sublimation[23] and is indicative of an *H*-aggregate as elucidated in Fig. 8.1. An *H*-aggregate is formed when the transition dipole moments are parallel aligned. Here the transition dipole moment is along the molecular backbone, and analysis of the extinction measurements as a function of angle has shown that the molecules themselves are indeed aligned almost perpendicular to the substrate.

Note that the radiative lifetime of an *H*-aggregate is larger than that of an isolated molecule. However the measured lifetime of the fluorescence from a complete monolayer (0.8 ns) is shorter than the lifetime for the fluorescence from the single molecules in solution (1.0 ns) and from the lifetime for substrates with only partial coverage (1.0 ns). From this it can be concluded that additional intermolecular interactions between 5T molecules in the complete monolayer reduce the probability for photon emission and lead to a change in the bandshape of the fluorescence as expected for an *H*-aggregate. Analysis of the full fluorescence decay trace of the complete monolayer, indicates contributions from species with lifetime exceeding 1 ns, indicating heterogeneity in the population of emitting species.

The extinction spectrum of the fully covered SAM is almost identical to that of a quinquethiophene single crystal.[35,36] Apparently the two dimensional polycrystalline monolayers have a similar optical transition as three dimensional single crystals, which demonstrates that in oligothiophene crystals the intermolecular interactions within one layer molecules are stronger than the interlayer electronic coupling.

Interestingly, the band shape of the extinction shows no significant variation with coverage, a fact which becomes apparent after normalizing the spectra to unit intensity at 3.45 eV as shown in the right side of the Fig. 8.4a. Even the extinction of substrates after 5 min incubation time is similar to that of a fully covered SAM. The size of the islands is then in the order of 1 μm which gives an upper limit for the length scale needed to form an *H*-aggregate.

The fluorescence spectra of the monolayers on quartz are presented on a semi-logarithmic scale in Fig. 8.4c. Similar spectra have been obtained for monolayers on Si-monitor wafers. Despite the fact that analysis of extinction spectra has shown that all monolayers are *H*-aggregates the fluorescence spectra are a strong function of coverage. Fully covered SAMs obtained upon many hours incubation time (the red and orange lines) show a typical *H*-aggregate fluorescence. The peak is red shifted with respect to that of the single molecule and the intensity is low because the optical transition is forbidden as elucidated in Fig. 8.1. In contrast, the partially covered SAMs show apart from the *H*-aggregate emission at 1.9 eV, a strong fluorescence at higher photon energies. The peak positions correspond to that of the isolated molecule. Hence the luminescence at higher photon energy originates from single molecules, either isolated on the substrates or physisorbed at the edges of the assembled islands. Contrary to *H*-aggregates the optical transition in single molecules is allowed. Hence their contribution swamps the total fluorescence spectrum. To illustrate this further, in the fluorescence spectrum for the substrate with exposure time of 4 hr, contributions from both single molecules and aggregates can be discerned, while the extinction spectrum is clearly dominated by the aggregated species. This can be explained considering that individual single and aggregated 5T molecules contribute with equal weight to extinction. In contrast, the weight for single molecules in fluorescence is much higher than for aggregated species because of their much higher fluorescence quantum yield. Hence in an almost complete monolayer, a small number of single chromophores can still overwhelm the contribution of the aggregated 5T molecules and so fluorescence is a sensitive method to monitor the final stages of closed monolayer formation.

8.4 Conclusion

The photophysics of self-assembled monolayers of a quinquethiophene (5T) derivative on Si monitor wafers and quartz substrates has been investigated. The coverage has been varied by varying the incubation time in the solution. The coverage has been determined from XPS measurements. The good agreement between XPS and extinction measurements shows that the self-assembly ends upon formation of a fully covered monolayer. The monolayers behave as *H*-aggregates. The fluorescence of fully covered

monolayers is weak and red shifted as compared to that of isolated single molecules. At the same time the extinction is blue shifted. The parallel packing of the molecules is confirmed by analysis of the extinction as a function of angle of incidence. The molecules are oriented almost perpendicular to the substrate. The extinction spectra are similar for fully and partially covered monolayers that contain only self-assembled islands. Even the smallest islands are *H*-aggregates. To accurately determine the length scale for *H*-aggregate formation smaller islands then investigated here are required. The extinction spectra are furthermore similar to that of a 5T single crystal which demonstrates that in oligothiophene crystals the intermolecular interactions within one layer molecules are stronger than the interlayer electronic coupling.

References

(1) A. Yang, M. Kuroda, Y. Shiraishi, T. Kobayashi, *J. Chem. Phys*. **1998**, *109*, 8442.

(2) C. Ziegler, H. S. Nalwa, Handbook of Organic, Conductive Molecules and Polymers, **1997**, vol. 3, John Wiley and S. Chichester.

(3) D. Fichou (Ed.), Handbook of Oligo- and poly-Thiophenes,Wiley-VCH, Weinheim, **1999**.

(4) L. Raimondo, M. Campione, M. Laicini, M. Moret, A. Sassella, P. Spearman, S. Tavazzi, *Appl. Surf. Sci.* **2006**, *253,* 271.

(5) R. Colditz, D. Grebner, M. Helbig, S. Rentsch, *Chem. Phys.* **1995**, *201*, 309.

(6) R. S. Becket, J. S. Melo, A. Macanita, F. Elisei, *Pure. Appl. Chem*. **1995**, 67, 9.

(7) P. Emele, D. U. Meyer, N. Holl, H. Port, H. C. Wolf, F. Wurthner, P. Bauerle, F. Effenberger, *Chem. Phys.* **1994**, *181*, 417.

(8) M. Defaux, F. Gholamrezaie, J. Wang , A. Kreyes, U. Ziener , D. V. Anokhin, D. A. Ivanov, A. Moser, A. Neuhold, I. Salzmann, R. Resel, D. M. de Leeuw, S. C. J. Meskers, M. Moeller, A. Mourran, *Adv. Mater.* **2012**, *24*, 973.

(9) J. J. Hopfield, *Phys. Rev.* **1958***, 112,* 1555.

(10) S. Tanaka, Y. Katano, Y. Kimura, T. Yoshinari, S. Nagasaka, H. Itoh, Y. Kuriyama, *Phys. Stat. Solidi A* **2010***, 207*, 1474.

(11) M. Muccini, E. Lunedei, C. Taliani, D. Beljonne, J. Cornil, J. L. Brédas*, J. Chem. Phys*. **1998**, *109*, 10513.

(12) F. C. Spano, L. Silvestri, P. Spearman, L. Raimondo, S. J. Tavazzi, *J. Chem. Phys*. **2007**, *127*, 184703.

(13) W. Kulig, P. Petelenz, *Phys. Rev. B* **2009**, *79,* 094305.

(14) P. Petelenz, W. Kulig, *Chem. Phys.* **2008**, *343*, 100.

(15) P. Petelenz, W. Kulig, *Phys. Rev. B* **2009**, *80*, 115127.

(16) a) A. Stradomska, P. Petelenz, *J. Chem. Phys.* **2009**, *131*, 044507. b) A. Stradomska, P. Petelenz, *J. Chem. Phys.* **2009**, *130*, 094705.

(17) A. Stradomska, P. Petelenz, *Acta Phys. Pol. A* **2007**, *112*, 161.

(18) E. Da Como, M. A. Loi, M. Murgia, R. Zamboni, M. J. Muccini, *Am. Chem. Soc.* **2006**, *128*, 4277.

(19) M. A. Loi, E. Da Como, F. Dinelli, M. Murgia, R. Zamboni, F. Biscarini, M. Muccini*, Nature mater.* **2005**, *4*, 81.

(20) F. C. Spano, L. Silvestri, P. Spearman, L. Raimondo, S. Tavazzi, *J. Chem. Phys.* **2007**, *127*, 184703.

(21) H. J. Egelhaaf, J. Gierschner, J. Haiber, D. Oelkrug, *Opt. Mater*. **1999**, *12*, 395.

(22) F. Gholamrezaie, S. G. J. Mathijssen, E. C. P. Smits, T. C. T. Geuns, P. A. van Hal, S. A. Ponomarenko, H. G. Flesch, R. Resel, E. Cantatore, P. W. M. Blom, D. M. de Leeuw, *Nano Lett.* **2010**, *10*, 1998.

(23) E. C. P. Smits, S. G. J Mathijssen, P. A. van Hal, S. Setayesh, T. C. T. Geuns, E. Cantatore, H. J. Wondergem, O. Werzer, R. Resel, M. Kemerink, S. Kirchmeyer, A . M. Muzafarov, M. Aziz, S. A. Ponomarenko, B. de Boer, P. W. M. Blom, D. M. de Leeuw, *Nature* **2008**, *455*, 956.

(24) S. G. J. Mathijssen, E. C. P. Smits, P. A. van Hal, H. J. Wondergem, S. A. Ponomarenko, A. Moser, R. Resel, P. A. Bobbert, M. Kemerink, R. A. J. Janssen, D. M. de Leeuw, *Nature Nano. Tech.* **2009**, *4*, 674.

(25) H. -G. Flesch, S. G. J. Mathijssen, F. Gholamrezaie, A. Moser, A. Neuhold, J. Novak, S. A. Ponomarenko, Q. Shen, C. Teichert, G. Hlawacek, P. Puschnig, C. Ambrosch-Draxl, R. Resel, D. M. de Leeuw, *J. Phys. Chem. C* **2011**, *115*, 22925.

(26) M. Orrit, D. Möbius, U. Lehmann, H. Meyer, *J. Chem. Phys*. **1986**, *85*, 4966.

(27) H. Nakahara, K. Fukuda, D. Mobius, H. Kuhn, *J. Phys. Chem*. **1986**, *90,* 6144.

(28) F. C. Spano, *Acc Chem. Res*. **2010**, *43*, 429.

(29) K. Miyano, *Appl. Surf. Sci.* **1997**, *113,* 299.

(30) S. A. Ponomarenko, O. V. Borshchev, T. Meyer-Friedrichsen, A. P. Pleshkova, S. Setayesh, E. C. P. Smits, S. G. J. Mathijssen, D. M. De Leeuw, S. Kirchmeyer, A. A. M. Muzafarov, *Organometallics*, **2010**, *29*, 4213.

(31) B. Milian-Medina, D. Wasserberg, S. C. J. Meskers, E. Mena-Osteritz, P. Bauerle, J. Gierschner, *J. Phys. Chem. A* **2008**, *112*, 13282.

(32) H. J. Egelhaaf, P. Bäuerle, K. Rauer, V. Hoffmann, D. Oelkrug, *J. Mol. Struct.* **1993**, *293*, 249.

(33) C. van der Marel, M. Yildirim, H. R. J. Stapert, *Vac. Sci. Technol. A* **2005**, *23*,1456.

(34) S. Tavazzi, M. Laicini, L. Raimondo, P. Spearman, A. Borghesi, A. Papagni, S. Trabattoni, *Appl. Surf. Sci.* **2006**, *253*, 296.

(35) G. Mazur, P. Petelenz, M. Slawik, *Chem. Phys.* **2012**, *13*, 92.

(36) S. Tanaka, Y. Katano, Y. Kimura, T. Yoshinari, S. Nagasaka, H. Itoh, Y. Kuriyama, *Phys. Stat. Sol. A* **2010**, *207*, 1474.

Chapter 9

Ordered semiconducting self-assembled monolayers on polymeric surfaces utilized in organic integrated circuits

A two-dimensional highly ordered self-assembled monolayer (SAM) directly grown on a polymer surface is reported in this chapter. Semiconducting SAMs are utilized in field-effect transistors and combined into integrated circuits as 4-bit code generators. The driving force to form highly ordered SAMs is the packing of the liquid crystalline molecules caused by the interactions between the linear alkane moieties and the π-π stacking of the conjugated thiophene units. The fully functional circuits demonstrate long-range order over large areas, which can be regarded as the start of flexible monolayer electronics.

9.1   Self-assembled monolayer on a polymeric surface

The realization of the first chemisorbed self-assembled monolayers (SAMs) in the 1980s inspired many to study its formation and characterize its properties.[1,2] Since then, SAMs are applied to, e.g., change the wetting properties of materials,[3] adapt the work function of metals,[4,5] build large-area molecular junctions,[6] or fabricate ultrathin dielectrics.[7,8] Self-assembly is advantageous from a technological point of view because it is one of the few practical strategies for making ensembles of nanostructures.[9] In selfassembled monolayer electronics, the basic building block is the self-assembled monolayer field-effect transistor (SAMFET), in which the semiconductor is a single molecular layer spontaneously formed on the gate dielectric. Recently the first SAMFETs were reported and combined into integrated circuits. The demonstration of real logic functionality makes self-assembly the ultimate technology for bottom-up mass production of organic electronics. However, up to now SAMFETs were made using thermally grown SiO_2 as the gate dielectric.[10] The high processing temperature prevents a direct transfer of the existing technology to the application in flexible electronics. Processing on foil has a limited temperature budget of about 200 °C. Therefore a prerequisite to incorporate SAMs as active layers in flexible electronics is to grow ordered monolayers on organic dielectrics processed at low temperatures. SAM formation on metals and oxides has been studied extensively.[3] Monolayers of thiols on gold grow dynamically, while silane SAMs on SiO_2 grow through the development of islands.[11] In general, SAMs cannot be directly formed on a blank, $i.e.$, unmodified, polymer surface.[12] A buffer layer is necessary to act as a bridge between the polymer surface and the SAM. For instance polyethylene and poly(dimethylsiloxane) have first been functionalized with a thin silicate layer onto which the actual SAM has been formed.[13] Additionally (aminopropyl)triethoxysilane was grafted as a buffer layer on poly(ethylene terephthalate).[12] Little is known about the growth mechanism.[13] Only recently it was shown that silane molecules can stick to a blank rubrene surface.[14] However highly ordered densely packed SAMs on polymers have not yet been reported.

To create semiconducting SAMs on an organic dielectric, the formation of a monolayer itself is not sufficient. In a monolayer transistor the layer thickness is comparable to that of the accumulation layer. In that case, structural imperfections, as voids or grain boundaries, lead to a deteriorated charge carrier mobility. Hence, efficient charge transport can only occur when the SAM is highly ordered. Here, it has been shown that the semiconducting SAMs not only are able to grow on organic dielectrics but also exhibit long-range order and allow for charge transport over micrometer distances. This SAMFETs comprising an organic dielectric exhibit the same performance as their hybrid, SiO_2 based, counterpart. Subsequently over a hundred SAMFETs were integrated into self-assembled monolayer circuits. The functional circuit, processed at low temperature, paves the way for flexible self-assembled monolayer electronics. It has been speculated that the origin for the formation of the highly ordered SAM on the blank polymer substrate is the liquid crystalline nature of the molecules employed.

9.2 Characterization of the Self-assembled monolayer

Self-assembled monolayer field-effect transistors are fabricated in a bottom-gate, bottom-contact architecture, as illustrated in Fig. 9.1a. First, a 50 nm Au layer is deposited onto the substrate and patterned using standard photolithographic and wet etching techniques to build the transistor gate and a first interconnect layer. An epoxy-based negative photoresist, SU8, is then spin-coated onto the wafer acting as the gate dielectric. Instabilities in the surface of the dielectric may occur because the molecules are mobile and the surface can resemble a viscous fluid.[15] To prevent instabilities such as swelling, the photoresist was cross-linked. The generic chemical structure is shown in the inset of Fig. 9.1a.

SU8 was chosen because it is a well-studied compound used in electronics[16,17] and, most importantly, because it contains epoxy groups, which are easily converted to –OH groups upon exposure to an oxygen plasma. Subsequent to the deposition of the gate dielectric, holes are photochemically defined to form the vertical interconnects (vias). A second Au layer is deposited on the stack and patterned to define the source and drain contacts together with a second interconnect layer.[18]

As semiconducting molecules chloro[11-(5'''-ethyl-2,2':5',2'':5'',2''':5''',2''''-quinquethien-5-yl) undecyl]-dimethylsilane was used as described previously.[10] The chemical structure of the self-assembled molecules is shown as inset in Fig. 9.1b. However, the molecules do not have a chemical interaction with the cross-linked polymeric gate dielectric.

To impose a driving force toward self-assembly, the gate dielectric was activated using an oxygen plasma. The activated surface was hydrolyzed by submerging the substrate in water. The functional groups formed by the plasma treatment are undoubtedly heterogeneous in both type and distribution.[19] The processing conditions did not optimizaed to obtain the highest number of silanol groups as reported to be crucial for SAM formation on SiO_2. After the water treatment, the substrate was blow dried and put in a dry toluene solution containing the active molecules for 2 days. The devices were measured after annealing in vacuum (10^{-5} mbar) at 130 °C to remove traces of solvent.

The microstructure of the SAM was investigated by grazing incidence X-ray diffraction. Fig. 9.2. shows the diffracted intensity integrated over the q_z direction, corrected for the background intensity from the polymer substrate underneath. The black line shows the integrated values whereas the red line shows a fit to the experimental data to determine the exact peak position. The diffracted intensity is presented as a color map in the inset of Fig. 9.2. as a function of perpendicular and in-plane scattering vectors, q_z and q_p. The horizontal line at q_z = 0.06 Å^{-1} is due to diffuse scattering from the sample surface at the critical angle as described by Yoneda.[20] Most important are the vertical lines, the so called Bragg rods.[21] They demonstrate in-plane order arising from the thiophene units; the rod shape arrives from the absence of periodicity perpendicular to the SAM. The Bragg rods of the monolayer are well-

defined, but they show low scattering intensity because of the remaining strong background intensity from the polymer substrate underneath.
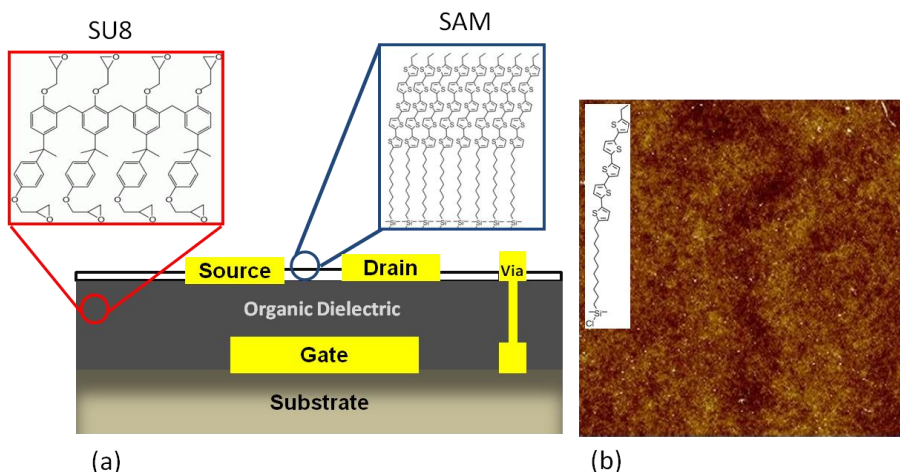

Figure 9.1. Schematic cross section of a SAMFET with an organic dielectric. (a) From bottom to top: a rigid monitor wafer, gold gate line, organic dielectric, gold source and drain electrodes, and SAM. (b) AFM topography of the monolayer grown on the organic dielectric ($9 \times 9 \ \mu m^2$), the z axis is 25 nm. The inset shows the chemical structure of the molecule.

Due to the very low electron density contrast between the polymer substrate and the monolayer itself, a very poor peak to background ratio is found. The small inplane width of the rods is a clear evidence of high order and large crystalline 2D domains within the monolayer. From the peak positions a rectangular unit cell can be determined which contains two molecules in a herringbone packing that is comparable to reported crystal structures of oligothiophenes.[22]

The Bragg rods can be indexed as the (1,1) and (0,2) reflections of a rectangular unit cell with lattice constants a = 5.49 Å and b = 7.81 Å, identical to the values previously obtained for SAM formation on SiO_2.[23] The shape of the Bragg rods in reciprocal space (decay of the intensity along q_z at constant q_p) shows upright standing molecules because the maximum intensity occurs at the Yoneda reflection.[20]

The morphology was investigated by atomic force microscopy (AFM) measurements on different spots on the sample. A typical spatial map of the topography is presented in Fig. 9.1b showing a fully covered smooth monolayer. If present, bilayers or voids could easily have been resolved.[23] A smooth surface alone could be due to the absence of molecules. To explicitly establish the presence of the semiconducting molecules, the electrical transport was characterized.
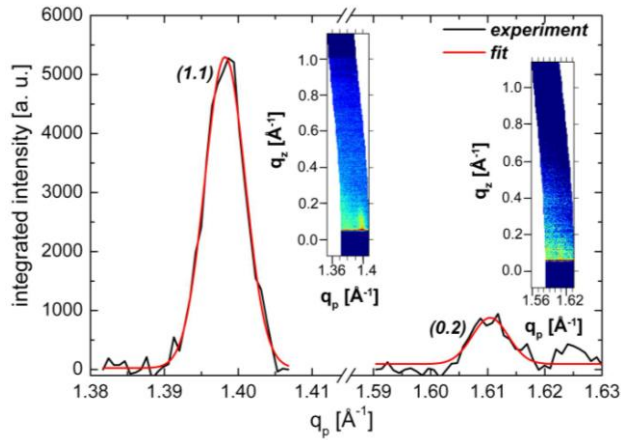
Figure 9.2. Grazing-incidence diffraction measurements. The diffracted intensity integrated over the q_z direction, corrected for background as a function of in-plane scattering vector q_p. The black line represents the actual measurement whereas the red line shows a fit to the experimental data to determine the exact peak position. The insets show the diffraction intensity from the Bragg rods in their reciprocal space maps. The (1,1) and (0,2) reflection are indicated.

A typical transfer characteristic of a transistor with concentric source and drain contacts, a channel length of 20 μm, and a channel width of 1000 μm is shown in Fig. 9.3. The extracted device mobility for the linear and saturation regime is about 0.02 cm^{2}V^{-1}s^{-1}, identical to the mobility obtained in SAMFETs comprising SiO$_2$ as gate dielectric.[10] The observed gate-controlled modulation of the source-drain current, in combination with the AFM measurements taken in the transistor channel is a direct evidence for the presence of the formation of a semiconducting self-assembled monolayer on the organic gate dielectric.

Figure 9.3. Transfer characteristic of a SAMFET with concentric source and drain employing a organic dielectric. The inset shows a photomicrograph of the transistor.

9.3 SAM in organic integrated circuits

The SAMFETs exhibit a positive threshold voltage. Any integrated circuits comprising these transistors should therefore be based on "$V_{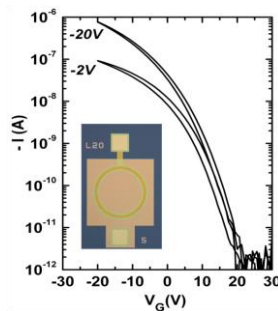gs}$ = 0" logic,[18,25] using inverters with the gate of the load shorted with the source. The basic operation of the inverter can be interpreted as a voltage divider controlled by the input voltage. When the input voltage is low (V_{in} = V_{dd}), the driver transistor is turned on and the output voltage is pulled up from logic 1 to logic 0.[24,25] When the input voltage is high (V_{in} = 0), the output voltage is pulled down to V_{dd} because the load transistor is chosen much wider than the driver. Fig. 9.4. shows the output signal of the inverter as a function of the input voltage (V_{in}). Voltage inversion is observed.
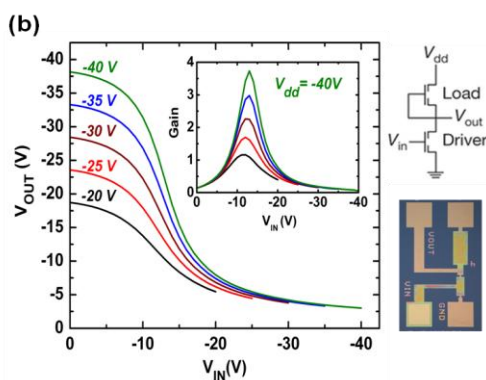
Figure 9.4. Input-output characteristic of an inverter for different supply voltages. The inset shows the signal gain as a function of V_{in} measured at different supply voltages V_{dd}, color coded as the main panel and under the graph a photomicrograph of the voltage inverter is shown.

The inset of Fig. 9.4. illustrates the output gain as a function of V_{in}, measured at different supply voltages. The observed gain is similar to the one obtained in conventional thin film organic inverters[25] and inverters based on SAMFETs with a SiO_2 gate dielectric.[10]

Inverters were combined into seven-stage ring oscillators. A buffer stage was added to determine the switching frequency. The ring oscillators were measured at a supply voltage of -32 V over a resistor with an oscilloscope. An oscillation frequency, f, of about 2 kHz was obtained as shown in Fig. 9.5. Realization of real logic functionality requires a small parameter spread in mobility and threshold voltage.

Over a hundred SAMFETs using polymeric dielectric in 4-bit code generators in which the ring oscillators act as the clock generator were combined. The code generator also contains hard-wired memory, a four-bit counter, decoder logic, and a load modulator. The output of the code generator is presented in Fig. 9.5. The bit rate is around 0.5 kbit/s at a supply voltage of -42 V. The circuit performance is similar to

that of state-of-the-art organic integrated circuits developed for organic radio frequency identification transponders.[26]

By now it is well established that at room temperature alkanesilane SAMs on SiO$_2$ grow in islands.[11] The silane molecules are first physisorbed at the hydrated silicondioxide surface, where hydrolysis of the SAM molecules takes place. Via a condensation reaction the SAM covalently binds to the interface. The self-assembly can be driven by the lipophilic interactions between the linear alkane moieties and by the enthalpic van der Waals forces. In the initial period the monolayer grows in a disordered liquid-like state and, with time, islands grow laterally and their size is limited by diffusion.

The surface coverage increases until a densely packed fully ordered SAM is obtained. Here, the selfassembling molecule consists of an aliphatic chain and a thiophene core each having the possibility to drive the selfassembly. On SiO$_2$, the growth mechanism has been studied by AFM and SKPM measurements on partially and fully formed monolayers. Incomplete monolayers grow in islands comparable to alkanesilanes on SiO$_2$. The electrical connection in between grains, with possibly different crystallographic orientations, was shown not to hamper the electrical transport.[23] On SU8, in complete monolayers imperfections occur as voids could not be identified. The electrical transport measurements discussed above show a comparable performance to SAMFETs optimized with SiO$_2$ as gate dielectric.

9.4 Conclusion

The occurrence of highly ordered densely packed SAMs directly on a polymeric surface can be tentatively explained as follows: first a few anchoring points are made by plasma oxidation. The monodentate molecules physisorb on the hydrated surface where they can covalently bind and subsequently grow into a compact SAM. The driving force is packing of the liquid crystalline molecules caused by the interaction between the linear alkane moieties and the π-π stacking of the conjugated thiophene units. Defects due to uncontrolled self-condensation are prevented by the use of a monodentate anchoring group. The hydroxyl groups on the surface have not been optimized as reported to be crucial for SiO$_2$. Still, proper SAM formation was observed, which could suggest that the microstructure is an umbrella motif consisting of a 2D ordered densely packed monolayer directly attached to the polymer substrate.
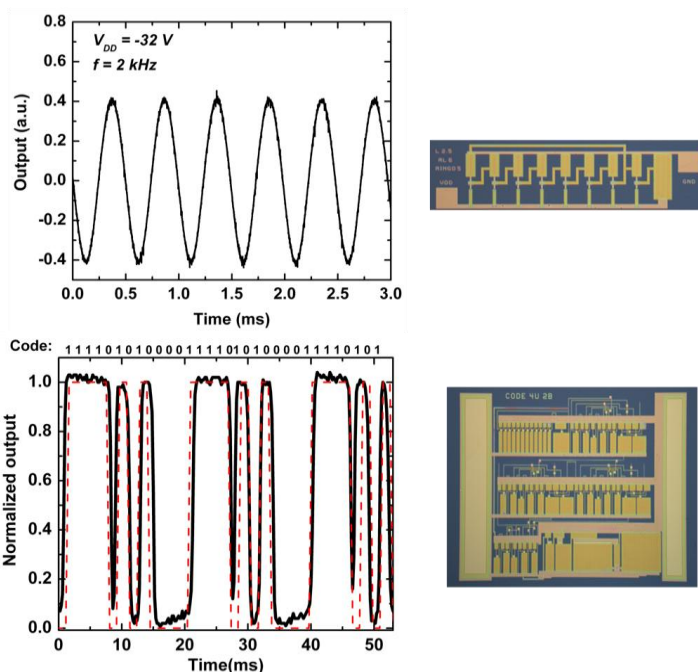
Figure 9.5. (top); Output signal of a seven-stage ring oscillator measured at a supply voltage of -32 V. (below) Output of a 4-bit code generator. The preprogrammed code is indicated above the diagram and by the red dotted line. The optical photomicrograph of each device shown next to its graphs.

Refrences

(1) R. G. Nuzzo, D. L. Allara, *J. Am. Chem. Soc.* **1983**, *105*, 4481.

(2) J. Sagiv, *J. Am. Chem. Soc.* **1980**, *102*, 92.

(3) A. Ulman, *Self-assembled monolayers of Thiols*; Academic Press: San Diego, CA, **1998**; Vol. 24.

(4) B. de Boer, A. Hadipour, M. M. Mandoc, T. van Woudenbergh, P. W. M. Blom, *Adv. Mater.* **2005**, *17*, 621.

(5) S. G. J. Mathijssen, P. A. van Hal, T. J. M. van den Biggelaar, E, C. P. Smits, B. de Boer, M. Kemerink, R. A. J. Janssen, D. M. de Leeuw, *Adv. Mater.* **2008**, *20*, 2703.

(6) H. B. Akkerman, P. W. M. Blom, D. M. de Leeuw, B. de Boer, *Nature* **2006**, *441*, 69.

(7) S. A. DiBenedetto, A. Facchetti, M. A. Ratner, T. J, Marks, *Adv. Mater.* **2009**, *21*, 1407.

(8) H. Klauk, U. Zschieschang, J. Pflaum, M. Halik, *Nature* **2007**, *445*, 745.

(9) G. M. Whitesides, B. Grzybowski, *Science* **2002**, *295*, 2418.

(10) E. C. P. Smits, S. G. J. Mathijssen, P. A. van Hal, S. Setayesh, T. C. T. Geuns, K. A. H. A. Mutsaers, E. Cantatore, H. J. Wondergem, O. Werzer, R. Resel, M. Kemerink, S.

Kirchmeyer, A. M. Muzafarov, S. A. Ponomarenko, B. de Boer, P. W. M. Blom, D. M. de Leeuw, *Nature* **2008**, *455*, 956.

(11) S. Onclin, B. J. Ravoo, D. N. Reinhoudt, *Angew. Chem. Int. Ed.* **2005**, *44*, 6282.

(12) J. Xiang, P. Zhu, Y. Masuda, K. Koumoto, *Langmuir* **2004**, *20*, 3278.

(13) M. K. Chaudhury, *Biosens. Bioelectron.* **1995**, *10*, 785.

(14) M. F. Calhoun, J. Sanchez, D. Olaya, M. E. Gershenson, V. Podzorov, *Nat. Mater.* **2008**, *7*, 84.

(15) A. Ulman, *Organic Thin Films and Surfaces: Directions for the Nineties in Thin Films* Academic Press: San Diego, CA, **1995**; Vol. 20.

(16) D. M. de Leeuw, G. H. Gelinck, M. Matters, US Patent 6635406, **2003**.

(17) H. S. Kim, E. Plis, A. Khoshakhlagh, S. Myers, N. Gautam, Y. D. Sharma, L. R. Dawson, S. Krishna, S. J. Lee, S. K. Noh, *Appl. Phys. Lett.* **2010**, *96*, 033502.

(18) E. Cantatore, T. C. T. Geuns, G. H. Gelinck, E. van Veenendaal, A. F. A. Gruijthuijsen, L. Schrijnemakers, S. Drews, D. M. de Leeuw, *IEEE J. Solid-State Circuits* **2007**, *42*, 84.

(19) G. S. Ferguson, M. K. Chaudhury, H. A. Biebuyck, G. M. Whitesides, *Macromolecules* **1993**, *26*, 5870.

(20) Y. Yoneda, *Phys. Rev.* **1963**, *131*, 2010.

(21) P. Fenter, In *Self-Assembled Monolayers of Thiols*; A. Uhlman, Academic Press: San Diego, CA, **1991**.

(22) D. Fichou, *Handbook of Oligo- and Polythiophenes*; Wiley-VCH: Weinheim and New York, **1999**.

(23) S. G. J. Mathijssen, E. C. P. Smits, P. A. van Hal, H. J. Wondergem, S. A. Ponomarenko, A. Moser, R. Resel, P. A. Bobbert, M. Kemerink, R. A. J. Janssen, D. M. de Leeuw, *Nat. Nanotechnol.* **2009**, *4*, 674.

(24) M. Spijkman, E. C. P. Smits, P. W. M. Blom, D. M. de Leeuw, Y. Bon Saint Come, S. Setayesh, E. Cantatore, *Appl. Phys. Lett.* **2008**, *92*, 143304.

(25) E. Cantatore, E. J. Meijer, *Proceedings of the 29th European Solid State Circuits Conference*, **2003**.

(26) G. H. Gelinck, H. E. A. Huitema, E. van Veenendaal, E. Cantatore, L. Schrijnemakers, J. B. P. H. van der Putten, T. C. T. Genus, M. Beenhakkers, J. B. Giesbers, B. H. Huisman, E. J. Meijer, E. M. Benito, F. J. Touwslager, A. W. Marsman, B. J. E. van Rens, D. M. de Leeuw, *Nat. Mater.* **2004**, *3*, 106.

Summary

       In recent years organic semiconductors have attracted considerable attention for application in electronic devices such as solar cells, photodetectors, light-emitting diodes and field-effect transistors. The advantages of the use of polymers are their unique electrical and mechanical properties. The electrical transport properties can be tailored by modification in chemical design. The mechanical flexibility in combination with solution processing provides the opportunity to produce low-cost electronics on large area substrate such as glass and plastic.

       At this moment for large area processing a top-down technology is used. Thin films are applied by evaporation, ink jet printing or spin coating and patterned using photolithography. A promising technology for organic electronics is bottom-up self-assembly, where molecules self-organize into complex patterns and structures without human intervention. By selectively patterning a substrate, in combination with the appropriate molecules, the self-assembly process can be directed, hereby eliminating subsequent patterning steps as needed in a top-down approach. The most used type of self-assembly is formation of self-assembled monolayers (SAMs). Despite being only a single molecular layer thick, the SAM can change the macroscopic mechanical and electrical properties of surfaces.

       The basic building block of organic electronics is the organic field-effect transistor (OFET); a microelectronic switch that is used to manipulate the resistance. Control of the key device parameters of OFETs such as field-effect mobility and threshold voltage is crucial. SAMs can play an important role in controlling these parameters. The effect of the SAM depends on the chemical composition of the comprising molecules and on the location in the device, viz. on the gate dielectric or on the source and drain electrodes.

       In chapter 2 of this thesis the charge injection in OFETs is discussed. SAMs are applied onto the metal electrodes to tune the work function. The charge injection into the semiconductor can be enhanced or suppressed. SAM modified electrodes however, can influence the morphology of the semiconductor close to the contacts and thereby enhance the charge injection as well. In chapter 3, the SAM modified electrodes in two geometries of OFETs are presented, to investigate how SAMs can affect the charge injection in different transistor geometries. In a bottom-contact, top-gate OFET geometry, the SAM is well defined and the charge injection is greatly enhanced. In a bottom-contact, bottom-gate layout the SAM at the edge of the electrode is less ordered and the charge injection is reduced. Both chapters 2 and 3 discuss how the presence of a SAM on the electrodes influences the charge injection. Apart from a change in workfunction, the main effect is a change in the microscopic ordering of the semiconductor.

       Controlling the threshold voltage in OFETs is important for the operation of organic circuits for instance by determining the noise margin of logic gates. It has been reported that a SAM applied on the SiO_2 gate dielectric can change the threshold voltage. In chapter 4, the origin of the threshold voltage shift is investigated. Using SKPM, the microscopic mechanism is revealed. By exfoliating the semiconductor after electrical

characterization and subsequent probing of the surface potential of the exposed gate dielectric, it is shown that the threshold voltage shift is due to charge trapping by the SAMs.

SAMs made from conjugated molecules can act as semiconducting layers in an OFET. In chapter 5, it is shown that monolayer OFETs can surprisingly be made by simple spin coating. Septithiophenes have been spin coated onto a SiO_2 surface where they self-organize into a monolayer by π-π interaction. The electrical and optical properties of the monolayer have been investigated. The mobility of the semiconductor is comparable with that of a bulk layer of the same material. The attachment between SAM and gate dielectric is by physisorption. The small binding energy yields a layer that is instable at high temperatures. Desorption then deteriorates the electrical transport properties.

To improve the temperature stability, a chemical reaction with the surface is required. A quinquethiophene derivative with an anchoring group has been used to chemically bind to the SiO_2 surface. In chapter 6, the preparation of the monolayer in a transistor, a so-called self-assembled monolayer field-effect transistor (SAMFET), is described. The synthesis of the SAM molecules results in a mixture of molecules. One molecule contains a silane anchoring group that can chemically react with the SiO_2 gate dielectric. The other molecule is inert. The ratio of the compounds in the solution has been varied. Surprisingly, the inert molecule is essential to obtain a densely packed SAM. With only reactive molecules in the solution multilayers are obtained. The molecules already react with each other before assembling on the surface. The inert molecules control the speed of the SAM formation. By adjusting the ratio and processing conditions such as time and temperature dense monolayers can be obtained.

The microstructure of a quinquethiophene SAMs has been studied as a function of temperature by grazing incidence x-ray diffraction. In chapter 7 it is shown that different phases are observed depending on the thermal history of the sample. In the pristine state and at elevated temperature, the molecules stand upright on the surface. At elevated temperature the domain size remains the same but the molecules start to tilt. Up to 520 K an almost reversible isotropic expansion of the unit cell has been observed. At higher temperatures the domains irreversibly melt. The two-dimensional ordering in the SAM is induced by the layer formation process. The single-crystalline domains with polygonal shapes are formed with a lateral size in the micrometer range. The crystal structure shows a certain variation of both the lattice constants and the molecular packing. The variations can be related to the specific nature of self-assembled monolayers formed by partial covalent bonding of the molecules to the substrate.

The packing of the molecules in the SAM has been investigated using optical spectroscopy. Oligothiophenes are currently under intense investigation due to their potential application in organic electronics. In the quantum mechanical description of the lower excited states of the oligothiopene crystals, it is often assumed that the electronic interaction between molecules parallel aligned in a single layer is much larger than the electronic interactions between molecules in different layers. The photophysical studies performed in chapter 8 on a quinquethiophene monolayer reveal spectroscopic properties that are very similar to those of the corresponding 3D crystal. This supports the often used assumption that the intralayer excited state interactions dominate the interlayer coupling.

The SAMFETs made with SiO$_2$ as the gate dielectric cannot be used for flexible electronics as the substrate is not bendable. In chapter 9, the formation of a highly ordered, densely packed SAM on a bare polymer surface is reported. The formation is tentatively explained. First a few anchoring points are made by plasma oxidation. The SAM molecules then covalently bind to these hydrated anchoring points. With time a fully covered monolayer is formed. The driving force is packing of the liquid crystalline molecules due to the interaction between the linear alkane moieties and the π-π stacking of the conjugated thiophene units. The resulting SAMFETs have been combined into integrated circuits as 4-bit code generators. The fully functional circuits demonstrate long-range order over large areas, which can be regarded as the start of flexible monolayer electronics.

Samenvatting

In de afgelopen jaren hebben organische halfgeleiders steeds meer aandacht gekregen vanwege mogelijk gebruik in elektronische toepassingen zoals zonnecellen, fotodetectors, lichtemitterende diodes en veldeffect transistors. De belangrijkste voordelen van organische halfgeleiders zijn hun mechanische flexibiliteit en elektrische transporteigenschappen die kunnen worden gemodificeerd door de chemische structuur te veranderen. De mechanische flexibiliteit in combinatie met verwerking uit oplossing maakt het mogelijk om extreem goedkope elektronica op grote schaal te produceren.

Nu wordt er voor het maken van elektronica over grote oppervlaktes een top-down technologie gebruikt. Dunne films worden aangebracht door middel van opdampen, printen of spincoaten en gepatroneerd met fotolithografie. Een veelbelovende techniek voor organische elektronica is bottom-up zelfassemblage, waarbij moleculen zichzelf formeren in complexe patronen en structuren zonder menselijke interventie. Door het selectief patroneren van een substraat, in combinatie met geschikte moleculen, kan het zelfassemblage proces worden gestuurd, waarmee de latere patroneerstappen van een top-down proces kunnen worden geëlimineerd. De meest gebruikte vorm van zelfassemblage is de formatie van zelfgeassembleerde monolagen (SAMs). Ondanks het feit dat een SAM bestaat uit maar één laag moleculen, kunnen SAMs de macroscopische mechanische en elektrische eigenschappen van een oppervlak veranderen.

De bouwsteen van organische elektronica is de organische veldeffect transistor (OFET); een micro-elektronische schakelaar die gebruikt wordt om de weerstand te manipuleren. Beheersing van de belangrijkste parameters van de OFET, zoals de veldeffect mobiliteit en drempelspanning, is cruciaal. SAMs kunnen een belangrijke rol spelen bij het beheersen van deze parameters. Het effect van de SAM hangt af van de chemische samenstelling van het betreffende molecuul en van de positie in de transistor; hetzij op het gate diëlektricum of op de source- en drainelektrodes.

In hoofdstuk 2 wordt de ladingsinjectie in OFETs besproken. SAMs zijn aangebracht op de elektrodes om de werkfunctie te manipuleren. De injectie van lading in de halfgeleider kan worden verbeterd of onderdrukt. Elektrodes die met een SAM zijn bedekt kunnen echter ook de morfologie van de halfgeleider bij de contacten, en hiermee de ladingsinjectie, beïnvloeden. In hoofdstuk 3 worden de elektrodes in twee verschillende types OFETs met SAMs besproken, waarbij het effect van SAMs op de ladingsinjectie in deze verschillende types wordt geëvalueerd. In een transistor met de elektrodes onder de halfgeleider en de gate erboven, is de SAM goed gedefinieerd op de plaats waar de lading van de elektrode in the halfgeleider wordt geïnjecteerd en wordt de injectie sterk verbeterd. Voor een transistor met zowel de gate als de elektrodes onder de halfgeleider is de SAM op de plaats van ladingsinjectie slecht geordend en de ladingsinjectie is verminderd. Hoofdstuk 2 en 3 bespreken hoe een SAM aangebracht op de elektrodes de ladingsinjectie kan beïnvloeden. Behalve een verandering in de

werkfunctie is het grootste effect een verandering in de microscopische ordening van de halfgeleider.

Beheersing van de drempelspanning in OFETs is belangrijk voor de werking van organische schakelingen, bijvoorbeeld omdat de noise margin van logische poorten er door wordt bepaald. Er is al gepubliceerd dat een SAM aangebracht op het SiO_2 gate diëlektricum de drempelspanning kan beïnvloeden. In hoofdstuk 4 is de oorsprong van de verschuiving van de drempelspanning onderzocht. Met behulp van Scanning Kelvin Probe Microscopy (SKPM) is de microscopische oorzaak verklaard. Door het afpellen van de halfgeleider na de elektrische metingen en het vervolgens meten van de oppervlaktepotentiaal van het blootgelegde gate diëlektricum is aangetoond dat de drempelspanningsverschuiving wordt veroorzaakt door vastzittende lading die is gevangen door de SAM.

SAMs die zijn gemaakt van geconjugeerde moleculen kunnen functioneren als halfgeleidende lagen in een OFET. In hoofdstuk 5 is aangetoond dat werkende OFETs met slechts een monolaag halfgeleider verrassend genoeg kunnen worden gemaakt door middel van spincoaten. Septithiofenen gespincoat op een SiO_2 oppervlak vormen een monolaag door zelfassemblage met behulp van de π -π interactie van de geconjugeerde delen van het molecuul. De elektrische en optische eigenschappen van de monolaag zijn onderzocht. De mobiliteit van de halfgeleider is vergelijkbaar met het bulkmateriaal. De verbinding tussen het molecuul en het gate diëlektricum is gevormd door fysisorptie. De kleine bindingsenergie levert een laag op die instabiel is bij hogere temperatuur. Door desorptie verslechteren dan de elektrische transporteigenschappen.

Om de stabiliteit bij hogere temperatuur te verbeteren is een chemische reactie met het oppervlak vereist. Een molecuul afgeleid van quinquethiofeen met een hechtingsgroep is gebruikt om chemisch te binden met het SiO_2 oppervlak. In hoofdstuk 6 is beschreven hoe een halfgeleidende SAM in een OFET, een zogenaamde SAMFET, wordt geformeerd. De synthese van de SAM moleculen resulteert in een mix van moleculen. Eén soort moleculen bevat een hechtingsgroep van silaan en kan chemisch reageren met het SiO_2 diëlektricum. De andere soort is inert. De verhouding tussen de twee soorten moleculen in de oplossing is gevarieerd. Verrassend is dat de inerte soort essentieel is voor het vormen van een goede, dicht gepakte, SAM. Met alleen reactieve moleculen in een oplossing reageren de moleculen al met elkaar voordat ze zich formeren op het oppervlak. De inerte moleculen beheersen de snelheid van de SAM-formatie. Door het aanpassen van de verhouding moleculen en de procesomstandigheden zoals tijd en temperatuur kunnen monolagen met dichte pakking worden verkregen.

De ordening van de moleculen in een SAM is onderzocht met behulp van optische spectroscopie. Oligothiofenen zijn momenteel het onderwerp van intensief onderzoek vanwege hun potentiële toepassing in organische elektronica. In de kwantummechanische beschrijving van de laaggeëxciteerde toestanden van oligothiofeenkristallen wordt vaak aangenomen dat de elektronische interactie tussen de moleculen die parallel liggen in een enkele laag veel groter is dan tussen moleculen in verschillende lagen. De in hoofdstuk 8 beschreven fotofysische onderzoeken op een quinquethiofeen monolaag laten spectroscopische eigenschappen zien die zeer sterk lijken op het bijbehorende 3D kristal. Dit ondersteunt de vaak gehanteerde veronderstelling dat de interacties veroorzaakt door

de geëxciteerde toestanden binnenin een laag domineren over de koppeling tussen de lagen onderling.

De SAMFETs gemaakt met SiO_2 als gate diëlektricum kunnen niet worden gebruikt voor buigbare elektronica, aangezien de onderlaag niet buigzaam is. In hoofdstuk 9 is de formatie van een hooggeordende, dicht gepakte SAM op een plastic oppervlak beschreven. Eerst worden enkele hechtpunten gemaakt door een behandeling met zuurstofplasma. De SAM moleculen binden dan chemisch met deze gehydrateerde hechtpunten. Mettertijd wordt een volledig bedekte monolaag gevormd. De drijvende kracht is het pakken van de vloeibaar kristallijne moleculen door interacties tussen de lineaire alkaangroepen en de door π –π interactie veroorzaakte stapeling van de geconjugeerde thiofeen onderdelen. De resulterende SAMFETs zijn gecombineerd in geïntegreerde schakelingen zoals 4-bit codegeneratoren. De volledig functionele schakelingen vertonen ordening over grote afstanden over macroscopische oppervlaktes, waardoor dit kan worden beschouwd als het begin van flexibele monolaag elektronica.

List of publications

1. *"Manipulation of charge carrier injection into organic field-effect transistors by self-assembled monolayers of alkanethiols"*
Kamal Asadi, <u>Fatemeh Gholamrezaie</u>, Edsger C. P. Smits, Paul W. M. Blom and Bert de Boer, *J. Mater. Chem*. **2007**, *17*, 1947.

2. *"Single-layer pentacene field-effect transistors using electrodes modified with self-assembled monolayers"*
Kamal Asadi, Yu Wu, <u>Fatemeh Gholamrezaie</u>, Petra Rudolf and Paul W. M. Blom, *Adv. Mater.* **2009**, *21*, 4109.

3. *"Ordered semiconducting self-assembled monolayers on polymeric surfaces utilized in organic integrated circuits"*
<u>Fatemeh Gholamrezaie</u>, Simon G. J. Mathijssen, Edsger C. P. Smits, Tom C. T. Geuns, Paul A. van Hal, Sergei A. Ponomarenko, Heinz. -G. Flesch, Roland Resel, Eugenio Cantatore, Paul W. M. Blom and Dago M. de Leeuw, *Nano Lett.* **2010**, *10*, 1998.

4. *"Controlling charge injection by self-assembled monolayers in bottom-gate and top-gate organic field-effect transistors"*
<u>Fatemeh Gholamrezaie</u>, Kamal Asadi, Romero Kicken, Bea Langeveld-Voss, Dago M. de Leeuw and Paul W. M. Blom, *Synthetic. Met.* **2011**, *161*, 2226.

5. *"Microstructure and phase behavior of a quinquethiophene based self-assembled monolayer as a function of temperature"*
Heinz -G. Flesch, Simon G. J. Mathijssen, <u>Fatemeh Gholamrezaie</u>, Armin Moser, Alfred Neuhold, Jiri Novak, Sergei A. Ponomarenko, Quan Shen, Christian Teichert, Gregor Hlawacek, Peter Puschnig, Claudia A. Draxl, Roland Resel and Dago M. de Leeuw, *J. Chem. Phys.* **2011**, *115*, 22925.

6. *"Charge trapping by self-assembled monolayers as the origin of the threshold voltage shift in organic field-effect transistors"*
<u>Fatemeh Gholamrezaie</u>, Anne-Marije Andringa, W. S. Christian Roelofs, Alfred Neuhold, Martijn Kemerink, Paul W. M. Blom and Dago. M. de Leeuw, *Small*, **2012**, *8*, 241.

7. *"Solution processable septithiophene monolayer transistor"*
Matthieu Defaux, <u>Fatemeh Gholamrezaie</u>, Jingbo Wang, Andreas Kreyes, Ulrich Ziener, Denis V. Anokhin, Dimitri A. Ivanov, Armin Moser, Alfred Neuhold, Ingo Salzmann, Roland Resel, Dago M. de Leeuw, Stefan C. J. Meskers, Martin Moeller and Ahmed Mourran, *Adv. Mater.* **2012**, *24*, 973.

8. "*Fluorescence from self-assembled monolayers of a quinquethiophene derivative*"
<u>Fatemeh Gholamrezaie</u>, Mindaugas Kirkus, Simon G. J. Mathijssen, Dago M. de Leeuw and Stefan C. J. Meskers, *J. Phys. Chem. A*, **2012**, *116, 7645*.

9. *"N-type self-assembled monolayer field-effect transistors and complementary circuits"*
Andreas Ringk, Xiaoran Li, <u>Fatemeh Gholamrezaie</u>, Edsger C. P. Smits, Alfred Neuhold, Armin Moser, Gerwin H. Gelinck, Roland Resel, Dago M. de Leeuw and Peter Strohriegl, *Submitted,* **2012**.

10. "*Organic field-effect transistors as a test-bed for molecular electronics: a combined study with large-area molecular junctions*"
Kamal Asadi, Ilias Katsouras, Jan Harkema, <u>Fatemeh Gholamrezaie</u>, Edsger C. P. Smits, Fabio Biscarini, Paul W. M. Blom and Dago M. de Leeuw, *Submitted,* **2012**.

11. *"Structural and electrical properties of asymmetrically substituted sexithiophene monolayers"*
Jingbo Wang, Wim H. de Jeu, <u>Fatemeh Gholamrezaie</u>, Ulrich Ziener, Sergei A. Ponomarenko, Ulrich Rücker, Matthias A. Ruderer, Eva M. Herzig, Peter Müller-Buschbaum, Dago M. de Leeuw, Martin Moeller and Ahmed Mourran, *Submitted,* **2012**.

12. *"Quantum electrodynamical model for optical properties of self-assembled monolayers of a quinquethiophene derivative"*
Stefan C. J. Meskers, <u>Fatemeh Gholamrezaie</u>, Mindaugas Kirkus, René A. J. Janssen and Dago M. de Leeuw, *in preparation.*

Acknowledgments

This thesis would not have been possible without the help of many people, who I would like to acknowledge now. I will start with my supervisor Dago, whose support allowed me to overcome the obstacles that almost derailed my PhD career at the very beginning. Dear Dago, many thanks for all the things you did for me during the time I was in the Philips Research Laboratory in Eindhoven; I really enjoyed working with you in your cluster. I am also very grateful to our group leader: Dear Paul, it is difficult to find the words for thanking you for all your care in these years. From the time I came to your group as a master student up until now, your smile always gave me lots of hope. With a heavy heart I would like to mention here Bert, who was my first supervisor. His course in the Topmaster program in Nanoscience was so interesting that it attracted me to the group of Molecular Electronics - Physics of Organic Semiconductor. Bert was a very kind person and his premature passing was a huge loss to the team and to all who knew him. Dear Stefan, you are one of the few scientists that I have met who poses such extreme patience and kindness towards your students. Thanks for the collaborations which started during my PhD and for your guidance, now that I become a post-doc under your supervision.

I would like to thank my reading committee: Prof. Petra Rudolf, Prof. Roland Resel and Prof. Michel Orrit for the time spent on my thesis and Dr. Ryan C. Chiechi for accepting to be in my committee.

I would like to thank all members of our small cluster in Philips for making a special working environment. Dear Simon, Edsger and Paul, many thanks for your care and support. I will always remember you; Simon – for your special patience, Edsger – for the hours of amazing discussion triggered by a single question and Paul (the yellow character) – for your help and networking that make lab work much easier. Anne-Marije, you were not only my colleague and my roomie but also a good friend. We had lots of fun going to conferences together, to summer school in Leuven, Nice, China and San Francisco. I have lots of nice memories with you. Mark-Jan, your remarkable help in the last months before my defense with checking my thesis and translating my summary in Dutch cannot be forgotten. Thank you! Also Christian, Mengyuan, Patrick, Sepas and Tom in our cluster. Next to this, I would like to acknowledge the people from the Photonic Materials and Devices group, for the interesting GWO and nice lunch meetings. Many thanks to Hans van Sprang for accepting me in the group of Photonic Materials and Devices to do my PhD project at Philips Research Laboratories.

I acknowledge the Dutch Polymer Institute (DPI) and the Zernike Institute for Advanced Materials for the financial support and thanks to DPI Program Coordinator in the area of Functional Polymer Systems (FPS) Dr. John A.E.H. van Haare.

My gratitude also goes to the professors from Zernike Institute for Advanced Materials for their support and/or the nice courses I had with them: Prof. van Loosdrecht, Prof. Maria Loi, Prof. Petra Rudolf, Prof. Thom Palstra, Prof. Bart van Wees, Prof. Cees Hummelen, Prof. Nasser Kalantar and many others.

During my time in Philips, I have collaborated with many groups on various projects. I would like to thank all my collaborators around the world from Austria, Germany and Italy for the joint projects that at the end made for great publications. I would like to mention a few names here: Prof. Roland Resel, Prof. Sergei Ponomarenko, Dr. Ahmed Mourran, Dr. Martijn Kemerink, Prof. Peter Strohriegl, Dr. Eugenio Cantatore, Heinz, Jingbo, Andreas, Xiaoran. And others who inspired me: Prof. Richard Friend, Prof. Quyen Nguyen, and Prof. George Malliaras.

I would like to acknowledge people from MEPOS group in Groningen for making an exceptional environment and unforgettable memories with lots of fun: Auke, Afshin, Alex and your dear wife Oksana for great days in Santa Barbara, Claudia, Date, Dorota, Eek, Francseco, Gert-Jan, Herman – your cozy house "Casa di Herman", Hylke – my inspiration doing lots of adventure, Illias – great trip with you around north Greece, Irina, Gia, Jan Anton, Jan K., Johan, Kamal, Marianna – full of happiness and thank you to be one of my paranymph, Martijn K., Martijn L., Milo, Paul de B., Yuan. And dear Renate and Jan Harkema, without you the group could not survive.

Many thanks to my new colleagues in the group of Molecular Materials and Nanosystems in Eindhoven University of Technology. Dear Rene, to me you are the source of positive energy and happiness that creates the unique atmosphere we all enjoy. Dr. M. Wienk, Daniele, Dhritiman, Domenique, Gijs, Mindaugas, and rest of the group, and Ratheesh – thank you so much for your help in my new projects. Stanislav and Wenshan, you are very cool office mates!

Kristizi, my girly, we had lots of great moments of gossiping in Groningen. Nice trip to Barcelona, Rome, Valencia and Torino. Thank you for being my paranymph. Saeedeh, honey, you are the best friend ever. But you are even more – the elder sister that I never had. I could not use words to describe your care for me. When you came to Groningen I was so happy and the same goes for Mehrsima. Our long friendship was strengthened when the small group was finally complete. I felt home in your lovely house every time I came to Groningen and I had the best moments in the last years, making lots of fun and jokes together.

I would like to express my gratitude to all my Persian friends which I met in the Netherlands in the past few years. We had a great time together, from dinners to concerts, to parties. Parisa and Mehdi, you are the embodiment of hospitality in a typical Persian way. Mehdi for his help to make cover of my thesis, Thanks! Salomeh – all just energy, with unforgettable Greece trip, Fariba – nice memories from Christmas trip to Belgium. Dear Leila – my house mate in first year in Groningen.

Samaneh, I do not know you for too long, but to me it is like we have known each other for ages! You are so very special to me; I cannot tell you how much I feel close to you. I also want to thank Afroz for the trip to lovely Prague, Amir – my travel buddy, Pilot Hamed for the adventurous flight and Mojtaba for the always open house. Morteza,

Raheleh, Saeed (you can be great poet one day) and Saeid, I was fortunate to absorb some of your incredible knowledge about everything in the world! Sara, Sahel and Narges, I will never forget our trip in the snowy winter ending up with a super Persian dinner in Germany. I hope that all these nice friendships continue even from faraway!

I want to express my warm feelings to all my Persian friends back home and around the world, who might be far, but at the same time are always close to me. Rofiedeh, Faranak, Ellahe, Nico, Reihaneh, Maryam, Firozeh, Azar, Azita, Sahar and Sara. Also people who directly or indirectly had an influence in my life.

I would like to thank my family, because without their patience it would not have been possible for me to continue my education. My mom let her only daughter go abroad while providing day to day support and my father like all fathers worried about his spoiled girl, but did not prevent her from following her dreams. My two dearest brothers, I always wanted to be as successful as you are, you were like my future dream when I was younger. Your advice and support is something I always need in my life. My kind sisters in law, who are like my real sisters, and my lovely nieces and nephew, to make me so happy and proud of having such a family.

Fatemeh